UC Merced
UC Merced Electronic Theses and Dissertations

Title

BIOPHYSICAL CONTROLS ON RHIZOSPHERE DYNAMICS

Permalink

https://escholarship.org/uc/item/0xv3t61v

Author

Albalasmeh, Ammar A.

Publication Date

2013

Peer reviewed|Thesis/dissertation

UNIVERSITY OF CALIFORNIA, MERCED

BIOPHYSICAL CONTROLS ON RHIZOSPHERE DYNAMICS

A dissertation submitted in partial satisfaction of the requirements

for the degree Doctor of Philosophy

in

Environmental Systems

(Soil Physics)

by

Ammar Ali Ahmad Albalasmeh

Committee in charge:

Teamrat A. Ghezzehei, Chair
Asmeret Asefaw Berhe
Francois Blanchette
Thomas C. Harmon

2013

The dissertation of Ammar Ali Ahmad Albalasmehis approved, and it is acceptable in quality and form for publication on microfilm and electronically:

Asmeret Asefaw Berhe

Francois Blanchette

Thomas C. Harmon

Teamrat A. Ghezzehei, Chair

University of California, Merced

2013

DEDICATION

To my father's soul, **Ali Albalasmeh**

To my beloved mother, **Muna Elmughrabi**

To my loving and supportive wife, **Hanan Almohammad**

To my exuberant, sweet, and kind-hearted little girl, **Jood Albalasmeh**

To all whom advised, assisted and put up with me, **Family and Friends**

TABLE OF CONTENTS

LIST OF TABLES

LIST OF FIGURES

ACKNOWLEDGMENTS

I would like to express my deepest appreciation to all those who provided me the possibility to complete this dissertation. First and foremost, I have great exhilaration to express my ingenuous gratitude to my advisor, Teamrat A. Ghezzehei, for his endless support, guidance and unwavering commitment to my success. Teamrat's philosophy, simplicity, ideas, endless knowledge in many subjects and passion for new findings were always inspiring. His kindness and generous response to my difficulties during the research work and outside it will remain a treasure in the memory forever.

I would also like to thank my committee members, Asmeret Asefaw Berhe, Francois Blanchette and Thomas C. Harmon, for their important comments, suggestions and discussion. A special thanks to Asmeret Asefaw Berhe for providing unlimited access to soil biogeochemistry lab's equipment.

Great thanks are extended to all closest friends and all graduate and undergraduate students in the school of Natural Sciences and the school of Engineering for their support and assistance during this work. I am especially indebted to Thomas Gebrenegus and Michael Kaiser for their friendship, support and encouragement.

I would like to thank Michael Dunlap for the help provided with the SEM and ESEM works through Imaging and Microscopy Facility (IMF) at University of California, Merced and Liying Zhao for the help provided with the TOC analyzer analysis through the Environmental Analytical Laboratory (EAL) at University of California, Merced.

I would like to pay my heartfelt thanks to my affectionate mother, Muna Elmughrabi, for her prayers, continuous encouragement and unconditional love. My brothers Ghaith and Mo'men and my sisters Ghadeer and Abeer have been great support and encouragement over these last 4 years.

Last, but most definitely nit least, I want to thank my wife, Hanan Almohammad, for being with me every step of the way. She has taken great care of me as I retreated into my selfish writing phase. Hanan served as my best friend and a great listener when I need some one to listen to me. I am grateful for having found a life partner who truly supports what I do. Also, I would like to thank my most important blessing in life, my daughter Jood.

I wish to express my sincere gratitude to everyone who, in their own way, helped me to complete this dissertation.

Merced.

Above All, I praise Allah for giving me the strength to start and finish this work.

<div align="right">Ammar A. Albalasmeh</div>

CURRICULUM VITAE

Ammar Ali Ahmad Albalasmeh

EDUCATION

Doctor of Philosophy in Environmental Systems   **2009-2013**
University of California, Merced   *Merced, California*

Master of Science in Natural Resources and Environment   **2005-2008**
Jordan University of Science and Technology   *Irbid, Jordan*

Bachelor of Science in Soil, Water and Environment   **2001-2005**
Jordan University of Science and Technology   *Irbid, Jordan*

RESEARCH EXPERIENCE

Graduate Research Assistant   **2009–2013**
University of California, Merced   *Merced, California*

TEACHING EXPERIENCE

Teaching Assistant   **2010–2012**
University of California, Merced   *Merced, California*

Teaching Assistant   **2006–2007**
Jordan University of Science and Technology   *Irbid, Jordan*

REFEREED JOURNAL PUBLICATIONS

Role of root exudates on rhizosphere water dynamics: effects on   **2013**
evaporation rate
In Preparation

Rhizosphere water dynamics: role of root exudates in mediating   **2013**
water retention
Vadose Zone Journal, submitted

Interplay between soil drying and root exudation in rhizosheath de-   **2013**
velopment
Plant and Soil, submitted

Association of Anionic extracellular polymers with sand   **2013**
Plant and Soil, submitted

A new method for rapid determination of carbohydrate and total   **2013**
carbon concentrations using UV spectrophotometry
Carbohydrate Polymers 97:253-261

Degradation of moist soil aggregates by rapid temperature rise under   **2013**
low intensity fire
Plant and Soil 362:335-344

Reclamation of highly calcareous saline sodic soils using Atriplex   **2011**
halimus and by-product gypsum
International journal of phytoremediation 13:873-883

REFEREED CONFERENCE ABSTRACTS

Rhizosphere water dynamics: role of exudates in mediating water   **April 2013**
retention and flow characteristics
European Geosciences Union (EGU)

Association Mechanisms of Sand with Anionic Extracellular Polysac-   **April 2013**
charides (EPS)
European Geosciences Union (EGU)

Soil aggregate formation: the role of wetting-drying cycles in the   **April 2013**
genesis of interparticle bonding
European Geosciences Union (EGU)

Root exudate as major player on soil-water retention dynamics   **Dec 2012**
American Geophysical Union (AGU)

How Low Temperature Fire Affect Soil Structure   **Apr 2012**
33rd Annual Central California Research Symposium

Conceptual Modeling of the Influence of Wetting and Drying Cycles   **Dec 2011**
on Soil Aggregation and Stabilization
American Geophysical Union (AGU)

Effects of Low-Temperature Fire on Soil Aggregate Stability   **Oct 2011**
ASA-CSSA-SSSA 75th Annual Meeting

Effects of Low-Temperature Fire on Soil Aggregate Stability (pre-   **Apr 2011**
liminary results)
32nd Annual Central California Research Symposium

Role of Wetting and Drying in Soil Aggregate Formation   **Nov 2010**
ASA-CSSA-SSSA 74th Annual Meeting

PROFESSIONAL AFFILIATION & SERVICES

European Geosciences Union (EGU)	**2013**
American Geophysical Union (AGU)	**2011**
Soil Science Society of America (SSSA)	**2010**
American Society of Agronomy (ASA)	**2010**
Jordanian Agricultural Engineers Association (JAEA)	**2005**
Manuscript Reviewer:	**Plant and Soil Journal**

ABSTRACT OF THE DISSERTATION

BIOPHYSICAL CONTROLS ON RHIZOSPHERE DYNAMICS

By

Ammar Ali Ahmad Albalasmeh

Doctor of Philosophy in Environmental Systems

(Soil Physics)

University of California, Merced, 2013

Teamrat A. Ghezzehei, Chair

Soil structure directly determines important soil physical properties including porosity, hydraulic conductivity, water retention, and mechanical strength. It also indirectly influences almost all biological and chemical processes that occur in soil. Conversely, the development, stability, and dynamics of soil structure are dictated by the very physical, chemical, and biological processes that occur within the structured soil. There is ample empirical evidence showing the effectiveness of wetting and drying in the presence of organic matter in soil aggregation and stabilization. However, the mechanisms that bond the particles together under this process need more investigation. The goal of this dissertation was to understand and develop quantitative description of the role of wetting and drying cycles in presence of exudates in the formation and stabilization of soil aggregates within the rhizosphere.

In this dissertation, I (a) developed a new, easy and rapid method to measure the

carbohydrate and total carbon concentrations using UV spectrophotometry, (b) examined whether the association between plant root and bacteria exudates with neutral sand particles occurred and defined the mechanism of this association, (c) developed a conceptual/mathematical model describe the soil aggregation mechanism in presence of exudates under multiple wetting and drying cycles, (d) examined the mechanisms that affect rhizosphere water dynamics and whether these dynamics are a result of the osmotic potential induced by root exudates or the soil structure modification that occurred because of these exudates, and (e) developed a mathematical model to quantitatively describe the experimental results of the effect of water potential induced by root exudates on water evaporation rate.

This dissertation presented a framework for in-depth understanding on how wetting and drying cycles in the presence of exudates promote soil aggregation and stabilization within the rhizosphere. It also advanced our understanding of the benefits of presence of root exudates in the rhizosphere on water retention and evaporation rate and provided the right-scale physics for high resolution computational modeling of water dynamics around the plant roots and root water uptake.

Chapter 1

Introduction

1.1 Background

Soil structure describes the arrangement of soil particles and the pore space located between them. A good aggregated soil (structured) is important for plant growth where it acts as storage spaces, doorways and passages for moisture, nutrients, organic carbon and gases (Ghezzehei, 2012). Soil aggregation is the result of complex interactions among biological, chemical, and physical processes in the soil (Marquez et al, 2004; Tisdall and Oades, 1982) as illustrated in Figure 1.1.

To understand the mechanism and the fundamental process behind soil aggregation in-depth, we will focus on one process affecting soil aggregation, wetting and drying cycles in the presence of plant root exudates (Figure 1.2).

Numerous studies have shown that stability of soil aggregates is significantly increased with the degree and repetition of drying. Pore-scale hydraulics and application of the classical capillary theory to the inter-aggregate contacts suggests that the inter-
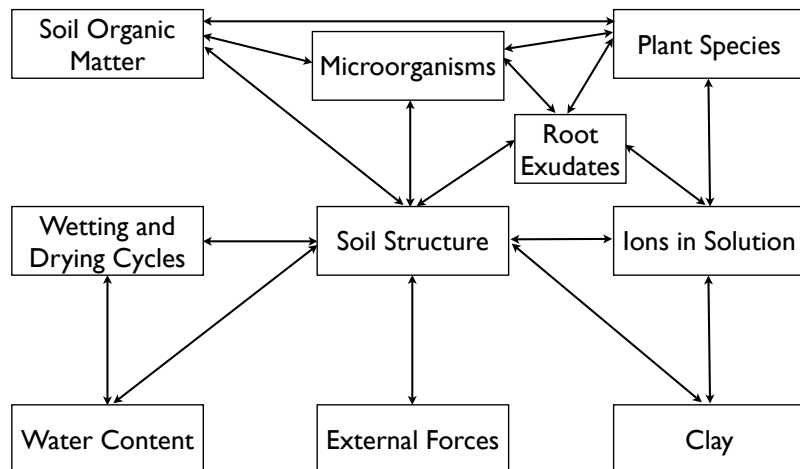
Figure 1.1: Factors influencing soil structure
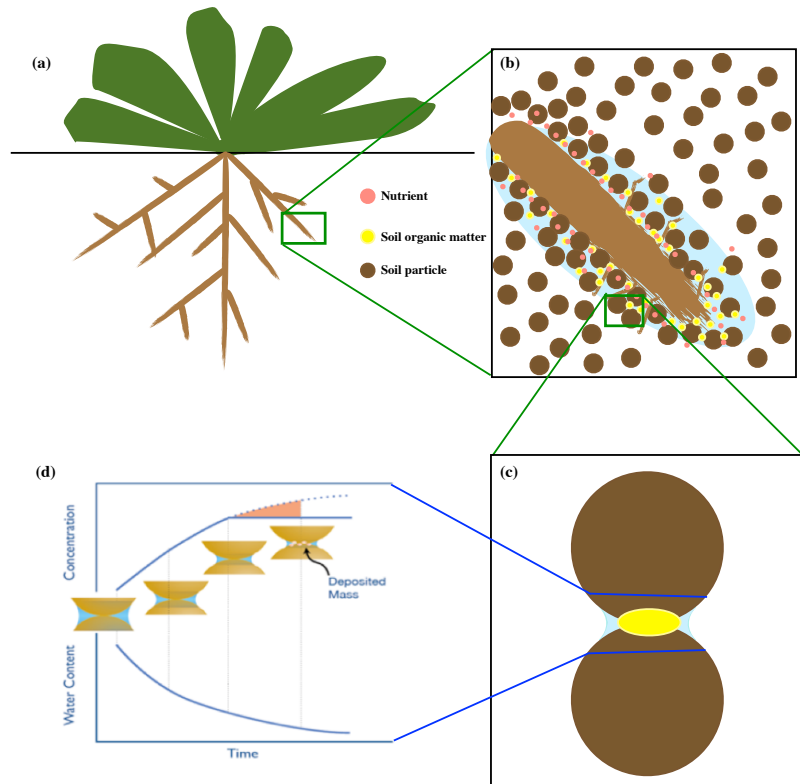
Figure 1.2: Schematic framework of plantsoil interaction. (a) The plant in the context of the soil plantatmosphere continuum, (b) processes on a single-root scale, (c) processes on the soil pore scale and (d) conceptual model of wetting drying cycles in the presence of root exudates

particle contact is the most likely place that will experience complete drying last. Thus, during the intervening period of drying, the suspended colloidal particles will migrate towards the inter-particle contact driven by the strong concentration gradients within soil aggregates that will be formed during drying as a result of water loss and increase the concentration of the suspended colloidal particles.

The root system has been described as the hidden half of a plant, playing a crucial role in plant growth. Less than a few millimeters around the root surface, the soil zone is significantly influenced by living roots, commonly known as rhizosphere, that the soil particles are strongly attached to one another as well as to the roots. In recent years, significant advances have been made in understanding biogeochemical transformations that occur in the rhizosphere (Dakora and Phillips, 2002; Neumann and Römheld, 2007; Lambers et al, 2009; Watt et al, 2006). In contrast, little is known about physical properties of the rhizosphere, its dynamics, and how they affect fluid flow and transport processes between soil and roots (Bengough, 2012; Hinsinger et al, 2009).

1.2   Scope of the Dissertation

As an overall theme, this dissertation research investigates not just *if*, but also *how* wetting and drying cycles in the presence of root exudates form and stabilize soil aggregates. Motivation for the research presented in this dissertation stems from the need to: (a) develop a rapid and cheap UV spectrophotometry method for carbohydrate concentration analysis, (b) understand the mechanism of physical attachment/association of sand and silt particles with organic polymers as a key process for aggregate formation by organic matter deposition, (c) develop applicable con-

ceptual and mathematical models for the distinct role of wetting and drying cycles in the transport and deposition of colloidal cementing agents at the most effective locations (inter-particle contacts), (d) understand the mechanisms by which root exudates deposited during wetting-drying cycle can alter soil water retention and (e) quantitatively describe the effect of the altered water potential status on evaporation rate.

1.3 Objectives of the Study

The overall aim of this dissertation was to understand soil aggregation process in-depth by looking at the root exudates as cementing agent transported by wetting and drying cycles to the most effective locations. The specific objectives to address one of the general questions/needs that motivated the research presented in this dissertation:

1. to develop an alternate for the colorimetric method of DuBois et al (1956) that reduce the reaction wait-time, improve accuracy of the measurements, eliminate the hazards posed by usage of phenol, and enabling direct correlation of light absorbance to total carbon concentration in aqueous solutions.

2. to provide a mechanistic explanation of the association of root and microbial exudates with sand and silt particles.

3. to formulate and test conceptual and mathematical models that describe the role of drying in soil aggregation as an agent for transport and deposition of binding agents.

4. to investigate how osmotic potential induced by root exudates affect the rhizosphere water dynamics.

5. to quantitatively study the effect of water potential induced by root exudate on water evaporation rate.

1.4   Organization of the Dissertation

The above research needs are addressed in five individual manuscripts, presented as self-contained chapters (2, 3, 4, 5 and 6, respectively). The chapters following this introduction each contribute to more understanding of aggregate formation process by wetting and drying cycles in presence of root exudates. Chapter 2 describes a new method for rapid determination of carbohydrate and carbon content concentrations developed to overcome some drawbacks of the traditional method of DuBois et al (1956). Such a rapid, cheap and easy method was required to analyze a very large number of samples involved in the sand-polysaccharides experiments reported in chapter 3. A key process for aggregate formation by organic matter deposition is the physical attachment/association of sand and silt particles with organic polymers, chapter 3 involve extensive experiments that allowed us to quantitatively describe the degree of association between various types organic polymers that represents exudates or plant roots and soil microorganisms. Chapter 4 deals with a conceptual and mathematical model for aggregate formation by wetting and drying cycles in presence of root exudates based. In this chapter, we also conducted several visualization experiments to test this hypothesis where we were able to show that aggregates of sand and silt particles can be formed by subjecting loose particles to wetting and drying cycles in the presence of dilute solutions of organic matter that mimic root exudates. Chapter 5 is concerned with the effect of root exudates and how they can alter soil water retention characteristics. Chapter 5 also differentiate between the effect of osmotic potential of root exudate and the capillary effect of aggregation

induced root exudates. Chapter 6. The purpose of this chapter is to extend the finding from previous chapter to quantitatively describe the effect of the altered water potential status on evaporation rate. Chapter 7 outlines an overall summary of the dissertation, conclusions and recommendations. A comprehensive list of bibliography cited in the dissertation is provided in the end.

A note on language: I wrote all chapters in the plural first-person, using the pronoun "we". I did this for two reasons, 1) all of these chapters are drafts of manuscripts that I will submit for publication with one or more co-authors who participated in their development (chapter 2 already submitted), and 2) I could not have imagined or completed this research without the dedicated assistance of many, many people, most of whom are listed in the Acknowledgements at the front of the dissertation. However, I take full responsibility for the data and ideas presented in this document.

Chapter 2

A New Method for Rapid Determination of Carbohydrate and Total Carbon Concentrations using UV Spectrophotometry[1]

abstract

A new UV spectrophotometry based method for determining the concentration and carbon content of carbohydrate solution was developed. This method depends on the inherent UV absorption potential of hydrolysis byproducts of carbohydrates formed by reaction with concentrated sulfuric acid (furfural derivatives). The proposed method is a major improvement over the widely used Phenol-Sulfuric Acid method developed

by DuBois et al (1956). In the old method, furfural is allowed to develop color by reaction with phenol and its concentration is detected by visible light absorption. Here we present a method that eliminates the coloration step and avoids the health and environmental hazards associated with phenol use. In addition, avoidance of this step was shown to improve measurement accuracy while significantly reducing waiting time prior to light absorption reading. The carbohydrates for which concentrations and carbon content can be reliably estimated with this new rapid Sulfuric Acid-UV technique include: monosaccharides, disaccharides and polysaccharides with very high molecular weight.

2.1 Introduction

The determination of carbohydrate concentration in aqueous solutions is very important component of several areas of environmental research (Fukasawa et al, 2012; Goupil et al, 2012; Raynaud et al, 2012; Takei et al, 2012; Yu et al, 2012; Zhang et al, 2012) as well as industrial applications in the petroleum (Zheng et al, 2012; Zhao et al, 2012; Fujieda et al, 2012; Pilavtepe et al, 2012; Trzcinski et al, 2012), pharmaceutical (Zha et al, 2012; Pereira et al, 2012; Bai et al, 2012; Lee et al, 2012; Coura et al, 2012), and food industries (Vriesmann et al, 2012; Golovchenko et al, 2012; Sheu and Lai, 2012; Rondan-Sanabria et al, 2012; Al-Sheraji et al, 2012). The wide diversity of carbohydrates involved in these areas has led to the development of numerous analytical techniques for measuring carbohydrate concentrations including chromatography (Mason and Slover, 1971; Prodolliet et al, 1995; Jahnel et al, 1998), capillary electrophoresis (Cortacero-Ramirez et al, 2004; ElRassi and Mechref, 1996; Soga and Serwe, 2000), infrared (IR) spectroscopy (Wang et al, 2011; Cadet, 1999; Robert and Cadet, 1998), light scattering detection (Suortti et al, 1998; Zhang et al,

2008) and Nuclear Magnetic Resonance (NMR) spectroscopy (Duquesnoy et al, 2008; Copur et al, 2003). Use of many of these methods requires considerable financial investment, advanced analytical skills, and time. One of the most versatile, relatively easy and cheap approaches for determination of carbohydrate concentrations is the colorimetric method based on reaction between hydrolyzed carbohydrate solution and a coloring reagent that develops color that is detectible in the visible range of the electromagnetic spectrum. Reagents commonly used for color development include phenol (C_6H_5OH) (DuBois et al, 1956), alkaline ferricyanide ($2\,K_4Fe(CN)_6$)(Englis and Becker, 1943), and anthrone ($C_{14}H_{10}O$)(Dreywood, 1946).

Among the colorimetric methods for carbohydrate analysis, the Phenol-Sulfuric Acid method of DuBois et al (1956) is so far the most reliable method and has been extensively used in a wide range of fields. At the time of writing this paper, more than 23,700 distinct peer-reviewed articles (including more than 1000 peer-reviewed articles in 2012 alone) were indexed by the Web of Science® (Thommpson Reuters) as citing the methods paper of DuBois et al (1956). The Phenol-Sulfuric Acid method depends on dehydration of hydrolyzed saccharides to furfural derivatives during reaction with concentrated sulfuric acid (Asghari and Yoshida, 2006; Bicker et al, 2003; DuBois et al, 1956; Hung et al, 1982; Itagaki, 1994; Lima et al, 2010; Rao and Pattabiraman, 1989). Further reaction of the furfural derivatives with phenol forms colored complexes that absorb light in the visible range, with a maximum absorbance at wave-length of 490 nm (DuBois et al, 1956; Rao and Pattabiraman, 1989).

Although it is easier to use than many of the available methods, the Phenol-Sulfuric Acid method has a few serious drawbacks. First, the coloring agent used in this method, phenol, poses multiple health hazards. Phenol and its vapors are corrosive to skin, eye, and respiratory system. Repeated and prolonged contact with skin can

cause dermatitis or second and third degree burns. Similarly, prolonged or repeated inhalation of phenol vapors causes lung edema. Long-term exposure to phenol also have serious impact on the central nervous system (it is a strong neurotoxin), kidneys, and liver (Michalowicz and Duda, 2007; Budavari, 1996; Lin et al, 2006). Phenol is one of 126 'Priority Pollutants' currently regulated by U.S. Environmental Protection Agency (Appendix A to 40 CFR Part 423). Secondly, the result of the standard Phenol-Sulfuric Acid method is presented in terms of glucose-equivalent concentrations. This representation may have potential limitations when dealing with complex carbohydrates that are not simple polymers of glucose. Finally, the chemical reactivity of carbohydrates with the derivatization reagent (sulfuric-acid) greatly depends on whether the carbohydrates are neutral or anionic. As a result, the molar absorption coefficients can greatly vary depending on the charge of the carbohydrates analyzed (Mecozzi, 2005).

The aim of this work was to develop an alternate for the colorimetric method of DuBois et al (1956) that alleviates the above listed drawbacks by reducing the reaction wait-time, improving accuracy of the measurements, eliminating the hazards posed by usage of phenol, and enabling direct correlation of light absorbance to total carbon concentration in aqueous solutions.

The motivation for this study was derived from the work of Itagaki (1994), who showed that aqueous solution of furfural has UV-light absorption maxima at 277 nm. Moreover, Itagaki (1994) showed that glucose and cellulose absorb UV light at 323 nm after hydrolysis by reaction with concentrated sulfuric acid. The bathochromic shift in absorption maxima from 277 nm to 323 nm was caused by the presence of sulfuric acid in solution (Kanetake and Otomo, 1988; Hammond and Modic, 1953; Premakumari et al, 2011; Srivastava and Kumar, 2007). It has been shown that the

bathochromic shift generally increases with the concentration of sulfuric acid used as solvent (Layne et al, 1963; LP, 1974; Itagaki, 1994).

In this paper, we will introduce a method for determination of sugar concentrations and carbon content of aqueous solutions that depends on the UV absorbance of furfural derivates produced by reaction with concentrated sulfuric acid. We will present a comparison between the standard Phenol-Sulfuric Acid method and the proposed Sulfuric Acid-UV method using aqueous solutions of neutral (glucose, fructose, sucrose, starch, dextran and actigum) and anionic (polygalacturonic acid (PGA) and xanthan) carbohydrates that are widely used in environmental research and industrial applications.

2.2 Materials and Methods

2.2.1 Reagents and Apparatus

All the chemicals used in the study were of analytical reagent grade. Glucose ($C_6H_{12}O_6$) was obtained from Sigma-Aldrich. Fructose ($C_6H_{12}O_6$), sucrose ($C_{12}H_{22}O_{11}$), starch (($C_6H_{10}O_5$)$_n$), phenol (C_6H_6O) and potassium hydroxide (KOH) were obtained from Fischer Scientific. Concentrated sulfuric acid (H_2SO_4) was obtained from ACROS. Polygalacturonic Acid (PGA) (($C_6H_8O_6$)$_n$), xanthan (($C_{35}H_{49}O_{25}$)$_n$) and dextran (($C_6H_{12}O_6$)$_n$) were obtained from MP Biomedicals. Actigum (($C_{24}H_{40}O_{19}$)$_n$) was obtained from Cargill company. Absorption measurements were made on a Thermo Scientific Evolution 300 UV-Vis Spectrophotometer.

A stock solution of each carbohydrate was prepared by dissolving 0.1 g of dry carbohydrate in 1 L of double milipore water (DDI). Because PGA is insoluble in water, it

was made soluble by addition of potassium hydroxide (KOH). It has been previously reported that 0.46 ml of KOH is required to dissolve 100 mg of PGA (Czarnes et al, 2000b). However, our preliminary experiments indicated that the pH of the prepared solution is better indicator of solubility of PGA. We found that the pH of the solution has to be raised to 12.4 for complete dissolution and this procedure was used throughout this study. Various dilutions of the stock carbohydrate solutions were made by pipetting a known volume of the stock solution and completing the volume with DDI water. The concentrations that were prepared for this study are: 0, 0.01, 0.03, 0.05, and 0.07 g/L.

2.2.2   Analytical Methods

In the paragraphs below we describe two methods that are based on light absorption in the visible and UV range: the Phenol-Sulfuric Acid Method (DuBois et al, 1956) and the proposed Sulfuric Acid-UV method, respectively.

Phenol-Sulfuric Acid Method

This is the most widely used colorimetric method to date for determination of carbohydrate concentration in aqueous solutions (DuBois et al, 1956). The basic principle of this method is that carbohydrates, when dehydrated by reaction with concentrated sulfuric acid, produce furfural derivatives. Further reaction between furfural derivatives and phenol develops detectible color. The standard procedure of this method is as follows. A 2 mL aliquot of a carbohydrate solution is mixed with 1 mL of 5% aqueous solution of phenol in a test tube. Subsequently, 5 mL of concentrated sulfuric acid is added rapidly to the mixture. After allowing the test tubes to stand for

10 minutes, they are vortexed for 30 seconds and placed for 20 minutes in a water bath at room temperature for color development. Then, light absorption at 490 nm is recorded on a spectrophotometer. Reference solutions are prepared in identical manner as above, except that the 2 mL aliquot of carbohydrate is replaced by DDI water. The phenol used in this procedure was redistilled and 5% phenol in water (w/w) was prepared immediately before the measurements.

Sulfuric Acid-UV Method

The procedure of the proposed Sulfuric Acid-UV method is as follows. A 1 mL aliquot of carbohydrate solution is rapidly mixed with 3 mL of concentrated sulfuric acid in a test tube and vortexed for 30 seconds. The temperature of the mixture rises rapidly within 10-15 seconds after addition of sulfuric acid. Then, the solution was cooled in ice for 2 minutes to bring it to room temperature. Finally, UV light absorption at 315 nm is read using UV spectrophotometer. Reference solutions are prepared following the same procedure as above, except that the carbohydrate aliquot is replaced with DDI water.

Total Carbon Analysis

One of the goals of this work was to determine if there is a linear relationship between the spectrophotometric absorption of the sugar solutions and the total carbon concentration of the aqueous solutions. For this purpose, the carbon concentration of all the sugars was measured using a Shimadzu TOC-Vcsh analyzer. However, total carbon analysis of xanthan and actigum solutions using the TOC analyzer was not reliable. Because these carbohydrates form viscous suspensions, the small volume of sample

extracted by the TOC analyzer needle is not necessarily representative. Therefore, we approximated the carbon content of these solutions as:

$$[C] = \frac{n\, M_{\mathrm{C}}}{M_{\mathrm{S}}} p\, S \tag{2.1}$$

where $[C]$ is theoretically calculated total carbon (in mass/volume), n is the number of C atoms in the basic unit of the carbohydrate molecule, M_{C} is molar mass of carbon atom, M_{S} is molar mass of a single unit of the carbohydrate molecule, p is the purity of the carbohydrate reagent used expressed as fraction, and S is the as-prepared concentration of the carbohydrate solution (in mass/volume) .

2.2.3   Interaction Time

We tested the effect of interaction time on the accuracy of both methods. This was done by varying the wait time after concentrated sulfuric acid is added to the carbohydrate solutions. Effect of time was tested on 0.01 and 0.07 g/L glucose solutions and wait times of 5, 15, 30, 45, 75, 105, 135 and 225 minutes.

2.2.4   Method Validation

The validation of the new method (Sulfuric Acid-UV method) was performed according to the International Conference on Harmonisation (ICH) guidelines (ICH Harmonized Tripartite Guidelines, 2005). Validation process was performed in terms of the following metrics: limit of detection (LOD), limit of quantification (LOQ), linearity, precision, and accuracy. In addition, the new method was tested for pos-

sible interference from solution components that absorb in the UV range of interest, primarily proteins and flavonoids.

The limit of detection (LOD) is the lowest analyte concentration that can be detected but not necessarily quantified as an exact value, where as the limit of quantification (LOQ) is the lowest analyte concentration that can be measured with suitable precision and accuracy (Currie, 1999). LOD and LOQ are calculated for carbohydrate concentration versus absorbance and total carbon versus absorbance relationships as

$$LOD = 3.52\sigma_b \tag{2.2}$$

$$LOQ = 16.67\sigma_b \tag{2.3}$$

where σ_b is the respective standard deviation of the blank.

The linearity of an assay refers to the ability of the assay to obtain response values that are related to the analyte concentration by a defined mathematical function. In quantitative terms, linearity is expressed as the regression coefficient for fitting the data points to a straight line . The linearity was evaluated by the least square regression method with triplicate determinations at each concentration level.

The accuracy of an analytical procedure describes how well the measured concentrations agree with accepted reference values. Accuracy was assessed in terms of the percentage relative error and mean percentage recovery. For this purpose, a separate set of triplicate samples were prepared and their concentrations were determined

using the fitted calibration equations. Percent relative error (δ) was determined as

$$\delta = 100\frac{[C]^* - [C]}{[C]} \tag{2.4}$$

where $[C]^*$ denotes carbohydrate concentration (carbon content) determined by the new method and $[C]$ is the prepared carbohydrate concentration (carbon content). Similarly, percent recovery (r) was calculated as

$$r = 100\frac{[C]^*}{[C]} \tag{2.5}$$

The precision of an analytical procedure expresses the closeness of agreement (degree of scatter) between a series of measurements obtained from multiple sampling of the same homogeneous sample under the prescribed conditions. The precision of an analytical procedure is usually expressed in terms of the standard deviation (SD) within the series of measurements.

To test for the possible interference from the presence of proteins and/or flavonoids in sample solutions, we tested the UV absorbance of bovine serum albumin (BSA) and cinnamic acid solutions that were subjected to the full procedure of the proposed Sulfuric Acid-UV method. The objective of this test was to check whether the reaction with concentrated sulfuric acid would reduce or eliminate the UV absorbance of these compounds that are known to absorb UV light in the target range.

2.2.5   Statistical Analysis

All measurements in this study were conducted on three replicate samples. All reported data points and spectra denote the means of the replicates. Error bars are not shown in the plots because the clutter makes it difficult to distinguish between the symbols that represent different carbohydrates. The mean and standard error of all the data reported in figures are provided in the electronic supplementary data. Data analysis was conducted using the statistical analysis software program R. Significant differences among means were analyzed by Tukey's HSD (honestly significant difference) test at probability level $\alpha < 0.05$.

2.3   Results and Discussions

Eight carbohydrates were tested in the study, including monosaccharides (glucose and fructose), disaccharide (sucrose), and polysaccharides (starch, actigum, dextran, PGA and xanthan). PGA and xanthan are inherently anionic carbohydrates while all the others are neutral.

2.3.1   Absorption Spectra

Light absorption in the entire visible range of the electromagnetic spectrum for all the carbohydrate solutions prepared according to Phenol-Sulfuric Acid method (DuBois et al, 1956) is presented in Appendix A, Figure A.1. The figures depict the fraction of the light absorbed (y-axis) as a function of wave length (x-axis). All of the carbohydrates, with the exception of PGA, have absorption maximum at 490 nm, in agreement with the original method (DuBois et al, 1956; Rao and Pattabiraman,

1989). All concentrations of PGA showed peak absorption at 478 nm. However, in the remainder of this paper, the standard 490 nm absorption is used consistently for PGA as well as the rest of the carbohydrates.

Similarly, UV light absorption in the full UV light spectrum for all the carbohydrate solutions prepared according to Sulfuric Acid-UV method is presented in Appendix A, Figure A.2. All of the carbohydrates, with the exception of PGA, showed maximum absorption at 315 nm. Note that this absorption peak is slightly smaller than that reported by Itagaki (1994) (322 nm). This slight bathochromic shift is related to differences in sulfuric acid concentration in the analyzed aliquots. All concentrations of PGA had maximum absorption at 297 nm. However, in the remainder of this paper, absorption at 315 nm is used for PGA in order to be consistent with the rest of the carbohydrates.

2.3.2   Effects of Reaction Time

The Phenol-Sulfuric Acid method requires several minutes for visible color development. In contrast, the proposed Sulfuric Acid-UV method is based on UV light absorption of the dehydrated carbohydrate, which requires only several seconds to be completed. Thus, one of the attractive features of the proposed method is time saving.

In Figure 2.1, the reaction time after addition of sulfuric acid was added to the carbohydrate solution is compared with the scaled absorbance for both methods. The scaled absorbance was calculated by dividing the absorbance at each time by the absorbance at 225 minutes, which we consider as the stable reading. From these results it is evident that the Phenol-Sulfuric Acid method requires > 30 minutes
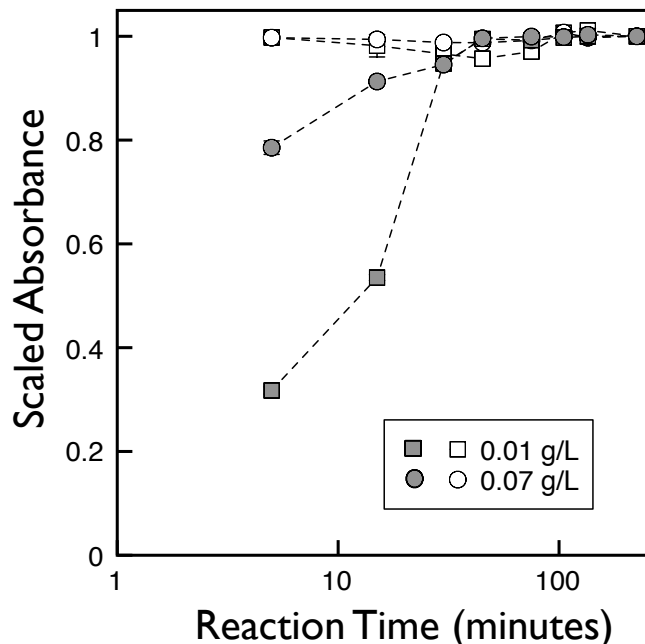
Figure 2.1: Comparison the effects of reaction time on the absorbance for Phenol-Sulfuric Acid method (filled symbols) and the Sulfuric Acid-UV Method (open symbols) for two concentrations of glucose. Note that the scaled absorbance denotes the absorbance at each reaction time normalized by the absorbance at 225 minutes, for the respective method and concentration.

for full coloration of the furfural derivatives by reaction with phenol. Similar wait time recommendation was previously reported by DuBois et al (1956) and (Rao and Pattabiraman, 1989). In contrast, the UV absorption of the furfural in the proposed method reaches stable level rapidly as soon as the reaction between the carbohydrates and the concentrated sulfuric acid is completed (most likely within a few seconds). Our observations are consistent with those of Itagaki (1994) who reported that UV absorbance of furfural does not change over time, remaining stable for up to five days.
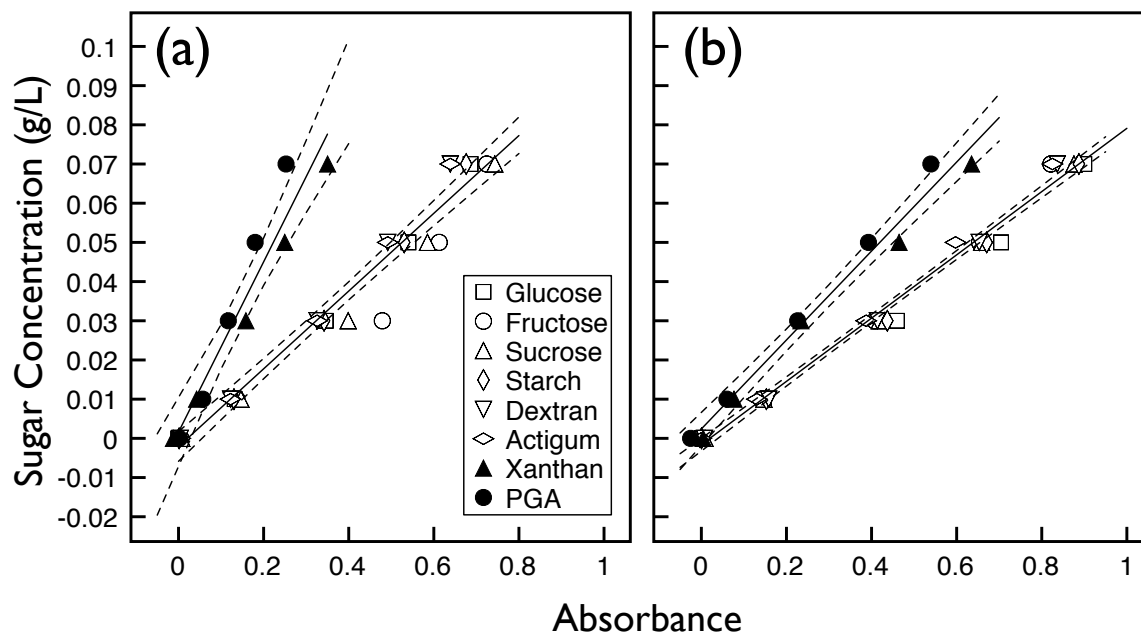
Figure 2.2: Absorbance response to different carbohydrate concentrations using the (a) Phenol-Sulfuric Acid method and (b) Sulfuric Acid-UV method. The solid lines represent linear regression fit to the data and the broken lines represent 95% confidence interval of the regression line. Note that the filled symbols represent the anionic sugars while the opened symbols represent the neutral sugars. For the statistical data see table 2.1

2.3.3 Measurement of Carbohydrate Concentrations

Figure 2.2 shows the relationship between the absorbance (x-axes) and the concentration of different carbohydrates in g/L (y-axis) for both the Phenol-Sulfuric Acid method (Figure 2.2a) and the Sulfuric Acid-UV method (Figure 2.2b). In Table 2.1 we show the coefficients of linear regression lines individually fitted to all the carbohydrate data plotted in Figure 2.2 for both methods.

Table 2.1: Coefficients of the standard curves obtained for the carbohydrates (Figure 2.2) (corresponding to the absorbance versus the carbohydrate concentrations)

Sugar	Method	Slope	Intercept	Regression coefficient (R^2)	Mass Absorptivity** ($cm^2 g^{-1}$)
Glucose	Phenol-Sulfuric Acid	0.1009 [AB]	-0.0024	0.992	11.34 (0.13)
	Sulfuric Acid-UV	0.0762 [a]	-0.0017	0.992	14.25 (0.07)
Fructose	Phenol-Sulfuric Acid	0.0903 [A]	-0.0034	0.947	13.07 (0.18)
	Sulfuric Acid-UV	0.0833 [a]	-0.0017	0.992	13.11 (0.08)
Sucrose	Phenol-Sulfuric Acid	0.0939 [AB]	-0.0033	0.988	12.57 (0.14)
	Sulfuric Acid-UV	0.0802 [a]	-0.0018	0.998	13.58 (0.07)
Starch	Phenol-Sulfuric Acid	0.1028 [AB]	-0.0025	0.992	11.17 (0.13)
	Sulfuric Acid-UV	0.0786 [a]	-0.0018	0.996	13.98 (0.08)
Dextran	Phenol-Sulfuric Acid	0.1098 [AB]	-0.0028	0.993	10.51 (0.13)
	Sulfuric Acid-UV	0.0836 [a]	-0.0026	0.994	13.66 (0.12)
Actigum	Phenol-Sulfuric Acid	0.1158 [B]	-0.0025	0.981	9.73 (0.11)
	Sulfuric Acid-UV	0.0851 [a]	-0.001	0.998	12.43 (0.05)
Xanthan*	Phenol-Sulfuric Acid	0.1933 [C]	0.0015	0.998	4.88 (0.09)
	Sulfuric Acid-UV	0.108 [b]	0.0014	0.995	8.46 (0.10)
PGA*	Phenol-Sulfuric Acid	0.2888 [C]	-0.0032	0.994	4.20 (0.24)
	Sulfuric Acid-UV	0.1232 [b]	0.0026	0.999	7.28 (0.12)
Neutral	Phenol-Sulfuric Acid	0.2172	-0.0021	0.959	11.40 (0.16)
	Sulfuric Acid-UV	0.0807	-0.0016	0.990	13.50 (0.09)
Anionic	Phenol-Sulfuric Acid	0.2172	0.0016	0.935	4.54 (0.18)
	Sulfuric Acid-UV	0.1135	0.0024	0.983	7.78 (0.13)

Values within each method followed by the same letter are not significantly different at the $\alpha = 0.05$ probability level according to Tukey's honestly significant difference (HSD) test.

* Anionic carbohydrate

** Mean (coefficient of variation (CV))

Before further discussing the merits of the proposed method, it is important to ascertain that the measured absorbance is indeed dependent only on the solution concentration. This concept is mathematically summarized in the Beer-Lambert Law that relates the measured absorbance to solution properties and the sample geometry

$$A = \epsilon [C] l \tag{2.6}$$

were A is the absorbance, ϵ [L^2/M] is the mass absorptivity, C [M/L^3] is the concentration and l [L] is the path length of the sample. We chose to use mass absorptivity (instead of molar absorptivity) because the molar mass of some of the carbohydrates used in this study (including actigum, dextran, PGA, starch and xanthan) is known only as a range of values. Equation (2.6) was fitted to all the individual samples that were analyzed. The mean and coefficient of variation of the calculated mass absorptivity values are reported in Table 2.1 for each carbohydrate as well as for the neutral and anionic carbohydrates collectively. The coefficient of variation is generally low indicating that Beer-Lambert law is obeyed.

The results in Figure 2.2 and in Table 2.1 clearly show that there is strong linear correlation between the carbohydrate concentrations and light absorbance, measured using both methods. Moreover, these results indicate that there is distinct difference in the concentration-absorbance relationships between the neutral carbohydrates and the anionic carbohydrates, as indicated by slopes of the regression fits to the neutral and anionic carbohydrates (reported as lines in Figure 2.2). Similar difference in absorption coefficients between neutral and anionic carbohydrate for the Phenol-Sulfuric Acid method was also noted previously by Mecozzi (2005). These observations suggest that the rate of conversion from carbohydrate to furfural derivatives, upon dehydration by sulfuric acid, is not the same for neutral and anionic carbohydrates. Thus,

the original Phenol-Sulfuric Acid method (DuBois et al, 1956), which uses glucose solutions as calibration standards, may not be directly applicable for anionic carbohydrates without appropriate adjustment for the calibration curves (Mecozzi, 2005).

A closer look at Figure 2.2a and the slopes of the regression lines of the Phenol-Sulfuric Acid method (Table 2.1) reveals that there were statistically significant differences, albeit small, amongst some of the standard curves of the neutral carbohydrates. In contrast, there was no statistically significant difference amongst the regression slopes of the neutral carbohydrates measured using the Sulfuric Acid- UV method (Figure 2.2b). These differences are also reflected in the coefficient of determination (R^2) values of the regression lines fitted to all the neutral and anionic carbohydrates separately (reported as lines in Figure 2.2). For both methods, there were no differences in regression slopes between the pair of anionic sugars. In addition, note that the separation between the neutral and anionic regression lines is smaller in the proposed Sulfuric Acid-UV method.

The above observations are consistent with the fact that all the neutral carbohydrates are broken down to similar base sugar molecules when hydrolyzed. The statistically significant variability amongst the neutral carbohydrates, when measured using the Phenol-Sulfuric Acid method, is probably a result of slight inconsistencies in the coloration of the furfural derivatives by Phenol. Thus, the significantly better consistency of the proposed Sulfuric Acid- UV method can be explained by (a) direct dependence on the UV absorption potential of the furfural derivatives and (b) avoidance the need for a separate color development process.

Finally, the 95% confidence intervals of the grouped regression fits indicate that the maximum errors of the Phenol-Sulfuric Acid method (computed at the mid-point of the measured absorbance range for each carbohydrate group and method) are

$\pm 6.5\%$ and $\pm 14.4\%$ for the neutral and anionic carbohydrates, respectively. The corresponding error levels of the proposed Sulfuric Acid-UV method are $\pm 2.8\%$ and $\pm 7.5\%$, respectively. Thus, the proposed method cuts the measurement error by as much as half.

2.3.4   Measurement of Total Carbon Content

In many applications, the total carbon content, rather than the bulk carbohydrate concentration, is the more desirable measure. To this end, we tested whether the absorbances measured according to the Phenol-Sulfuric Acid method and the proposed Sulfuric Acid-UV method are strongly correlated with total carbon content of the solutions. The carbohydrate concentrations reported in Figures 2.2 were converted to total carbon content using two approaches: (a) approximated from the carbohydrate composition and solution concentration according to Eq. 3.1 and (b) direct measurement of the carbon content of all the solutions using TOC analyzer. The calculated and measured total carbon content values of all the carbohydrate solutions, except those of actigum and xanthan, were in strong agreement as indicated by the tight distribution of the data points around the 1:1 line in Figure 2.3a. However, the measured carbon concentrations of actigum and xanthan suspensions were significantly lower than the calculated values. Similar observations were also noted byother researchers (Fontes et al, 2005) who analyzed total carbon content of suspensions. Likely causes for this underestimation of measured carbon content include (a) the suspended carbohydrates settle prior to extraction by the auto-sampler of the TOC analyzer and/or (b) the sampling needle is too fine to extract representative sample from the suspension. Therefore, the calculated total carbon content values of actigum and xanthan are used in the remainder of the discussions.
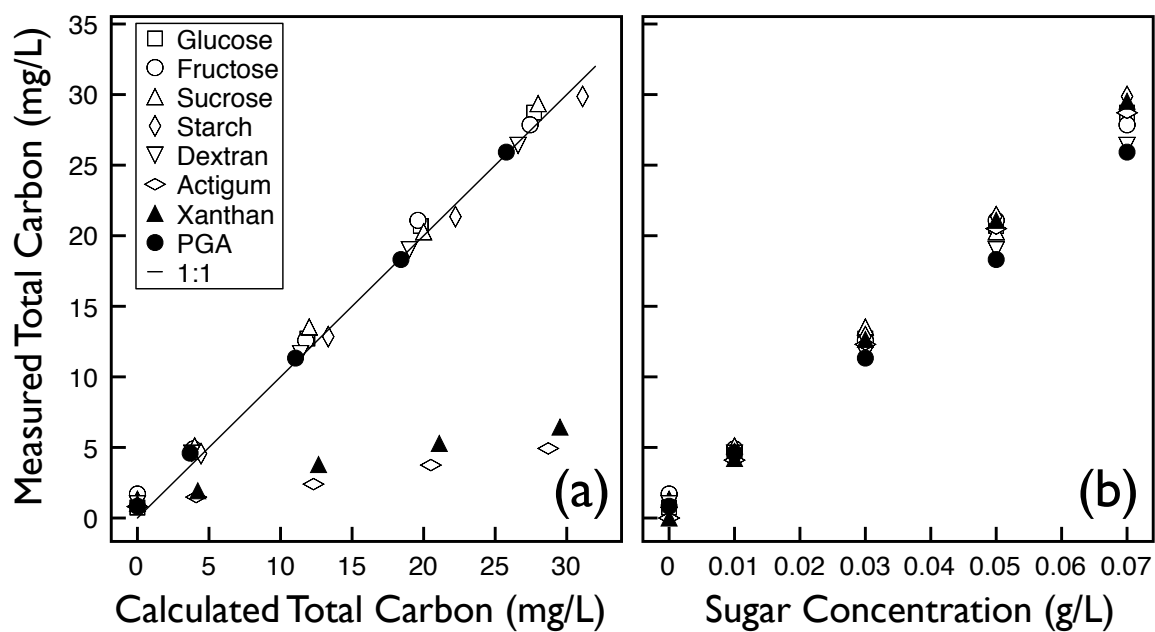
Figure 2.3: Relationship between the calculated and measured total carbon for the different carbohydrate used (a) and the correlation between the total measured carbon content and carbohydrate concentrations (b). Note that calculated carbon content is used for actigum and xanthan in part (b) because the measured carbon content was unreliable (see text for explanation).

In Figure 2.3b, the carbon content (mg/L) of the carbohydrate solutions is compared with the corresponding total carbohydrate concentrations. The coefficients of linear regression equations fitted individually to all the carbohydrates in Figure 2.3b are provided in Table 2.2. The very high coefficients of determinations ($R^2 \geq 0.998$) of the regression fits are indicative of the precision with which the samples used in this study were prepared and the analyses were performed. It is also important to note that there were small but statistically significant differences among the slopes of the regression equations given in Table 2.2. Thus, there is no universal rule for conversion from total carbohydrate concentration to carbon content (and vice versa).

Table 2.2: Coefficients of the measured total carbon content measurements obtained for different carbohydrate concentrations (Figure 2.3B) (corresponding to the total carbon content in mg/L versus the carbohydrate concentration)

Sugar	Slope	Intercept	Regression coefficient (R^2)
Glucose	400.05 [cd]	0.7065	1
Fructose	381.39 [cd]	1.4205	0.999
Sucrose	395.95 [c]	1.2516	0.998
Starch	414.89 [c]	0.6514	1
Dextran	362.83 [ab]	0.9359	1
Actigum[*]	410.1[bd]	0	1
Xanthan[*]	421.83 [cd]	0	1
PGA	354.95 [a]	0.8412	1

Values followed by the same letter are not significantly different at the $\alpha = 0.05$ probability level according to Tukey's honestly significant difference (HSD) test.
* calculated total carbon

By combining the data reported in Figures 2.2 and 2.3b, we derived relationships between the total carbon content of the carbohydrate solutions and absorbance values measured using the Phenol-Sulfuric Acid and Sulfuric Acid-UV methods (Figure 2.4). The coefficients of linear regression equations fitted individually to all the carbohy-
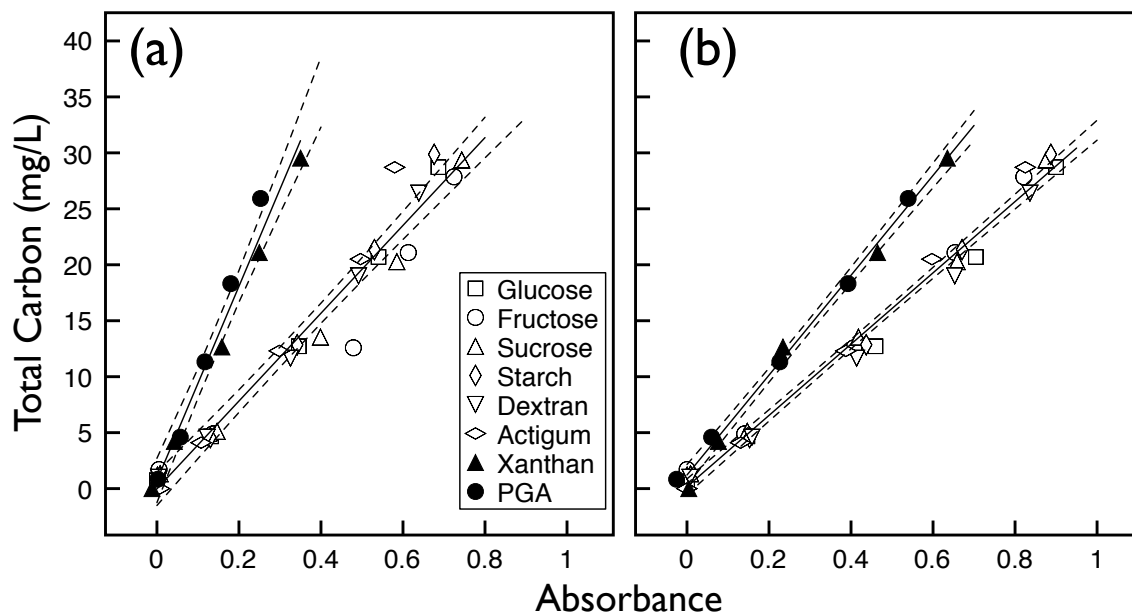
Figure 2.4: Absorbance response to total carbon content for different carbohydrate concentrations using Phenol-Sulfuric Acid method(a) and Sulfuric Acid-UV method (b). The solid lines represent linear regression fit to the data and the broken lines represent 95% confidence interval of the regression line. Note that the filled symbols represent the anionic sugars while the opened symbols represent the neutral sugars. For the statistical data see table 2.3

drates are reported in Table 2.3. Comparison of the coefficients of determination of individual carbohydrates reported in Table 2.1 with those in Table 2.3 reveals that there was no gain or loss of measurement accuracy for either method.

In addition, linear regression lines were fitted to the neutral and anionic groups of carbohydrates. The maximum errors of the Phenol-Sulfuric Acid method at 95% confidence level (computed at the mid-point of the measured absorbance range for each carbohydrate group and method) are $\pm6.1\%$ and $\pm8.4\%$ for the neutral and anionic carbohydrates, respectively. The corresponding error levels of the proposed Sulfuric Acid-UV method are $\pm2.9\%$ and $\pm4.2\%$, respectively. It is important to highlight the fact that the error level of the proposed Sulfuric Acid-UV method is half of the Phenol-Sulfuric Acid method. In addition, note that the error in both methods

Table 2.3: Coefficients of the standard curves obtained for the carbohydrates (Figure 2.4) (corresponding to the absorbance versus total carbon)

Sugar	Method	Slope	Intercept	Regression coefficient (R^2)
Glucose	Phenol-Sulfuric Acid	40.377 [AB]	-0.2551	0.991
	Sulfuric Acid-UV	30.464 [a]	0.0330	0.991
Fructose	Phenol-Sulfuric Acid	34.423 [A]	0.1426	0.945
	Sulfuric Acid-UV	31.810 [a]	0.7525	0.993
Sucrose	Phenol-Sulfuric Acid	37.155 [AB]	-0.0582	0.985
	Sulfuric Acid-UV	31.749 [a]	0.5364	0.995
Starch	Phenol-Sulfuric Acid	42.587 [AB]	-0.3816	0.988
	Sulfuric Acid-UV	32.565 [a]	0.0622	0.992
Dextran	Phenol-Sulfuric Acid	39.776 [AB]	-0.0550	0.991
	Sulfuric Acid-UV	30.286 [a]	0.0024	0.993
Actigum	Phenol-Sulfuric Acid	47.499 [B]	-1.0154	0.981
	Sulfuric Acid-UV	34.913 [a]	0.4228	0.998
Xanthan*	Phenol-Sulfuric Acid	81.536 [C]	0.6349	0.998
	Sulfuric Acid-UV	45.574 [b]	0.6042	0.995
PGA*	Phenol-Sulfuric Acid	102.590 [C]	-0.2869	0.995
	Sulfuric Acid-UV	43.714 [b]	1.7694	0.998
Neutral	Phenol-Sulfuric Acid	39.231	-0.0225	0.960
	Sulfuric Acid-UV	31.848	0.1701	0.988
Anionic	Phenol-Sulfuric Acid	86.733	0.7281	0.976
	Sulfuric Acid-UV	44.612	1.2159	0.994

Values within each method followed by the same letter are not significantly different at the $\alpha = 0.05$ probability level according to Tukey's honestly significant difference (HSD) test.
* calculated total carbon

is significantly diminished when used for measuring carbon content as opposed to carbohydrate concentration (Figure 2.2) of the anionic solutions.

2.3.5   Method Validation

Analytical characteristics of the Sulfuric Acid-UV method were evaluated in terms of LOD, LOQ, linearity, accuracy and precision. These validation tests were performed using the combined calibration equations that were fitted to the absorbance

vs sugar concentration and absorbance vs carbon content data of the neutral as well as anionic sugars collectively. The LOD and LOQ for the sugar concentration calibration equations calculated using Equations (2.2) and (2.3) are 0.002 and 0.01 g/L, respectively. From these results, it is readily apparent that the LOD values are an order of magnitude lower than the lowest concentration used for the calibrations. The LOQ on the other hand is equal to the lowest concentration used in the calibrations. Therefore, the new method and the provided calibrations are considered applicable for quantitative measurement within the the range of the concentrations used in this study; i.e. sugar concentrations of $0.01 - 0.7$ g/L. The linearity of the sugar concentration and carbon content calibration equations are provided in Tables 2.1 and 2.3, respectively. The observed R^2 values ($R^2 \geq 0.983$ and $R^2 \geq 0.988$, respectively) are considered high for the intended purpose of the method. The accuracy and precision of the new method are reported in Table 2.4. Accuracy of the method was tested in terms of percent relative error (δ) and percent recovery (r), which were calculated using Eqs 2.4 and 2.5, respectively. In general, the new method can be considered to be accurate to within 3.6%. The standard deviation (precision) of the replicate validation samples is reported in Table 2.4, which is generally low indicating high precision measurement. Note that the smaller SD, the better precision.

Table 2.4: Accuracy and Precision of the Sulfuric Acid-UV Method.

| Sugar | Prepared | | Measured | | | | % Recovery | | % Relative Error | |
	sugar Conc. (g/L)	Carbon Content (mg/L)	sugar Conc. (g/L)	SD*	Carbon Content (mg/L)	SD*	sugar Conc.	Carbon Content	sugar Conc.	Carbon Content
Glucose	0.010	4.667	0.010	0.0024	4.788	0.0035	100.00	102.59	0.00	2.59
	0.030	12.717	0.031	0.0023	12.941	0.0095	103.33	101.76	3.33	1.76
	0.070	28.723	0.070	0.0010	28.260	0.0042	100.00	98.39	0.00	1.61
Starch	0.010	4.560	0.010	0.0055	4.661	0.0021	100.00	102.19	0.00	2.19
	0.030	12.850	0.031	0.0091	12.941	0.0089	103.33	100.71	3.33	0.71
	0.070	29.867	0.071	0.0064	28.993	0.0015	101.43	97.07	1.43	2.93
PGA	0.010	4.595	0.010	0.0035	4.428	0.0018	100.00	96.37	0.00	3.63
	0.030	11.330	0.029	0.0055	11.700	0.0102	96.67	103.27	3.33	3.27
	0.070	25.923	0.068	0.0064	26.823	0.0110	97.14	103.47	2.86	3.47

* Standard Deviation

The test for interference showed that UV absorbance of BSA and cinnamic acid is reduced but not completely eliminated after hydrolysis by reaction with concentrated sulfuric acid. Therefore, it is concluded that that the proposed method is not appropriate for samples that absorb in the UV range without any pre-treatment. As a precaution it is recommended that prior to using the proposed Sulfuric acid-UV method, samples should be pre-screened to test if they have UV absorbance.

The reduction of UV absorbance upon hydrolysis suggests that it is possible that small quantities of protein/flavonoid impurities might be admissible, if their UV absorbance is reduced below the detection limit. The admissible level of UV absorbance of untreated samples must be established by systematic analysis of wide range of proteins and flavonoids mixed with carbohydrates at varying concentrations and proportions.

2.4   Conclusion

The proposed Sulfuric Acid-UV method represents a major improvement to the widely used carbohydrate characterization by Phenol-Sulfuric Acid method. The advantages of the proposed method is linked to the elimination of phenol for visible coloration of the furfural derivatives and instead capitalization on the UV absorption potential of furfural. This modification not only avoids the health and environmental hazards of phenol use but also cuts measurement error by as much as half while significantly reducing measurement time. Therefore, we can conclude that the proposed Sulfuric Acid-UV method is suitable for safer and high-throughput analysis of diverse carbohydrates in research and industrial applications. However, the Sulfuric Acid-UV method is not to be used for samples that have UV absorbance before treatment as this may indicate possible interference by protein and/or flavonoid impurities.

Chapter 3

Association of Anionic Extracellular Polymers with Sand

abstract

Association of sand and silt particles with polysaccharides is a key process for aggregate formation. Particularly, the formation of rhizosheath is a striking evidence of strong adhesion of plant roots and microorganisms exudates with coarse-grained soil particles. This study was designed to test the mechanisms of how exudates of plant roots and microorganisms are associated with sand. Polygalacturonic Acid (PGA) and xanthan, were used as a representation of exudates of plant root and bacteria, respectively. Association experiments were carried out by mixing sand with polysaccharide at different pH and concentrations. The association/attachment is pH dependent. PGA was associated at much higher rate than xanthan. With increase in the concentration, the degree of association of PGA increased. However, xanthan peaked in the mid-range concentrations and declined at higher concentrations within

the examined range. The size of the sand particles showed no effect on the degree of association of PGA while it increased with sand particle size in xanthan. The degree of association is inversely related to the mineral surface area for both polysaccharides. The association degree depends on molecular configuration and charge density of the polysaccharides. Hydrogen bonds seem to be highly relevant for the association.

3.1   Introduction

An essential step in soil aggregation and structure development is the association (attachment) of mineral constituents of soil with organic matter (Ghezzehei, 2012). Soil organic matter is composed of partially decomposed debris including dead roots and microorganisms (Kögel-Knabner, 2002; Vogt et al, 1986), aboveground foliage (Godbold et al, 2006; Kögel-Knabner, 2002; Vogt et al, 1986), as well as polysaccharides exuded by roots and microorganism (Guidi et al, 1977; Martin, 1971). Although polysaccharides represent a small fraction of the soil organic matter (Olness and Clapp, 1975), they have been shown to be responsible for the enhanced soil aggregation typically observed in the vicinity of plant roots and microorganisms (Abiven et al, 2007; Alagoez and Yilmaz, 2009; Czarnes et al, 2000a; Morel et al, 1991; Tisdall and Oades, 1982). This phenomenon is particularly evident in the case of rhizosheaths–a narrow volume of soil around roots where soil particles are strongly adhered to the root and one another (de León-González et al, 2006; Ma et al, 2011; Smith et al, 2011; Sprent, 1975; Watt et al, 1994).

There has been extensive research on association of polysaccharides with charged clay particles and oxides (Qi and Laskowskib, 2006; Parfitt, 1972; Jucker et al, 1997; Parfitt and Greenland, 1970; Greenland, 1965b; Clapp et al, 1962; Clapp and Emerson, 1972;

Olness and Clapp, 1975). These studies have shown that the primary mechanisms by which organic matter is strongly attached to the charged clay surface include (a) polyvalent cation bridging between the clay exchange sites and the polysaccharides (Qi and Laskowskib, 2006; Somasundaran, 1969; Weisseborn et al, 1995) as well as (b) direct hydrogen bonding of organic macromolecules with the clay minerals and oxides (Guidi et al, 1977; Jucker et al, 1997; Parfitt and Greenland, 1970). Thus, the degree of association between polysaccharides and charged surfaces can be related to the nature and concentration of cations present (Dontsova and Bigham, 2005; Parfitt, 1972), surface area and exchange capacity of the minerals (Chenu et al, 1987; Theng, 1982), as well as molecular weight, functional group composition, pH, and molecular configuration of the polysaccharides (Chenu et al, 1987; Guidi et al, 1977; Parfitt and Greenland, 1970; Parfitt, 1972; Clapp et al, 1962; Clapp and Emerson, 1972; Olness and Clapp, 1975). For example, higher degree of association of polysaccharides with montmorillonitic clays than kaolinitic clays has been attributed to the larger specific surface area of montmorillonite (Chenu et al, 1987; Theng, 1982).

In contrast, the mechanism of association of silt- and sand- size particles with organic matter (particularly, polysaccharides) has not been studied as extensively. There is ample empirical evidence for the formation of strong bonding of organic matter with sand particles. Particularly, the formation of rhizosheath is a striking evidence of strong adhesion of certain class of organic matter with coarse grained (mostly sandy) soil particles (Czarnes et al, 2000a; de León-González et al, 2006; Ma et al, 2011; Nambiar, 1976; Smith et al, 2011; Sprent, 1975; Watt et al, 1994). These associations appear to be similar to attachment of clay minerals on sand particles via hydrogen bonding between oxygen atoms of the silica molecules that make up the bulk of both sand and clay minerals (Sideri, 1936).

The overarching goal of this study was to provide a mechanistic explanation of the association of root and microbial exudates with sand and silt size particles. Particularly, this study was concerned with association of sand with Polygalacturonic Acid (PGA) and xanthan, which are analogs of the exudates of roots (Gessa and Deiana, 1990, 1992; Morel et al, 1987; Traore et al, 2000; Wright and Northcote, 1974) and bacteria (Chenu, 1993; Clapp and Emerson, 1972; Hart et al, 2001; Milas and Rinaudo, 1986), respectively. The specific objective of this study was to experimentally test a hypothesized conceptual model of association between quartz particles and long-chain polysaccharides.

3.1.1 Conceptual Model of Association

The following conceptual model of association between silica and polysaccharides was formulated to enable systematic description of the processes and factors that are responsible for aggregation of sand and silt sized soil particles. In the following description, the term "degree of association" is used to explain the mass of polysaccharide macromolecules that are strongly adhered to a unit mass of sand or silt media. The most common constituent of the sand fraction in soils is silica (silicon dioxide, SiO_2). The silica molecules are bonded to one another through covalent bonds (Fig. 3.1a), in which every silicon atom is surrounded by four covalently bonded oxygen atoms. In an aqueous environment, the outwardly projecting oxygen atoms are able to form hydrogen bonds with water molecules as shown in Fig. 3.1b (Qi and Laskowskib, 2006). The primary mechanism of association between polysaccharides and sand particles is hypothesized to be similar hydrogen bonding between hydroxyl branches of polysaccharides and silica surface (Fig. 3.1c). However, for this association to proceed the hydrogen-bond linkage between the hydroxyl and the carboxyl groups of the
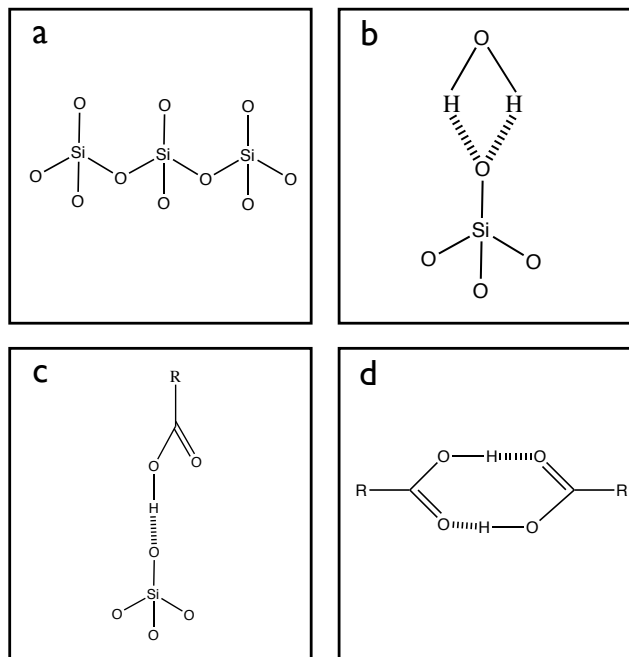
Figure 3.1: Conceptual model. (a) covalent bond formed between silica molecules, (b) hydrogen bond between sand and water, (c) hydrogen bond between the polysaccharides and sand and (d) hydrogen bond between polysaccharides

polysaccharides (Fig. 3.1d) as well as between water and silica must be broken.

Anionic polysaccharides carry a net negative charge due to the carboxyl group, where the density of the negative charge is known and shown experimentally and through models to be pH dependent. The point of zero charge (pzc) describes the pH at which a particular molecule or surface carries no net electrical charge. Below pzc the molecules carry a net positive charge and above pzc they carry a net negative charge. When the solution pH is not at the pzc, internal repulsion between like-charged branches of the macromolecules result in expansion of the macromolecules. Therefore, the degree of association between anionic polysaccharides and sand is expected to decrease with increasing deviation of the pH from pzc (first prediction).

Polysaccharides found in soils greatly vary in the molecular size and structure (Clapp et al, 1962; Greenland, 1965a; Guidi et al, 1977; Parfitt and Greenland, 1970; Qi and

Laskowskib, 2006) and it is expected that these differences play a role in the degree of their association with sand particles. One key difference between polysaccharides is the branching of the macromolecules. In branched polysaccharides, the anionic (carboxylic) ends are located very close to each other, inducing a high negative charge density and strong electrostatic repulsions. The resulting rigid conformation of such macromolecules is not favorable to attachment of the macromolecules to the surface of sand particles (Labille et al, 2005). Another key difference is the number of strands that make up the polysaccharide macromolecules. In general, triple helix conformation gives rise to a more compact macromolecular structure, thereby resulting in a higher degree of association than double helix or single stand macromolecules. Therefore, the second prediction of this conceptual model is that triple-helical and/or linear polysaccharides adhere to silica much more strongly than double-helical and/or branched polysaccharides.

In general, the degree of association must increase with increase molecular weight (molecular chain length) of the macromolecules. However, beyond a certain optimal chain length (Harris et al, 1966), an increase in the macromolecules size lowers the specific surface area of the macromolecules thereby decreasing the effectiveness of attachment to sand surfaces. Therefore, the third prediction of this conceptual model is that there is a positive correlation between the effective molecular weight of polysaccharides and degree of association. This correlation is reversed from positive to negative when the effective molecular weight (chain length) of the polysaccharides macromolecules exceeds a certain threshold.

In this study, we investigated the association between sand media of varying sizes and two types of polysaccharides (PGA and xanthan). These two polysaccharides were selected because they represent dominant constituents of root (Gessa and Deiana, 1990,

1992; Morel et al, 1987; Traore et al, 2000; Wright and Northcote, 1974) and bacterial (Chenu, 1993; Clapp and Emerson, 1972; Hart et al, 2001; Milas and Rinaudo, 1986) exudates, respectively. Moreover, because these polysaccharides differ in their density of hydroxyl and carboxyl functional groups, degree of branching, number of strands in their helical structures, and molecular weight they enable us to directly test the three major predictions of the above conceptual model.

3.2 Materials and methods

3.2.1 Reagents and Apparatus

All the chemicals used in this study were of analytical reagent grade. Potassium hydroxide (KOH) was obtained from Fischer Scientific. Concentrated sulfuric acid (H_2SO_4) was obtained from ACROS. Polygalacturonic Acid (PGA) and xanthan were obtained from MP Biomedicals. Samples were shaken and centrifuged by a Eberbach 6000 reciprocal shaker and Thermo Scientific Sorvall RC 6+ centrifuge, respectively. Absorption measurements were made using a Thermo Scientific Evolution 300 UV-Vis Spectrophotometer.

3.2.2 Sand

Quartz sand (Laguna Clay Company, Industry, California) was baked at 440°C for 16 hours to remove any preexisting organic matter and sieved to four different particle size ranges (Table 3.1) and stored in polyethylene containers for further use. Beckman Coulter LS 13 320 Laser Diffraction Particle Size Analyzer was used to determine the

Table 3.1: Sand analysis

ID	Mean (μm)	D50 (μm)	SSA^1 (m^2 g^{-1})	texture -	Clay %	Silt %	Sand %
S1	107.1	107.8	1.19	Sand	2.43	4.68	92.89
S2	210.3	204.0	0.70	Sand	1.48	2.11	96.41
S3	356.7	356.2	0.40	Sand	0.90	1.23	97.87
S4	609.4	597.1	0.24	Sand	0	0	100

[1] Specific Surface Area
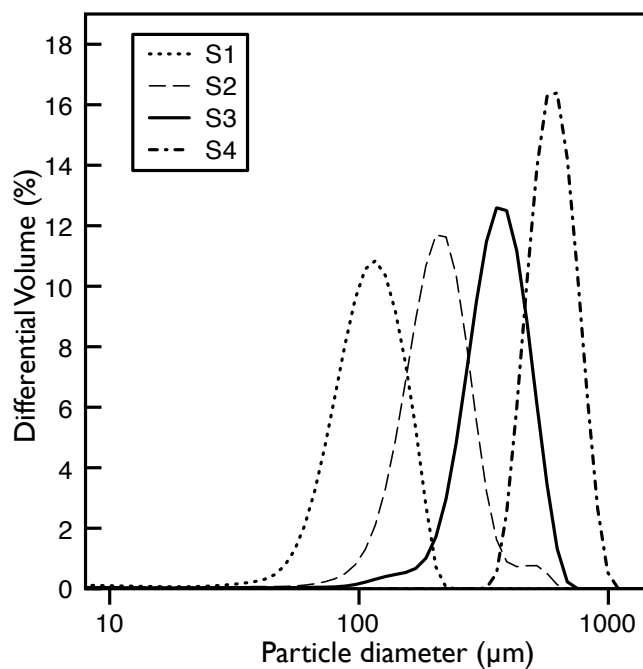
Figure 3.2: Particle size distribution of sand particles used in this experiment

particle size distribution reported in Fig. 3.2. Specific surface area (SSA) was measured using Beckman Coulter SA 3100 Gas Adsorption Surface Area Analyzer. The physical properties of the sands are provided in Table 3.1.

3.2.3 Polysaccharides

In this study we used two types of polysaccharides; PGA as a representative of plant root exudates and xanthan as a representative of bacterial exudates. Although both
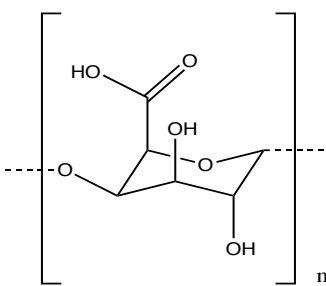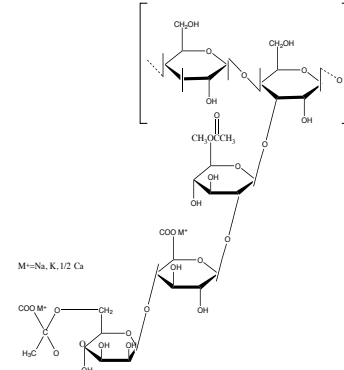
polysaccharides are anionic, they differ markedly in other properties, which allow us to test the predictions of the above conceptual model. The key differences between PGA and xanthan are summarized in Table 3.2. PGA has lower density of carboxyl and hydroxyl groups than xanthan, which allows us to test the first prediction. PGA has much lower molecular weight than xanthan, which allow us to test the second prediction. The basic unit of PGA molecule is unbranched linear arranged in triple-helical structure (see chemical structure). Whereas xanthan molecule is branched arranged in double-helical structure. The latter structural differences allow testing of the third prediction of the conceptual model.

Different concentrations of each polysaccharide were prepared by dissolving known mass of dry polysaccharide in 1 L of double millipore water (DDI). Because PGA is insoluble in water, it was made soluble by adjusting the pH to 12.4 using potassium hydroxide (KOH) (Albalasmeh et al, 2013).

3.2.4 Analytical Method

We used the Sulfuric Acid-UV method (Albalasmeh et al, 2013) to analyze the absorbance of the polysaccharide solutions used in this study. The procedure of the Sulfuric Acid-UV method is as follows. A 1 mL aliquot of polysaccharide solution is rapidly mixed with 3 mL of concentrated sulfuric acid in a test tube and vortexed for 30 seconds. The temperature of the mixture rises rapidly within 10-15 seconds after addition of sulfuric acid. Then, the solution was cooled in ice for 2 minutes to bring it to room temperature. Finally, UV light absorption at 315 nm is read using UV spectrophotometer. Reference solutions are prepared following the same procedure as above, except that the polysaccharide aliquot was replaced with DDI water.

Table 3.2: PGA and xanthan Polysaccharides Properties

	PGA	Xanthan
Primary Structure		
Molecular Weight (Da.)	$(26\text{-}70)\times 10^3$	$> 2\times 10^6$
Molecular Formula	$(C_6H_8O_6)_n$	$(C_{35}H_{49}O_{25})_n$
Carboxyl Group no.	1	3
Molecular Configuration (Conformation)	triple helix	double helix
Branching	linear	branched
Solubility in Water	insoluble	soluble
Viscosity[1]$(mPa.s)$	1.60^2	6.78^3
Turbidity[4](NTU)	1.62	63.35
Original Source	plant roots	Microbes

[1] for 2 g/L concentration
[2] Barre and Hallett (2009)
[3] Khouryieh et al (2007)
[4] for 0.5 g/L concentration

3.2.5   Sand-Polysaccharides Association

Association experiments were carried out by mixing known mass of sand with 15 mL volume of polysaccharide solutions of known concentration into 50 mL centrifuge tubes using a reciprocating shaker for specific time. Immediately after shaking, each sample was centrifuged at speed of 9900 rpm (with equivalent centrifugal force of 12000 g) for 20 minutes. The supernatant were analyzed for the concentration remaining in solution using a spectrophotometer. Control samples of polysaccharide solutions without sand were also treated and analyzed similarly.

The amount of associated polysaccharides with sand, q_e (mg g^{-1}) was calculated using the following equation:

$$q_e = \frac{(C_o - C_e)}{m} V \tag{3.1}$$

where C_o and C_e are the initial and equilibrium concentrations (mg/L) of polysaccharide in solution, V is the volume (L) of solution, and m is the mass of sand (g).

Preliminary experiments were carried out to determine the optimum agitation time and mass of sand that should be used in the main experiments of this study. The degree of association was compared for six different agitation periods of 0.5, 1, 2, 4, 8 and 24 hours. The maximum association for both polysaccharides was observed at 8 hours, with no further increase in the degree of association at 24 hours. Therefore the agitation time was set at 8 hours for the remainder of the study. The optimum mass of sand was also determined similarly by comparing five different masses of 2, 4, 6, 8 and 10 g. These pre-experiments showed maximum degree of association occurred

for the 10 g of sand that was used for the remainder of the study.

3.2.6 Effect of pH

Stock solutions of PGA and xanthan with 0.07 g/L concentration were prepared as described above. Then four different sub-volumes of the stock solutions were adjusted to pH levels of 4, 6, 8, and 11.5 (measured at $\approx 25°$ C) by addition of HCl or NaOH. The association of the PGA and xanthan with sand was then determined as described above by shaking 10 g of sand together with 15 ml pH adjusted solution for 8 hours.

3.2.7 Effect of Concentration

The dependence of polysaccharide-sand association on polysaccharide concentration was determined using the same procedure as in the effect of pH experiment. PGA and xanthan solutions of seven different concentrations (0.07, 0.15, 0.25, 0.35, 0.50, 0.75, and 1.00 g/L) were prepared as described above. Then the pH of the solutions were adjusted to 6 by addition of HCl or NaOH for PGA and xanthan solutions, respectively.

3.3 Results

3.3.1 Effects of pH

The effects of pH on the association densities of PGA and xanthan with different particle sizes of sand (S1-S4) are portrayed in Fig. 3.3, (distinct symbols are used

to differentiate between sand sizes). The data for PGA and xanthan are plotted in Fig. 3.3 a and b, respectively. pH values are plotted on the abscissae and the amount of polysaccharide associated with the sand media are plotted on the ordinates (mg/g). Each data point is an average of three replicates and the error bars indicate the standard error of the mean values.

The association of both polysaccharides, PGA (Fig. 3.3a) and xanthan (Fig. 3.3b) are pH-dependent in the entire range investigated, and the maximum association occurred at pH value of 6 for both polysaccharides. Within the range of pH investigated, it was observed that the degree of association decrease with increase in alkalinity. The pH dependence appears to be stronger in xanthan than PGA, while the overall degree of association was higher for PGA than xanthan (Fig. 3.3).

3.3.2   Effects of Concentration

The effect of the polysaccharide concentrations on the degree of sand-polysaccharide association is shown in Fig. 3.4. The four different sand media studied (S1-S4) are indicated using distinct symbols. The data for PGA and xanthan are plotted in Fig. 3.4 a and b, respectively. Polysaccharide solution concentration (0.07 - 1.00 g/L) is plotted on the abscissae and the amount of polysaccharide associated with the sand media (mg/g) are plotted on the ordinates. Each data point is a mean of three replicates and the error bars indicate the standard error of the means.

The results shown in Fig. 3.4 reveal three major differences between the behaviors of PGA and xanthan. First, PGA is associated with all the sand media at much higher rate than xanthan in the entire concentration range examined. Second, the sand size did not result in any discernible effect on the degree of association of PGA
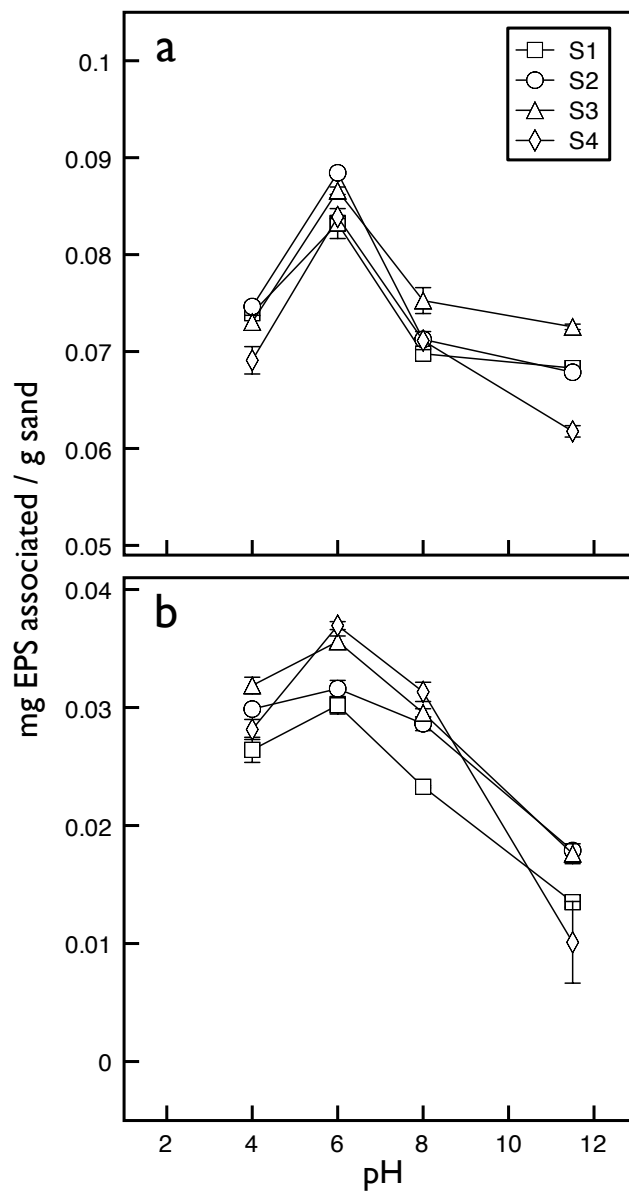
Figure 3.3: Effects of pH on polysaccharide-sand association. **a** PGA and **b** xanthan. Values are averages over three replicates of the treatments, with error bars representing standard error on y-axis
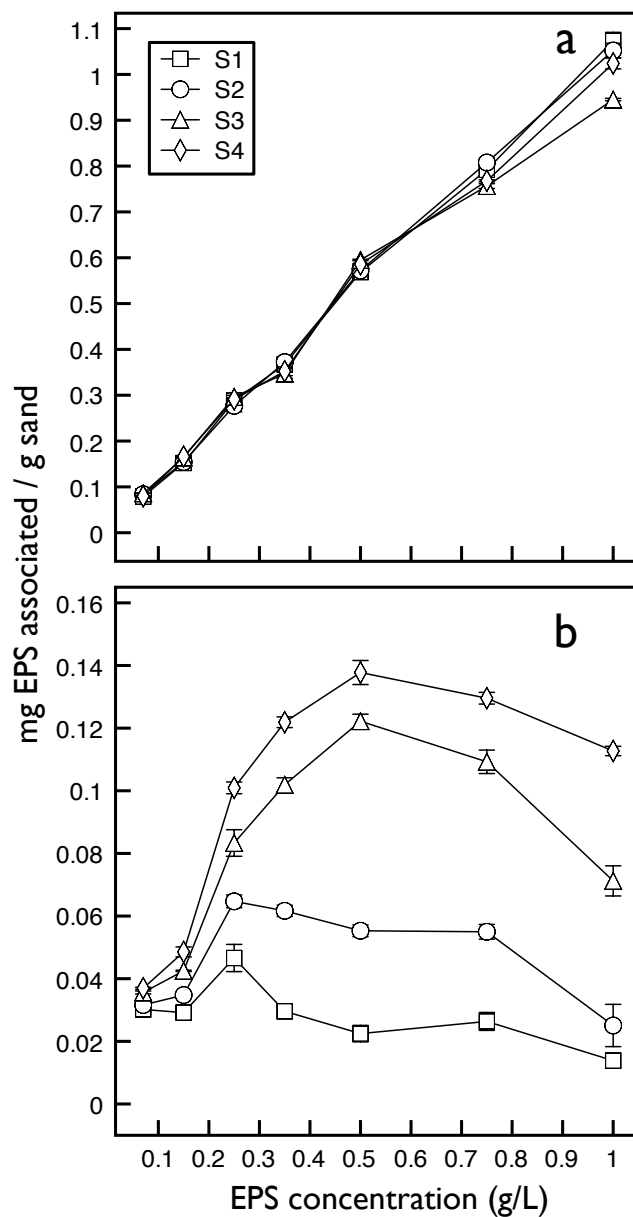
Figure 3.4: Effects of concentration on polysaccharide-sand association. **a** PGA and **b** xanthan. Values are averages over three replicates of the treatments, with error bars representing standard error on y-axis

with sand. In contrast, the degree of association of xanthan with sand increased with sand particle size. Finally, it was observed that, within the range of polysaccharide concentrations examined, the degree of association of PGA with sand increased with concentration nearly linearly. For xanthan, however, the degree if association with sand peaked in the mid-range concentrations and declined at higher concentrations.

To reveal dependence of the polysaccharide-mineral association on surface area of the sand media, the data from Fig. 3.4 was replotted in Fig 3.5 in terms of the ratio of associated polysaccharide mass to the specific surface area of the sand media (mg/m^2). These plots showed that the degree of association is inversely related to surface area for both polysaccharides in the entire range of concentrations examined.

3.4 Discussion

3.4.1 Effects of pH

The effect of pH on the association densities of PGA and xanthan with sand size particles is shown in Fig. 3.3. With the increase of the solution pH of PGA and xanthan above the pzc, the dissociation of the acid groups (R-COOH) is favored and the carboxyl group (COO^-) becomes negatively charged. Conversely, with decrease in pH below pzc, the acidic water donates more protons and the acid groups become positively charged ($COOH^+$). Therefore, deviation of the solution pH away from the pzc leads internal electrostatic repulsion between like charged groups. As a results, the macromolecules expand in size. Because xanthan has three times more carboxyl groups than PGA (Table 3.2), the charge density and internal expansion are higher in xanthan. The effect of this difference in charge density had two effects. First,
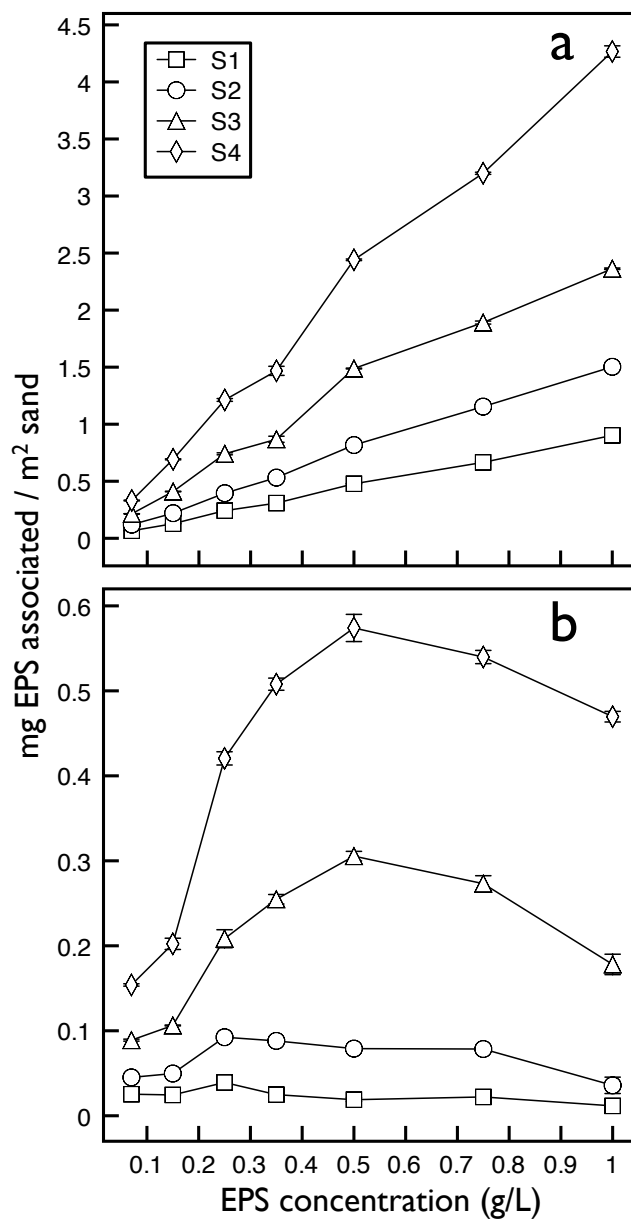
Figure 3.5: Effects of particle size on polysaccharide-sand association. **a** PGA and **b** xanthan. Values are averages over three replicates of the treatments, with error bars representing standard error on y-axis

with increasing pH the reduction in association was greater in xanthan than PGA. Second, the association degree with sand was much less in xanthan compared to PGA (Figure 3.3), which is in agreement with the first prediction of the conceptual model. These results are in agreement with Parfitt (1972) and Parfitt and Greenland (1970) who studied the adsorption of PGA on montmorillonite and Dontsova and Bigham (2005) who studied the adsorption of xanthan on montmorillonite. Even more, Parfitt (1972) report negative adsorption at higher pH because of coulombic forces between the negatively charged clay surface and xanthan.

3.4.2   Effects of Concentration

The results presented above show that anionic polysaccharides have the ability to adhere to neutral sand media, albeit to much less degree than with charged clays and oxides. Considering that silica surfaces have a high degree of affinity for molecular attraction via hydrogen bonding, we proposed that the similar mechanism is also responsible for the association of the polysaccharides. According to our conceptual model the amount of polysaccharides that is adsorbed by sand sized particles depends on the carboxyl groups content (Clapp et al, 1962), the molecular configuration (conformation) (Chenu et al, 1987) and molecular weight (Guidi et al, 1977).

In our study we observed that both polysaccharides, PGA and xanthan, were associated with sand of different particle size. However, the degree of association was much greater for PGA than for xanthan. Moreover, the degree of association for xanthan also increased with particle size. The differences in the association behavior between PGA and xanthan can be explained by the three predictions of the conceptual model.

First, xanthan has three times more carboxyl groups compared to PGA (Table 3.2).

Carboxyl groups are able to form hydrogen bonds with water and other carboxyl groups resulting in, for example, dimers that consist of structurally similar monomeric carboxylic acids. Therefore, with increasing carboxyl group content of organic molecules the formation of hydrogen bonds between them can lower the number of carboxyl groups available to interact with the surface of silicates. The higher carboxyl group content of xanthan should consequently lead to a lower degree of association compared to PGA , which is confirmed by our results (Fig. 3.4 and Fig. 3.5). This is also in agreement with Clapp et al (1962) who compared 16 anionic polysaccharides differing in their carboxyl content where lower carboxyl content led to more associations and hence higher aggregate stability. Moreover, the bridging ability of anionic polysaccharides was inversely related to the charge density.

Second, the triple helix of PGA gives rise to a greater degree of association with the surface of sand size particles than the double helix of xanthan does due to the more segments in the triple helix and the reduction of the macromolecules size. The latter increases the specific surface area of the molecules leading to a larger sand/solution interface and increased interactions per unit surface area . A similar observation was reported by Chenu et al (1987), who found that the triple helix of scleroglucan has more contact with clay than the single helix of dextran does. Additionally, the primary structure of the polysaccharides plays an important role for the association with silicate surfaces. Xanthan consist of a short disaccharide backbone repeat unit and trisaccharide side chains (Table 3.2), the anionic side chains are thus very close to each other inducing a high charge density, strong electrostatic repulsions, and thus a very rigid conformation, which is not favorable for bridging (Labille et al, 2005).

Third, we observed that with increasing EPS concentrations the degree of association for xanthan first increased and then decreased while for PGA the degree of association

continuously increased (Fig. 3.4 and Fig. 3.5). Hayahara and Takao (1968) found that there is an inverse relationship between the molecular weight of polymers and a critical concentration where no association can be observed anymore. Moreover, Harris et al (1966) reviewed related studies and reported that the addition of anionic polymers above certain concentrations led to enhanced dispersion of kaolinite particles held together by polymeric bridges also indicating reduced polymer-mineral interactions in dependence from type and concentration of the polymer. Because of the higher molecular weight of xanthan compared to PGA, xanthan should reach this tipping point at lower concentration than PGA, which is confirmed by our results (Fig. 3.4 and Fig. 3.5). Here, the critical concentration for xanthan was 0.5 g/l for the size classes S3 and S4 and 0.25 g/l for the size classes S1 and S2 (Fig. 3.4 and Fig. 3.5). This indicates that above the critical concentration at least for xanthan where no or reduced attached on silicate surfaces can be observed seems also to be influenced by the particle size.

3.5   Summary and conclusion

Two types of anionic polysaccharides, PGA and xanthan, were used in this study as a representation of plant root and microorganisms exudates, respectively. Because these polysaccharides have different characteristics (molecular weight, charge density and conformation), they enable us to directly test the predictions of our conceptual model. The experimental results presented in this study show that the degree of association of anionic polysaccharides with sand sized particles is pH dependent and increases with a decrease in the charge density and with an increase in the complexity of the molecular configuration of the polysaccharides. The mechanism of association involve hydrogen bond between sand and the polysaccharides.

In summary, it appears that the degree of attachment between the anionic polysac-charides and sand was found to be very strong. Note that the degree of association reported here reflects only the association that persisted after the vigorous shaking and centrifugation. Therefore, this study has conclusively demonstrated the fact that strong bonding of sand particles by polysaccharides is a plausible mechanism responsible for the formation of aggregates coarse soil particles (e.g. rhizosheath).

Chapter 4

Interplay Between Soil Drying and Root Exudation in Rhizosheath Development

Abstract

Wetting-drying cycles are important environmental processes known to enhance aggregation. However, very little attention has been given to drying as a process that transports mucilage to inter-particle contacts where it is deposited and serves as binding glue. The objective of this study was to formulate and test conceptual and mathematical models that describe the role of drying in soil aggregation through transportation and deposition of binding agents. We used an ESEM to visualize aggregate formation of pair of glass beads. To test our model, we subjected three different sizes of sand to multiple wetting-drying cycles of PGA solution as a root

exudates to form artificial aggregates. Water stable aggregate was determines using wet sieving apparatus. A model to predict aggregate stability in presence of organic matter was developed, where aggregate stability depends on soil texture as well as the strength, density and mass fraction of organic matter, which was confirmed experimentally. The ESEM images emphasize the role of wetting-drying cycles on soil aggregate formation. Our experimental results confirmed the mathematical model predictions as well as the ESEM images on the role of drying in soil aggregation as an agent for transport and deposition of binding agents.

4.1 Introduction

Roots of several plants form a coating of soil particles—commonly referred to as *rhizosheath*—that are strongly attached to one another as well as to the roots. Rhizosheath is believed to play important role in nutrient and water uptake and in mitigation of environmental stresses (Czarnes et al, 2000a; de León-González et al, 2006; Ma et al, 2011; Nambiar, 1976; Smith et al, 2011; Sprent, 1975; Watt et al, 1994). The radial extent of the rhizosheath is roughly the same as the length of root hairs (Ma et al, 2011; Watt et al, 1994). Because of this size similarity, formation of rhizosheath is attributed by some authors to the binding action of root hairs (Buckley, 1982; Ma et al, 2011; McCully, 1999a; Smith et al, 2011). However, Sprent (1975) studied the contact between roots and soil particles under high-magnification Scanning Electron Microscopy (SEM) and observed that the epidermal cells in the region were striated, which suggests the presence of mucilage (Old and Nicolson, 1975). Furthermore, Sprent (1975) noted that the root-hairs in the rhizosheath were far too short and did not enmesh the soil particles, indicating that the attachment of soil particles to roots is primarily a result of the gluing action of root mucilage (but not the engulfing effect

by root hairs).

Several studies have been carried out since then to investigate the effects of moisture regimes and sorption of mucilage on the formation of rhizosheaths (Czarnes et al, 2000a; Reid and Goss, 1981, 1982; Watt et al, 1993, 1994). Watt et al (1994) observed that rhizosheaths of maize and other mesophytic grasses are "thicker and held to the root with greater tenacity when formed in the drier soils of midsummer, and they are less substantial and more easily removed from roots growing in the wetter soils of early spring". A similar observation was made earlier by Nambiar (1976) in a laboratory experiment that exposed a small portion of the root length to <-1.5 MPa matric potential, while the whole plant remained under satiated moisture regime. These experiments revealed that sharply demarcated rhizosheath was formed only in the region that was exposed to dryness. The degree of adherence of soil particles and aggregates to roots has been investigated by subjecting the rhizosheath to external forces (e.g., shaking and ultrasonication) (Czarnes et al, 2000a; Sprent, 1975). These studies have shown that removal soil aggregates typically occurs by tensile rupture of the aggregates that are adhered to root surfaces (Czarnes et al, 2000a). These observations indicate that mucilage forms strong bonding between roots and soil particles.

A somewhat paradoxical feature of rhizosheaths is that they are generally wetter than the bulk soil although they are fully formed and attain maximal tenacity when the soil is exposed to drier conditions (Watt et al, 1994). It appears, therefore, that plants create rhizosheath by expenditure of hard-earned photosynthate (mucilage) as an adaptation mechanism. The increased moisture level is generally attributed to the hygroscopic nature of mucilage and this feature has been shown to play a major role in mobilization and uptake of nutrients (Ma et al, 2011; Nambiar, 1976; Smith et al,

2011)

It is evident from the foregoing discussions that soil aggregation in the rhizosheath is a product of an intricate interplay between the release of mucilage by plant roots and the moisture regime of the rhizosphere. Specifically, soil drying has been shown to be an essential requirement for rhizosheath development. The role of drying as a trigger for the release of mucilage in larger quantity to cope with environmental stresses is widely recognized mechanism (Hale et al, 1971). However, very little attention has been given to drying as a *process* that transports mucilage to micro-sites where it is deposited and serves as binding glue. The objective of this study was to formulate and test conceptual and mathematical models that describe the role of drying in soil aggregation as an agent for transport and deposition of binding agents. Although this study was motivated by the starkly discernible structure of the rhizosheath soil, the proposed mechanisms are postulated to be widely applicable to soil structure development in the bulk soil as well. In the remainder of this paper, we will present theoretical development of the proposed conceptual/mathematical models as well as testing of the models using experimental observations.

4.2   Theory

4.2.1   Geometric Model

Coarse grained soil is conceptualized as a pack of monodisperse spherical particles of radius R [m] and solid density of ρ_s [$kg\ m^{-3}$]. The bulk density of the pack is ρ_b
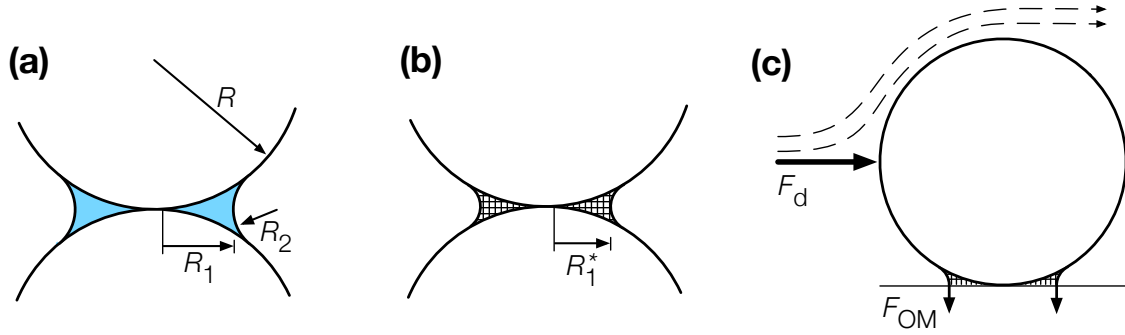
Figure 4.1: Conceptual description of the hypothesized mechanism of soil aggregation: (a) geometric definitions of capillary water; (b) schematic representation of deposited organic matter fabric; and (c) definitions of destabilizing drag force due to flowing water and adhesive force due to organic matter.

$[kg \ m^{-3}]$ so that the porosity is

$$\phi = 1 - \frac{\rho_b}{\rho_s} \qquad (4.1)$$

The remainder of this mathematical treatment is focuses on a single pair of particles, which is schematically represented in Fig. 4.1. The capillary pressure of water meniscus held between any pair of grains is defined by a pair of radii; R_1 [m] (concave towards the liquid) and R_2 [m] (concave towards the gas). The capillary pressure of the liquid is given by Young-Laplace equation as

$$\Psi = \gamma_w \left(\frac{1}{R_1} - \frac{1}{R_2} \right) \qquad (4.2)$$

where Ψ [Pa] is the capillary pressure and γ [N/m] is the surface tension of the liquid-gas interface. At this point, we define dimensionless quantities to facilitate the

mathematical treatment of the problem. Unless noted otherwise, lower-case Latin and Greek letter variables denote dimensionless versions of the corresponding upper-case dimensioned variables. Length dimensions are scaled by the radius of the particle as

$$\frac{r_1}{R_1} = \frac{r_2}{R_2} = \frac{1}{R} \tag{4.3}$$

Similarly, the the capillary pressure is non-dimensionalized as

$$\frac{\psi}{\Psi} = \frac{R}{\gamma} \tag{4.4}$$

Then, the dimensionless form of the Young-Laplace equation may be written as

$$\psi = \frac{1}{r_1} - \frac{1}{r_2} \tag{4.5}$$

The volume of liquid (v_L) for any combination of r_1 and r_2 can be determined using the method of volume of revolution (Ghezzehei and Or, 2000). The details of this approach is provided in appendix B. The ratio of the liquid volume [m^3] to solid volume [m^3] (note that each meniscus is associated with the equivalent of one sphere)

can be approximated by

$$\frac{v_L}{v_S} = \theta \frac{\rho_s}{\rho_b} = \left(1 + (c\psi)^d\right)^{-1} \tag{4.6}$$

where $c = 7/5$ and $d = 5/4$ are parameters obtained by fitting to the exact solution of the volume of revolution calculations. This compact representation accurately represents the exact mathematical formula with high degree of fidelity (coefficient of determination R^2=0.999). Similarly, the width of the capillary meniscus (r_1) can be expressed as a function of the capillary pressure

$$r_1 = \frac{2}{3} \left(1 + (a\psi)^b\right)^{-1/2} \tag{4.7}$$

where $a = 3/8$ and $b = 9/10$.

Concentration Dynamics

One basic premise of this conceptual model is that roots exude complex sugars in a aqueous solution (suspension). The exact concentration likely depends on the plant type, root age, and physiological stress level. Our starting state is known initial exudate mass released in to a finite initial volume of pore fluid, such that the initial concentration and volumetric water content are $[C]_\circ$ $[kg\ m^{-3}]$ and $\theta_\circ$, respectively. As the soil moisture evolves by wetting or drying, without any change to the mass of

exudates in the system, the concentration evolves with it as given by

$$[C] = [C]_\circ \frac{\theta_\circ}{\theta} \tag{4.8}$$

In particular, the concentration of the exudates increases with degree of dryness. As the concentration increases, the interaction among sugar neighboring molecules increases and we postulate that the organic matter begins to form gel (Fig. 4.1c). This gelling is hypothesized here as the root cause for the soil aggregation. This is supported by experimental observations that will be presented later. In addition, Al-balasmeh and Ghezzehei (2013a) have shown that organic matter is strongly attached to granular particles. In Fig. 4.2, the relationship between the water content (θ) and dimensionless concentration ($[C]/[C]^*$) is shown for two different levels of initial concentration ($[C]_\circ/[C]^*$). It is assumed that a permanent bond begins to form when the gel is formed. The strength of the bond formed between two particles is considered to be proportional to the size of the meniscus at the critical concentration when gel is formed $[C] = [C]^*$. The organic matter content of the unit system (mass ratio), after all the dissolved/suspended organic matter has been deposited is given by

$$X_{OM} = \frac{[C]_\circ \, \theta_\circ}{\rho_b} \tag{4.9}$$

The capillary pressure at this critical stage $\psi = \psi^*$ is obtained by substituting Eq.
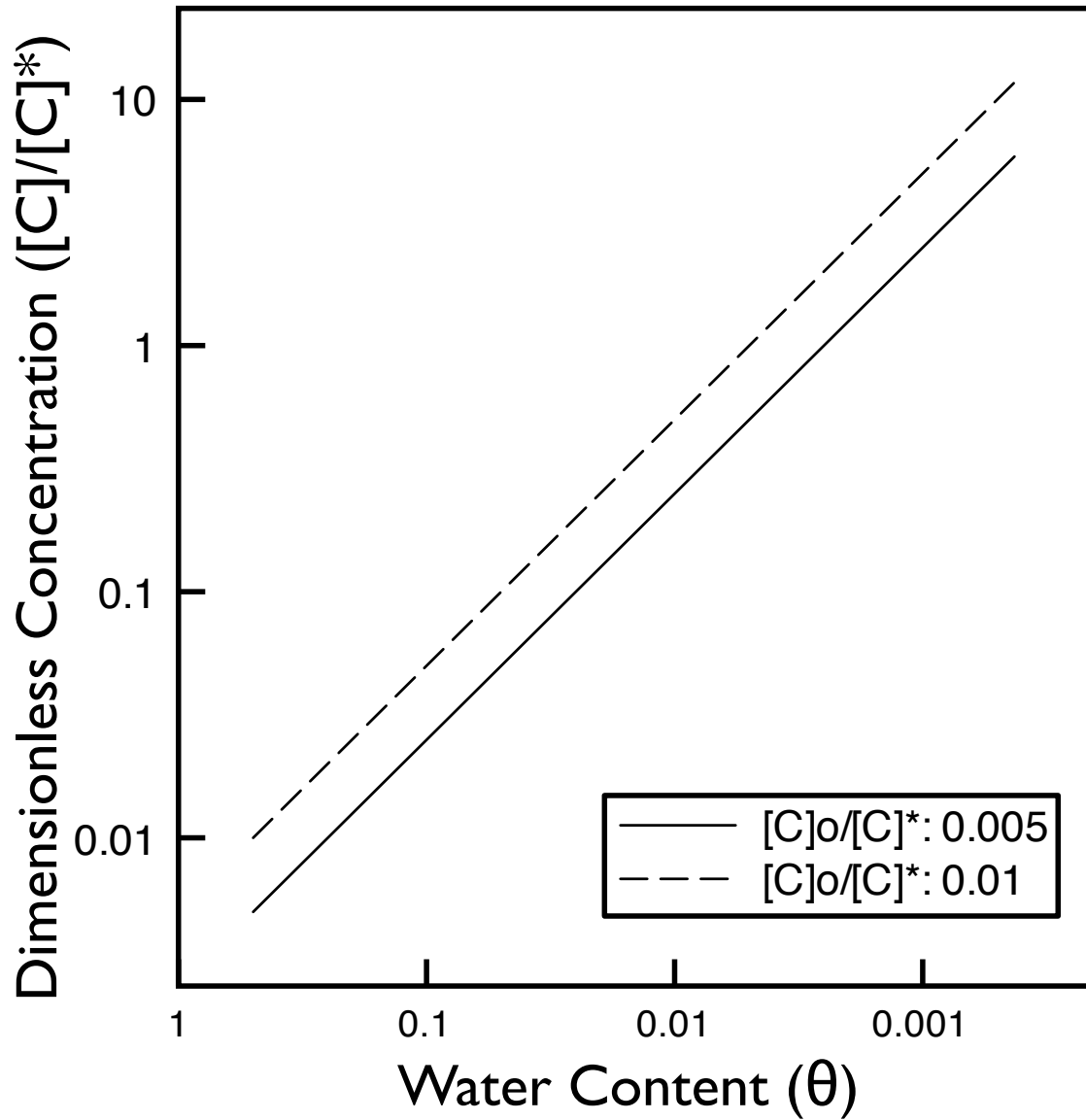
Figure 4.2: Evolution of the dimensionless concentration as a function of water content for two dimensionless initial concentrations, 0.005 $kg\ m^{-3}$ (solid line) and 0.01 $kg\ m^{-3}$ (dashed line)

(4.8) in Eq. (4.6)

$$\psi^* = \frac{1}{c}\left(\frac{\rho_b[C]^*}{\rho_s[C]_\circ\theta_\circ} - 1\right)^{1/d} \tag{4.10}$$

Finally, the relative strength of the inter-particle bond (Fig. 4.1b) is obtained by substituting Eq. (4.10) in Eq. (4.7)

$$r_1^* = \frac{2}{3}\left\{1 + \left(\frac{a}{c}\right)^b \left(\frac{\rho_b[C]^*}{\rho_s\theta_\circ[C]_\circ} - 1\right)^{b/d}\right\}^{-1/2} \tag{4.11}$$

Note that the critical concentration $[C]^*$ is considered here to be that concentration beyond which drying by evaporation and or plant uptake cease causes minimal shrinkage of the organic matter deposit. Therefore, this concentration also represents the dry density of the deposited organic matter fabric; i.e., $[C]^* = \rho_{OM}$. Then, Eq. (4.11) can be further simplified by using Eq. (4.9)

$$r_1^* = \frac{2}{3}\left\{1 + \left(\frac{a}{c}\right)^b \left(\frac{\rho_{OM}/\rho_s}{X_{OM}} - 1\right)^{b/d}\right\}^{-1/2} \tag{4.12}$$

4.2.2   Micromechanics

The force that keeps the particles bonded together is related to the tensile strength of the deposited organic matter as well as the adhesion of the organic matter on the soil

particles. The strength of soil aggregates is usually characterized by stability against external disruptive stresses. A commonly used method in soil physics research is water stable aggregation, which refers to the fraction of soil aggregates that remain intact after they are subjected to the action of flowing water in a wet-sieving apparatus. For the unit model we have at hand, the disruptive force resulting from the action of fluid passing past the pair of spheres can be represented in terms of drag force (Fig. 4.1c). Here we consider the plane of contact separating the two particles as the reference plane. The drag force acting on one of the spheres as a result of flow of water (Phares et al, 2000) is

$$F_d = \frac{\pi}{2}\rho_w v^2 C_D R^2 \tag{4.13}$$

where F_d [N] is the drag force, v $[m\ s^{-1}]$ is the fluid velocity past the center of the sphere, C_D is drag coefficient, and ρ_w $[kg\ m^{-3}]$ is the density of water. The moment of the drag force acting on the plane of contact between the two particles is then

$$I_d = \frac{\pi}{2}\rho_w v^2 C_D R^3 \tag{4.14}$$

where I_d [N.m] is the moment of the drag force.

The combined force of adhesion is assumed to be independent of the size of the bond and/or the sphere diameter. SEM images indicates that most of the deposited organic matter forms an outer shell of dense organic matter. Hence, the strength of the deposit is proportional to the perimeter of the deposit and the surface tension of

the ring

$$F_{OM} = 2\pi\gamma_{OM}r_1^*R \tag{4.15}$$

The strength of the contact bond that opposes the drag force is given by the moment of inertia (Wang, 1990)

$$I_{OM} = 2\pi\gamma_{OM}(r_1^*R)^2 \tag{4.16}$$

Then, the largest radius of particle pair $(R = R_{max})$ that will remain intact under given drag forcing (F_d) is obtained by equating equations (4.14) and (4.16) and solving for R

$$R_{max} = \frac{4\gamma OM}{\rho_w v^2 C_D}\frac{4}{9}\left\{1 + \left(\frac{a}{c}\right)^b \left(\frac{\rho_{OM}/\rho_s}{X_{OM}} - 1\right)^{b/d}\right\}^{-1} \tag{4.17}$$

In the above equation, γOM and ρ_{om} ($\rho_{om} = [C]^*$) represent the properties of the organic matter and ρ_w, v^2 and C_D represents the external disruptive environment used for testing stability of the aggregate bonding. Such experiments are rather difficult to be conducted using a single pair of particles. In the following, we will present an approximate method for upscaling the model to pack of particles.

Upscaling

Consider a pack of sand that is characterized by normal particle size distribution

$$F_R = \frac{1}{2}\left\{1 + \text{erf}\left(\frac{2R - \mu}{\sqrt{2}\sigma}\right)\right\} \tag{4.18}$$

where μ [m] and σ [m] are the mean and standard deviation of the particle diameter $(2R)$, respectively, and F_R is the cumulative mass fraction. In such a system, the pairing of soil particles is likely to involve particles of different sizes. For mathematical expediency, we will assume that strength of the bonds is determined by the largest of the pair. Thus, the fraction of the soil particles that will remain aggregated ($R \leq R_{\text{max}}$) can be calculated by substituting Eq. (4.17) in Eq. (4.18),

$$AS = \frac{1}{2}\left\{1 + \text{erf}\left(\frac{2R_{max} - \mu}{\sqrt{2}\sigma}\right)\right\} \tag{4.19}$$

When a standardized method is used to characterize aggregate stability, Eq. (4.19) defines aggregate stability in terms of soil texture (μ and σ) as well as the strength, density and mass fraction of organic matter (σ_{OM}, ρ_{OM}, and X_{OM} respectively).
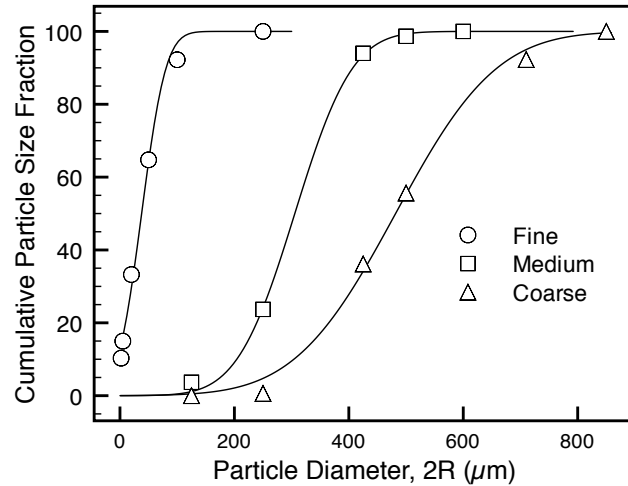
Figure 4.3: Particle size distribution of three media used in experimental testing of the hypothesized mechanism of soil aggregation.

4.3 Materials and Methods

4.3.1 Sand and EPS preparation

In order to test the hypothesized mechanism of soil aggregation, different sand sizes and polysaccharides concentration were used. Quartz sand (Laguna Clay Company, Industry, California) was baked at 440 °C for 16 hours to remove any pre-exist organic matter and sieved to three different particle sizes and stored in polyethylene containers for further use. Beckman Coulter LS 13 320 Laser Diffraction Particle Size Analyzer were used to determine the particle size distribution (Fig. 4.3).

Different concentrations of Polygalacturonic Acid (PGA) solution were prepared by dissolving known mass of dry PGA in double millipore water (DDI). Because PGA is insoluble in water, it was made soluble by adjusting the pH of the solution to 12.4 using potassium hydroxide (KOH) (Albalasmeh et al, 2013).

4.3.2   Environmental scanning electron microscopy (ESEM)

Fully hydrated, chemically unaltered samples were examined using a FEI XL30 environmental scanning electron microscope equipped with a field emission electron gun, a gaseous secondary electron detector (GSED) and a Peltier stage for controlling temperature. A few glass beads particles mounted directly on a Peltier cooling stage without further preparative treatment then a 75 μL of 0.1 g/L of PGA was added. The samples were kept under chamber pressure of 650 Pa water vapor during imaging.

4.3.3   Aggregate stability test

Water stable aggregate was determined using wet sieving method of Kemper and Rosenau (1986) . This test measures the resistance of aggregates against destructive force of flowing water. A fraction of the sand (M_1) were carefully transferred from the Büchner cups to a 4-cm diameter sieve with 250 μm mesh size. Then the sand was slowly pre-wetted by capillary rise from wet paper towel placed underneath the mesh, in order to minimize slaking. Then the sieves were submerged in tarred cans filled with water and shaken using a wet sieving apparatus (Eijkelkap Agrisearch Equipment, The Netherlands) at a regular up-and-down motion with a vertical distance of 1.3 cm and a rate of 35 cycles per minute for three minutes. The mass of sand collected in the can (M_2) was then determined after evaporating the supernatant water in oven. Then the percentage of the water stable aggregates (S) was calculated as

$$S = 100 \times \frac{M_1 - M_2}{M_1} \tag{4.20}$$

4.4 Results

4.4.1 Visualization of aggregate formation

Fig 4.4 shows scanning electron microscope images of aggregates formed by adding PGA and xanthan as representation of root and bacterial exudates, respectively. Fig. 4.5 shows some snapshots of the environmental scanning electron microscope (ESEM) images. ESEM enables moist materials to be viewed without a pre-treatment by controlling temperature and water vapor pressure and can be used to perform wetting/drying cycles without removing the sample from the ESEM chamber. The snapshots in Fig. 4.5 represent dynamic conditions of water content at multiple wetting and drying cycles where they show the changing in menisci shape as a function of water content change and transferring the dissolved/suspended organic matter toward the inter-particle contacts as the water content changing. This resembles the real field conditions where the water content continuously change as a function of fluctuations in the environmental conditions (e.g. humidity and temperature). Note that the shape of menisci at the drying stage is primarily controlled by the nature of the materials involved and this could explain the irregular menisci in Fig. 4.5 g and h.

4.4.2 Bond Growth and Aggregate stability

In Fig. 4.6 the dimensionless radius of the deposited organic matter bond (r_1^*) is plotted as a function of organic matter percent at different levels of relative organic matter density (ρ_{OM}/ρ_s). With increase percent of organic matter there is an increase in the corresponding dimensionless radius deposited width (r_1^*). However, with increase the
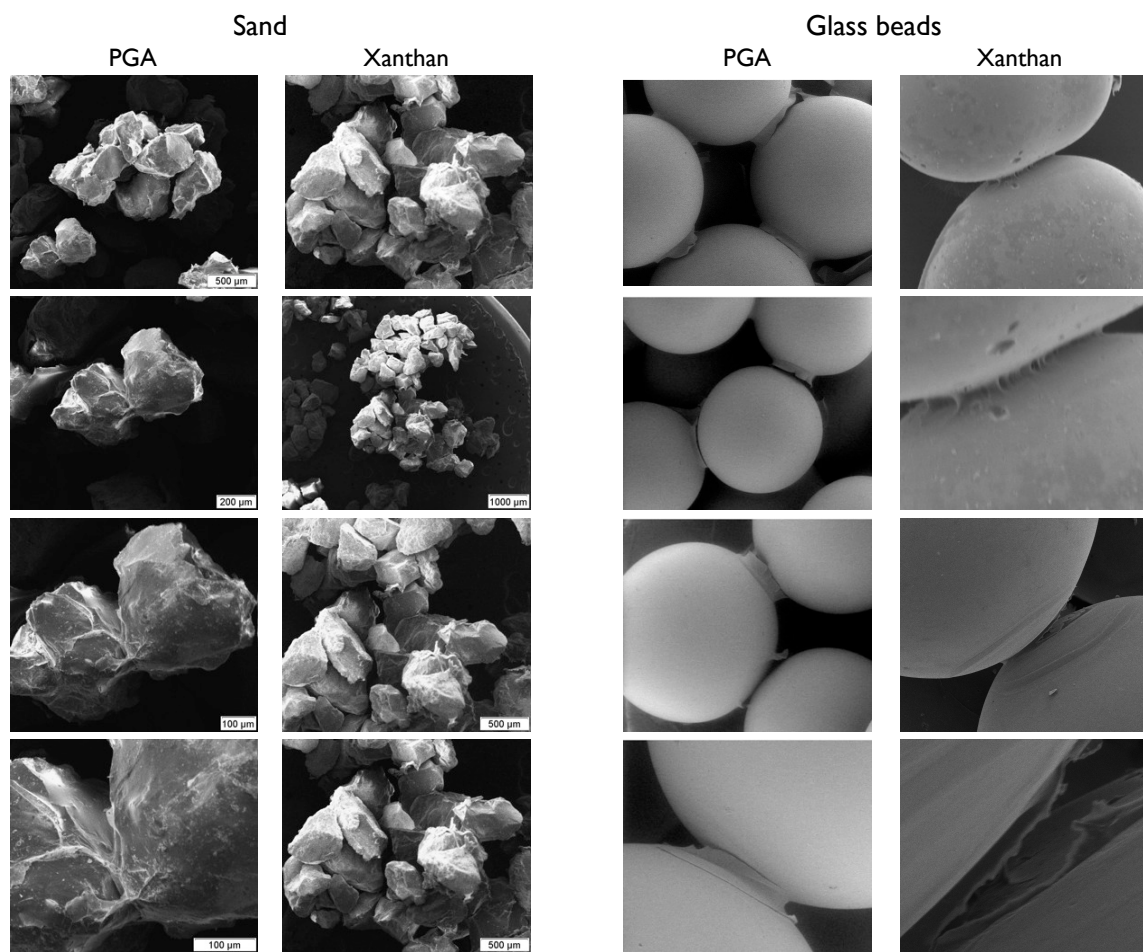
Figure 4.4: Visualization of formation of bond between sand particles (left) as well as glass beads (right) under Scanning Electron Microscopy
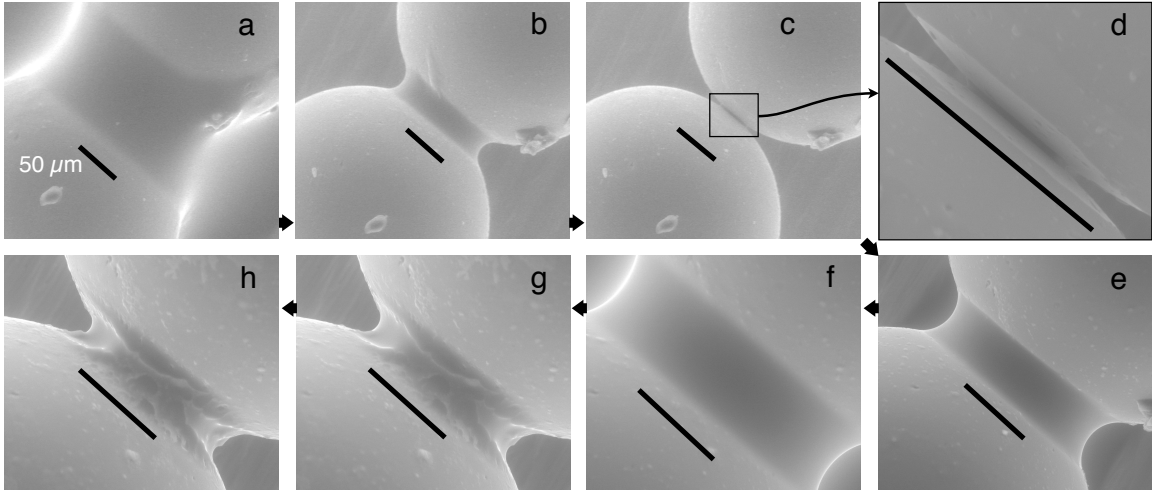
Figure 4.5: Visualization of formation of bond between two 300 μm glass beads under Environmental Scanning Electron Microscopy: (a)-(c) drying of glass beads bathed in PGA solution of 0.1 g/L; (d) close-up of deposited organic matter; (e)-(f) rewetting of glass beads by vapor deposition (pure water); (g) drying of re-wetted organic matter that forming a fabric that binds the particles together. Thick black in all images represent 50 μm

organic matter density (ρ_{OM}), which is equivalent to the critical concentration $[C]^*$ there is a decrease in the dimensionless radius of the deposited organic matter width (r_1^*). Note that the relative size of the bond is independent of the particle size and depends only on the relative organic matter percent and the density of the organic matter when it forms a bonding gel ($[C]^*$).

To test the hypothesized mechanism of soil aggregation, different sand sizes (Fig. 4.3) and polysaccharide concentrations were used. Water stable aggregate percentage as a function of organic matter percentage for the three different sizes of sand are depicted in Fig. 4.7. The results clearly show the effect of particle size (equation 4.18) and organic matter content (equation 4.17) on the water stable aggregate where the fine particles (Fig. 4.7a) showed higher water stable aggregate compared to coarse particles (Fig. 4.7c). At the same time, with increase the percent of organic matter, the corresponding water stable aggregate percentage increase for all particle sizes.
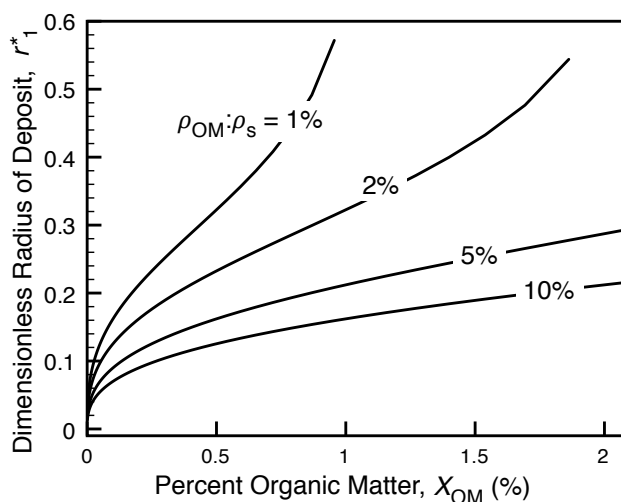
Figure 4.6: Relationship between dimensionless deposit width (r_1^*) and percent organic matter deposited in the contact region ($100 \times X_{OM}$) for four different levels of relative organic matter density (ρ_{OM}/ρ_s).
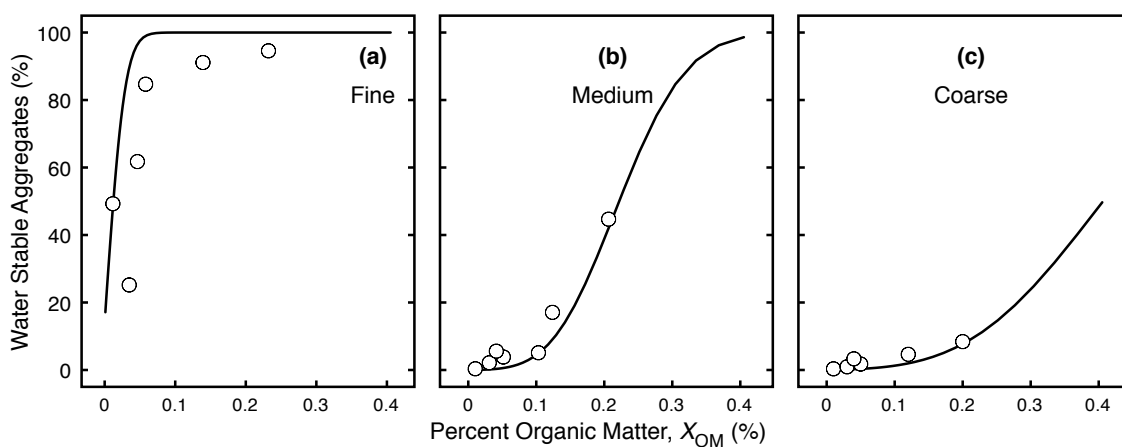
Figure 4.7: Relationship between water stable aggregates percentage and percent of organic matter for different particle sizes; (a) fine; (b) medium and (c) coarse sand. Open symbols represents the measured water stable aggregates percentage and the solid lines represents the water stable aggregates percentage from the model (equation 4.19)

4.5 Discussions

4.5.1 Visualization of aggregate formation

There is a lot of confusion as to how much, when, and where root exudates are released. McCully and co-workers have shown repeatedly the secretion of copious amounts of mucilage in root tips in very wet conditions (Guinel and McCully, 1986; McCully, 1999b; Sealey et al, 1995). But the volume may only be a reflection of the highly hygroscopic nature of these substances. The actual mass of organic matter released is not necessarily reflected in the visible volume of mucilage. The papers reviewed above suggest and show experimentally that the action of rhizodeposits (primarily formation of rhizosheath) is accentuated in dry regions and/or dry times around the roots. There is ample genetic and evolutionary research that shows these traits are associated with stress management and are more pronounced in xeric environments.

Sideri (1936) investigated the effect of drying on the irreversibility of the bond between clay and sand grains. He found that the adsorption of clay on sand grains is strongly dependent on drying. Similarly, Reid and Goss (1982) showed that drying increases the stabilizing efficacy of polysaccharide materials released in the root-zone of maize by increasing the adsorption of polysaccharides onto mineral surfaces. Increased polysaccharide concentrations could result from a greater release of organic materials from the roots and microorganisms subjected to drought (Roberson and Firestone, 1992); stimulation of soil microbial activities on rewetting; or removal of water from around dissolved or colloidal polysaccharides, particularly those in pores drained during the drying treatments. Wetting-drying cycles also promote soil aggregation by transporting large quantities of colloidal materials along the drying gradient. Park

et al (2007) showed that transport of dissolved organic matter towards the center of aggregates subjected to multiple wetting-drying cycles resulted in significant stabilization. In general, availability of dissolved and suspended cementing agents as well as wetting-drying cycles are complementary factors in promoting soil aggregation.

Fig. 4.5 suggests that fresh mucilage is weak in water holding capacity (Guinel and McCully, 1986). However, mucilage exposed to desiccation tends to have strong water holding capacity. This is shown in our ESEM experiments. Under drying conditions, polysaccharides respond by shrinking and adjusting their morphology (Sutherland, 2001), which is in agreement with our results in Fig. 4.5 g and h. Mechanistic explanation for how such fibrous structures are formed and made stable can be derived from SEM work of Gessa and Deiana (1990, 1992). Note that the difference between Fig. 4.5 c and d, which represents the end of the first wetting/drying cycle and Fig. 4.5 h, which represents the end of the second wetting/drying cycle. This difference reveals two important observations, the first is the strength of the bond that is formed between the two particles and the capability of these deposited materials on water holding capacity at such high degree of dryness.

4.5.2   Bond Growth and Aggregate stability

Soil organic matter role in soil aggregation and stabilization of most soils is well established (Tisdall and Oades, 1982). Increasing the concentration of organic matter leads to an increase in the number of contacts between the particles (Albalasmeh and Ghezzehei, 2013a), therefore increase the width of the deposited materials (equation 4.17), which is accompanied by strengthening of the fibrous structural bonds and thus increase the percentage of water stable aggregates (equation 4.19). In agreement with these results, Chenu and Guerif (1991) showed that the increase in tensile

strength is proportional to increase in the organic matter content as a result of increase the percentage of the contact points involving organic matter. Note that, Abiven et al (2009) in his review showed that to achieve such high water stable aggregate percentage it need much more organic matter than what is predicted by the proposed model (equation 4.17 and equation 4.19). This paradox in the percent of organic matter required to achieve the high water stable aggregates is due to the fact that not all organic matter compositions involve in the aggregation process. Although, polysaccharides represent a small fraction (5-20 %) of the total organic matter (Olness and Clapp, 1975), several studies (Abiven et al, 2007; Alagoez and Yilmaz, 2009; Czarnes et al, 2000a; Morel et al, 1991; Tisdall and Oades, 1982) showed their effectiveness in enhance soil aggregation. Note that, the polysaccharide concentration depends on the plant type, root age, and physiological stress level.

4.6   Summary and Conclusion

We developed a mathematical model to predict water stable aggregate percentage of different soil texture in presence of organic matter as cementing agent. The model showed that the water stable aggregate percentage depend on soil texture as well as the the strength, density and mass fraction of organic matter. The experimental results presented in this study provide evidences that support our mathematical model. The water stable aggregates of the experimental results was dependent on soil texture as well as organic matter concentration. The ESEM images emphasize the role of drying in soil aggregation as an agent for transport and deposition of binding agents.

Chapter 5

Rhizosphere Water Dynamics: Role of Root Exudates in Mediating Water Retention

Abstract

Plant roots alter soil properties at an expensive physiological cost, the role of their exudates on soil structure has been well documented. However, the effect of the hygroscopic nature of exudates on soil-water relations has not received much attention. Therefore, the overarching goal was to investigate the osmotic effect of exudates in isolation from changes in soil structure. We measured the water retention curves of porous media saturated by different concentration of Polygalacturonic Acid (PGA) as a representation of exudates of plant root as well as the water potential of pure PGA solutions at different concentrations using a WP4C Dewpoint Potentiameter. A

model of total water potential was developed based on combining the matric potential model of pure porous media and osmotic potential model of pure PGA solution at different concentrations where the total water potential was a function of PGA concentration. The experimental results of this study confirmed that plant root exudates are able to retain a considerable volume of water in soils at low water potential using less than 1% of PGA. Our results indicate that osmotic potential induced by PGA concentrations play a significant role in total water potential and water content.

5.1   Introduction

Roots develop in an environment, the soil, where it is hard to move and where resources, such as water, nutrients and air, are frequently scarce and patchy, so that roots have evolved to adapt and to influence their environment (Hinsinger et al, 2009). For this reason, plant roots and soil microorganisms alter soil properties (Walker et al, 2003), at an expensive physiological cost. Plants invest large portion of their photosynthetic carbon in developing highly specialized soils around individual roots, commonly referred to as *rhizosphere* (Sprent, 1975; Nambiar, 1976; Watt et al, 1994; Czarnes et al, 2000a; de León-González et al, 2006; Ma et al, 2011; Smith et al, 2011), which allows them to optimally exploit water and nutrient distributions in the soil (Morgan et al, 2005; Gao et al, 2011; Marschner, 2012).

One mechanism of rhizosphere alteration is through the release of exudates by plant roots. The amount of exudates produced by plant roots vary with the plant species, age, and environmental conditions. Gao et al (2011) has shown that the amount of root exudates decrease with distance from the root surface within the rhizosphere soil. The estimation of the quantity of carbon (C) released in soil via root exudates

vary depending on the method of collection, ranging from 50 to 2000 μg C/g soil/day (Meharg and Killham, 1991; Jones and Darrah, 1993; Cheng, 1996; de Graaff et al, 2010; Gao et al, 2011). There is also ample empirical evidence that shows that roots release higher quantities of exudates in response to water and/or nutrient stress (Roberson and Firestone, 1992; Watt et al, 1994; Sharp et al, 2004; Song et al, 2012). For example, Reid and Mexal (1977) showed that roots subjected to a lower water potential exuded more exudates than roots at higher water potential. Therefore, we can postulate that root exudates represent significant strategies for successful survival of plants under stressed conditions. It has been documented that rhizosphere soil is often more moist than bulk soil (Watt et al, 1994). This was recently confirmed using neutron radiography based high-resolution imaging of soil moisture around individual roots (Carminati et al, 2010).

Exudates can influence soil-water relations through at least two mechanisms: (a) alteration of soil aggregation and/or (b) direct effect on the soil water potential. The role of exudates on soil structure and aggregation has been documented by several researchers (Alami et al, 2000; Czarnes et al, 2000b; Kaci et al, 2005; McCully, 1999a; Watt et al, 1994). Recently, we presented experimental and mathematical description of the physical mechanisms of aggregation of coarse grained soils, including association of organic matter with sand (Albalasmeh and Ghezzehei, 2013a) and the formation of inter-particle bond (Albalasmeh and Ghezzehei, 2013b). However, the effect of the hygroscopic nature of exudates on soil-water relations has not received much attention and has been recently pointed out as one of the major knowledge gaps in the biophysical controls in rhizosphere hydrology (Bengough, 2012).

The primary components of soil water potential are gravitational, matric and osmotic. The osmotic and matric potentials are generally responsible for soil water retention

characteristic (WRC). The matric potential results from the combined effects of capillarity and adsorptive forces within the soil matrix while osmotic potential is due to the solute concentration in soil water (Hillel, 2004). Matric potential, therefore, is closely related to the soils mineralogical composition as well as the structure (pore size and pore size distribution). The overarching goal of this study was to investigate the osmotic effect of exudates in isolation from changes in soil structure. Specifically, this study was designed to address this knowledge gap through systematic quantification of the water potential effects of exudates at wider range of moisture and exudate concentration.

There is an experimental difficulty in isolating substantial amounts of purified root exudates (Morel et al, 1987) due to methodological challenges, for instance, differentiating between the root exudates and other sources of soluble carbon compounds and capturing the exudates before microbial assimilation (Phillips et al, 2008). To overcome such challenges and to standardize experiments, the majority of exudate related laboratory studies use model compounds that mimic root exudates. Root exudates are mostly composed of polygalacturonic acid (PGA) (Gessa and Deiana, 1990, 1992). This was in part confirmed by similarity of elemental composition of PGA and root exudates collected in the field from nodal roots of maize plants (Morel et al, 1987). They found that the elemental composition of PGA (36.5% C, 4.8% H and 52.1% O) is very close to that found in actual root exudate (38.2% C, 5.8% H and 44.1% O). Therefore, in this study PGA was used as a model for root exudates.

5.2 Materials and Methods

5.2.1 Glass beads and EPS preparation

The porous media used in this study were packs of spherical glass beads, baked at 440 °C for 16 hours in a muffle furnace to remove any possible organic matter. An anionic polysaccharide, Polygalacturonic Acid (PGA) was employed as representative of plant root exudates (Albalasmeh and Ghezzehei, 2013a). Different concentrations of PGA solution (Table 6.1) were prepared by dissolving known mass of dry PGA in double millipore water (DDI). Because PGA is insoluble in water, it was made soluble by adjusting the pH of the solution to 12.4 using potassium hydroxide (KOH) (Albalasmeh et al, 2013). Two major treatments were considered in this experiment, varying concentrations of aqueous solutions of PGA only and glass beads saturated by PGA solutions.

Table 5.1: PGA concentrations used through this study

Concentration			
g PGA L^{-1}	g PGA g^{-1} beads	%	(w/w) μg C g^{-1} beads*
0.1	0.00003	0.003	9.9
1	0.00026	0.026	97.7
5	0.00129	0.129	463.8
15	0.00394	0.394	1379.1
29	0.00775	0.775	2260.6

* Albalasmeh et al (2013)

5.2.2 Water potential measurements

The Dewpoint Potentiameter, also known as a chilled-mirror hygrometer, measures dewpoint and temperature very accurately in a closed space above the soil sample. The sealed chamber has a mirror and a condensation detector with precise temper-

ature control. At equilibrium, the water potential of the air in the chamber is the same as the water potential of the soil sample. When the first condensation appears on the mirror, the vapor pressure is measured and total potential can be calculated (Decagon Devices, 2010; Nam et al, 2010).

A WP4C Dewpoint Potentiameter (Decagon Devices, Inc., Pullman, WA, USA) was used in this study to measure the total water potential. The typical accuracy of the equipment is $\pm$ 0.05 MPa for potential from 0 to -5 MPa, and 1% for the values between -5 to -300 MPa. The WP4C Dewpoint Potentiameter was calibrated with 0.5 M KCl standard solution before performing the measurements. Five grams of glass beads saturated by 1.3 mL of PGA at different concentrations were prepared and placed in a sample cup, and the initial water content of the soil sample was measured. Then the sample was placed in the equipment for measurement, once it reaches equilibrium in the chamber and potential was recorded, the sample weight was measured and left uncovered. After a certain time, the sample cup was covered and left for equilibrium. After that, the sample was then placed into the equipment for another measurement. In the same way, we measured the water potential for the PGA only treatment. This procedure was repeated several times in five replicates for each treatment.

5.3   Results

The water retention characteristic curve of the clean glass beads (0 g/L PGA) treatment, is given in Fig. 5.1, where x-axis represents the effective saturation degree (Θ) and y-axis represent water potential (ψ) in bar. Note that the water potential is dependent only on the porous media and the water content and does not require

Figure 5.1: Water retention curve as driven by matric potential only. Each data point is an average of five replicates, with error bars representing standard error in y-axis.

presence of organic mater or solutes to take effect, in other words, the ψ_t is equal to ψ_m only. Each data point is an average of five replicates. The error bars indicate the standard error of the water potential values.

The water retention curve data (Fig. 5.1) were fitted to van Genuchten model (van Genuchten, 1980) over a wide range of potential using the following equation:

$$\psi_m = \frac{1}{\alpha}\left(\Theta^{-1/m} - 1\right)^{1/n} \tag{5.1}$$

where ψ_m [bar] is the matric potential; Θ is the effective saturation; α [bar^{-1}] and n are empirical fitting parameters; and $m = 1 - 1/n$. The effective saturation degree is defined as $\Theta = (\theta - \theta_r)/(\theta_s - \theta_r)$, which scales the water content (θ) with respect

to the saturated water content (θ_s) and residual water content (θ_r). Because it is rather difficult to define a bulk density of repacked glass beads, we did not convert the gravimetric water content values to volumetric values. Van Genuchten fitted parameters used to generate Fig. 5.1 are θ_s= 0.268, θ_r=0, α= 2.688 and n= 1.843.

The water potential as a function of PGA concentration for different initial PGA concentrations is shown in Fig. 5.2, where x-axis represents PGA concentration in g/L and y-axis represents water potential in bar (distinct symbols are used to differentiate between different initial concentrations). Note that the water potential is dependent only on the PGA concentration and does not require presence of porous media to take effect, in other words, the ψ_t is equal to ψ_o only. Each data point is an average of four-five replicates. Horizontal and vertical error bars indicate the standard error of the PGA concentration and water potential values, respectively.

Water potential (Osmotic potential) decreases linearly ($R^2 = 0.97$) as a function of PGA concentration (Fig. 5.2), which can be written as:

$$\psi_o = a \, C_{PGA} \tag{5.2}$$

where ψ_o [bar] is the osmotic potential; a [bar.L g^{-1}] is a proportionality constant that depends on the nature of the organic matter, in case of PGA, it is equal to 0.2972 and C_{PGA} is the concentration of PGA [g L^{-1}]. Note that, there are overlaps between the different initial concentration treatments as their concentration increase with time is due to the linearity relationship (Fig. 5.2 and Eq. 5.2).
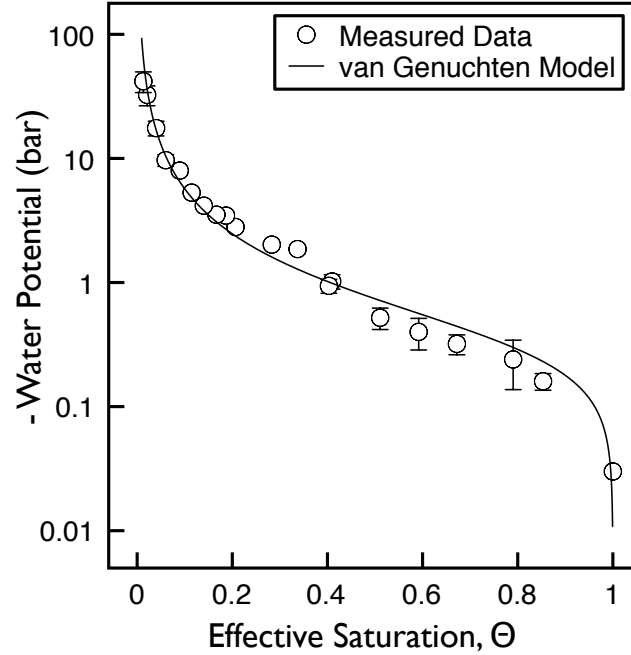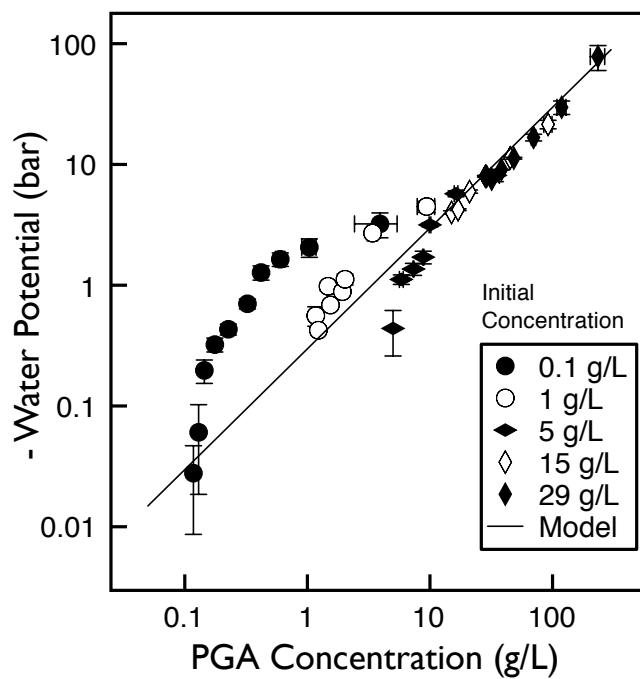
Figure 5.2: The water potential as driven by osmotic potential only. Each data point is an average of four to five replicates, with error bars representing standard error in both axis.

PGA concentration can be written as a function of gravimetric water content (θ)

$$C_{PGA} = C_o \frac{\theta_o}{\theta} \tag{5.3}$$

where C_o and θ_o are the initial PGA concentration and initial water content, respectively.

By substituting Eq. 5.3 in Eq. 5.2 will get the ψ_o as function of θ as:

$$\psi_o = a \, C_o \frac{\theta_o}{\theta} \tag{5.4}$$

The total water potential (ψ_t) is primarily consists of two components, matric potential (ψ_m) and osmotic potential (ψ_o). Therefore, ψ_t can be calculated by combining the matric potential (Eq. 6.10) and osmotic potential (Eq. 6.9) to be

$$\psi_t = \frac{1}{\alpha} \left(\Theta^{-1/m} - 1 \right)^{1/n} + a \, C_o \frac{\theta_o}{\theta} \tag{5.5}$$

The relationship between PGA concentration in g/L on x-axis and the water potential in bar on y-axis for different initial PGA concentration used in this study is depicted in Fig. 5.3. Each data point is an average of four-five replicates. Horizontal and vertical error bars indicate the standard error of the PGA concentration and water potential values, respectively.
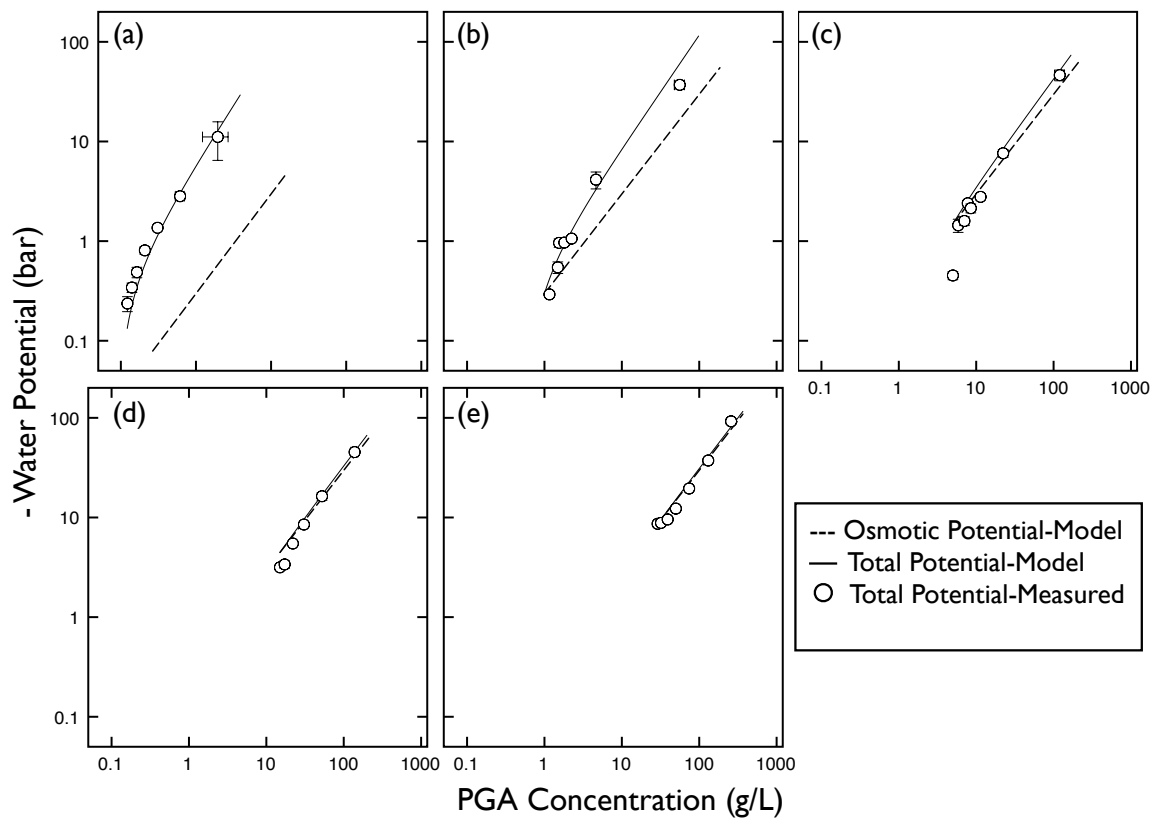
Figure 5.3: Effects of PGA concentration on total water potential of **a** 0.1 g/L, **b** 1 g/L, **c** 5 g/L, **d** 15 g/L, and **e** 29 g/L. Values are averages of four to five replicates of the treatments, with error bars representing standard error in both axis.

With the increase in the initial concentration of PGA, the difference between the osmotic potential (Eq. 6.9) and the total potential (Eq. 5.5) decrease. Moreover, at PGA concentration of 15 and 29 g/L, both of the potential (ψ_o and ψ_t) are merged together (Fig. 5.3). In other words, with the increase in the PGA concentration, the effect of osmotic potential become dominant and represents higher percentage of the total water potential. The contribution of osmotic potential in the total water potential at different initial PGA concentration is shown in Fig. 5.4, where the effective saturation is plotted on x-axis against the ratio of osmotic potential to the total water potential on y-axis. This format of presentation allow us to make direct comparison between the effect of different initial PGA concentration on the ratio of osmotic potential to the total water potential. Note that, the ratio is unity if the osmotic potential is equal to the total water potential (osmotic potential represents 100% of the total water potential). Fig. 5.4 shows that osmotic potential range from 0.08 to 0.96 at 0.5 effective saturation degree for 0.1 and 29 g/L, respectively.

The water retention characteristic curves for different initial concentrations of PGA are depicted on Fig. 5.5, where x-axis represents the gravimetric water content (g/g) and y-axis represents water potential (bar). Because it is rather difficult to define a bulk density of repacked glass beads, we did not convert these gravimetric water content values to volumetric values. Each data point is an average of four to five replicates. Horizontal and vertical error bars indicate the standard error of the water content and water potential values, respectively.

Fig. 5.5 shows that the osmotic potential appears to be significant in the total water potential compared to matric potential with the increase of PGA concentration, more specifically, when the PGA concentration increased above 5 g/L. In other words, with the increase in PGA concentration, the effect of osmotic potential become dominant
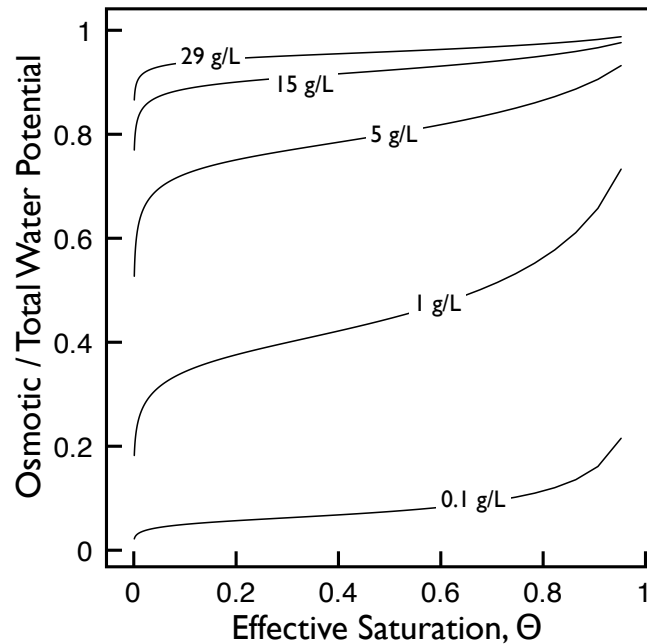
Figure 5.4: Effect of PGA concentrations on the ratio of osmotic potential to the total water potential

over the effect of matric potential (Fig. 5.5).

Fig. 5.6 shows the hydraulic function capacity on y-axis as function of water potential on x-axis. The hydraulic function capacity describe the ratio of water content change over the change of water potential.

5.4   Discussions

Our results (Fig 5.2) are consistent with those of Read et al (1999) who found that increased root exudates were associated with a decreased water potential. Read et al (1999) found that when the mucilage reached concentration of 1.2 g/L, the measured water potential was -0.6 bar, which is very close to the results of this study (Fig 5.2), the small difference in our measurements could be attributed to the error margin
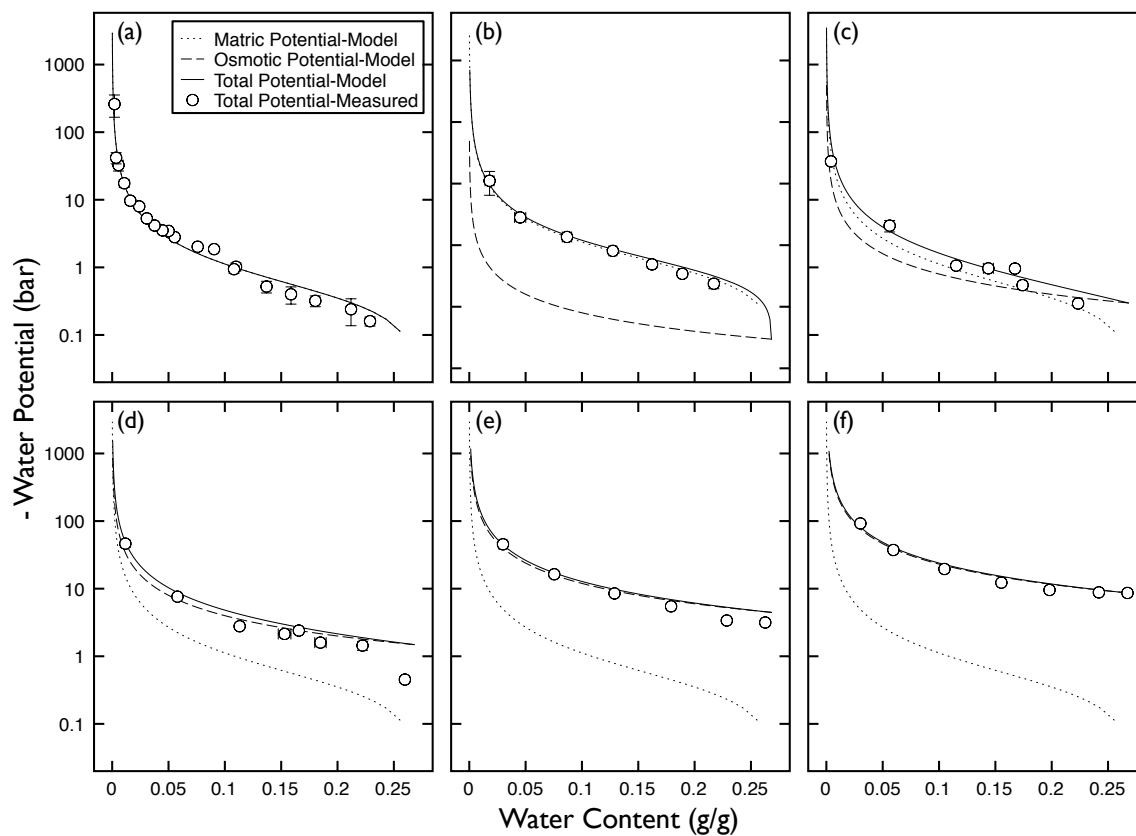
Figure 5.5: Water retention characteristic curve of **a** 0 g/L, **b** 0.1 g/L, **c** 1 g/L, **d** 5 g/L, **e** 15 g/L, and **f** 29 g/L. Values are averages of four to five replicates of the treatments, with error bars representing standard error in both axis.
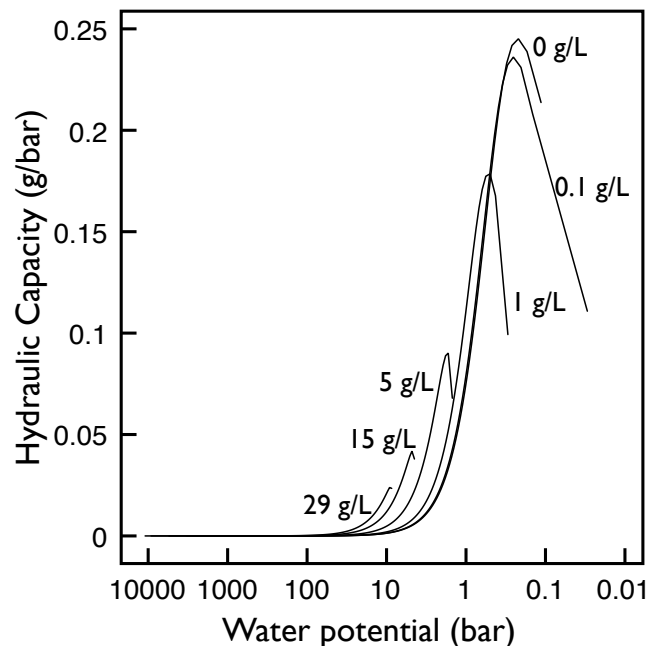
Figure 5.6: Effect of PGA concentrations on the hydraulic function capacity

of the WP4C at high water potential. Moreover, it is in agreement with McCully and Boyer (1997) who showed that air-dried mucilage from aerial maize roots had a water potential of -110 bar. Roberson and Firestone (1992) showed that EPS at -15 bar holds five times its weight in water while at -5 bar holds 10 times its weight in water. For comparison, our study showed that at -17 bar, the PGA holds 13 times its weight in water while at -6 bar holds 57 times it weight (Fig 5.2), this difference between our results and that of Roberson and Firestone (1992) could be attributed to the origin of the polysaccharides used in each study. In our study we used a model of plant root exudates and in their study they used a microorganism secretions. Moreover, Albalasmeh and Ghezzehei (2013a) showed that polysaccharides from plant root origin is more effective in association/attachment with sand than polysaccharides from microorganisms source due to the number of carboxyl group in each type of polysaccharides, which can be used to explain the difference in the amount of water held by EPS in both studies. The EPS strands act as a sponge with considerable

capacity to absorb water resulting in swelling of the matrix and progressive increase in spaces between the EPS strands (Or et al, 2007). However, this expansion depend on the carboxyl group content.

Our results show that the osmotic potential induced by PGA in solution plays significant role in the total water potential (Fig. 5.3). With the increase of PGA concentration, the difference between the osmotic potential and the total potential decreases until reaching the PGA concentration of 15 g/L where their values overlap. Moreover, we calculated the ratio of osmotic potential to the total water potential (Fig 5.4) to confirm the effect of osmotic potential in the total water potential as PGA concentration increases, which clearly shows that with the increase in PGA concentration there is an increase in the contribution of osmotic potential in the total water potential range from 0.22 to 0.99 for 0.1 and 29 g/L initial PGA concentration, respectively at saturation (high water potential).

Roberson and Firestone (1992) reported similar results where the amount of polysaccharide exerted from microorganisms in the water stressed treatments started to increase immediately as the water potential decreased and continued to increase. Bengough (2012) concluded that the more negative water potential measured for the nodal maize mucilage might be accounted for a greater accumulation of solutes, which give rise to more negative osmotic potential. Moreover, in soils, polysaccharides most often do not occur in dilute solutions; rather, they surround microorganisms and roots as more concentrated gels or slimes, particularly at low water potential (Chenu and Roberson, 1996), which is in favor to more pronounced effect of osmotic potential in the total water potential. However, a root tip growing through soil produces exudates continuously over a prolonged period (Walker et al, 2003). Therefore, this experiments (which involved a single application of the exudate) are likely to have

underestimated the influence that exudate may have.

The presence of mucilage in the rhizosphere has given rise to studies on its ability to absorb and retain water (Carminati and Vetterlein, 2012; Hinsinger et al, 2009; McCully and Boyer, 1997). However, the common explanation for the effect of these polymers in soil-water relations is primarily attributed to the soil structural modifications (matric potential effects) by addition of organic matter (Alami et al, 2000; Czarnes et al, 2000b; Kaci et al, 2005; McCully, 1999a; Watt et al, 1994). Our results (Fig. 5.5 and Fig 5.6) confirmed the previous observation by quantifying the effect of root exudate (PGA) presence on the water content and on the total water potential. Roberson and Firestone (1992) reported that when the external water potential decreases in a drying soil, soil microorganisms may retain water by increasing their internal solute concentration. In more recent studies, Bengough (2012) and Beruto et al (1995) explained the strong dependence of mucilage water potential on water content must lie in the combination of matric and osmotic potentials that together give rise to the total water potential. Our results showed that the osmotic potential induced by PGA in solution plays significant role in the amount of water held by the porous media (Fig. 5.5 and Fig 5.6). Roberson and Firestone (1992) in their study demonstrate the ability of bacterial exudates to retain water during desiccation at low water potential. Addition of PGA increased the amount of water held by the glass beads at all water potentials compared to the control (0 g/L PGA). Moreover, the amount of water held by glass beads is directly proportional to the concentration (Fig. 5.5).

It is surprising that the addition of small amounts of PGA (Table 6.1) to glass beads may result in disproportionally large increases in its water-retention capacity (Fig. 5.5). In a study by Chenu and Roberson (1996), it was observed that 1%

(w/w) addition of EPS results in a significant increase in water-retention capacity of unsaturated media, which is in agreement with our results. However, the highest concentration we used is less than 1% (Table 6.1). The presence of PGA substantially decrease the hydraulic function capacity (Fig 5.6). This reduction in hydraulic function capacity may provide significant additional time in which to make metabolic adjustments that allow plants and microorganisms to survive environmental stress. Same conclusion was reached by Roberson and Firestone (1992).

Few reports have addressed the effect of exudates into the rhizosphere water dynamics under water stress. Roberson and Firestone (1992) found that to adapt to a decrease in soil water potential, soil microorganisms may retain water by increasing their internal solute concentration. Chenu and Roberson (1996) found that the addition of 1% (w/w) EPS resulted in disproportionately increase in the water holding capacity, which is in agreement with previous finding by (Roberson and Firestone, 1992). Or et al (2007) confirmed the previous results. They indicated that EPS held 10 times its weight in water at -5 bar while at a lower water potential of -15 bar, it holds five times its weight in water.

5.5   Summary and Conclusion

The role of root exudates on soil water dynamics has been generally overlooked because exudates are (a) distributed in a narrow zone of soil around the roots, (b) biodegradable and (c) rapidly assimilated by soil microbes (Phillips et al, 2008),

We measured the water retention curves of porous media saturated by different concentration of PGA. A model of total water potential was developed based on combining the matric potential of pure porous media and osmotic potential of pure PGA

solution at different concentrations. The experimental results of this study confirmed that plant root exudates are able to retain a considerable volume of water in soils at low water potential using less than 1% of PGA. We showed that osmotic potential induced by PGA concentrations play a significant role in total water potential and water content. The above results were based on a single application of the exudate while in the natural conditions the root tip growing through soil produces exudates continuously over a prolonged period. Therefore, this results are likely to have underestimated the influence that exudate may have.

More experimental work is needed to properly unravel this fascinating and important observations on the effect of the osmotic potential of the root exudates and whether the very negative potentials are due to osmotic potential (increased concentration of solutes) or to the spacing between the polysaccharides chains in the formed gel-like structure becoming smaller with the increase in concentration and giving rise to more negative matric potentials. The presence of root exudate play important role in maintaing root water uptake for extended time periods. Therefore, more experiment is needed to properly study and show the effect of root exudates on evaporation rate.

Chapter 6

Role of Root Exudates on Rhizosphere Water Dynamics: Effects on Evaporation Rate

abstract

In a recent study, we quantified the water retention characteristic of root exudates, where root exudates are able to retain water under low water potential. Therefore, the goal of this study was to investigate the effect of root exudates on evaporation rate from porous media and whether exudates provide additional capillary effects. We visualized the formation of exudate gel and enhanced moisture retention using microscopic visualization and measured the evaporation rate from sand saturated by different initial concentrations of polygalacturonic Acid (PGA) as a representation of exudates of plant root. A model of evaporation rate was developed based on isother-

mal vapor diffusion. The results of the model predicted very well the experimental results. Both, the model and the experimental results, confirmed that plant root exudates are able to retain water in soils for longer time compared to the control treatment and a reduced evaporation rate was achieved with PGA concentrations as low as 1% of PGA. Therefore, the presence of root exudates play important role in maintaing root water uptake for extended time periods.

6.1   Introduction

The rhizosphere is the narrow zone of soil around the roots developed by plants through investing large portion of their photosynthetic carbon (Czarnes et al, 2000a; de León-González et al, 2006; Ma et al, 2011; Nambiar, 1976; Smith et al, 2011; Sprent, 1975; Watt et al, 1994) to enhance uptake of water and nutrients (Gao et al, 2011; Marschner, 2012; Morgan et al, 2005). Soil which is not part of the rhizosphere is known as bulk soil.

One way to translocate the carbon into rhizosphere is through the release of exudates by plant roots. Root exudate concentrations vary depending upon the species and the age of the plant and the environment in which a plant is growing, including soil edaphic, water stress and biological factors. Moreover, their concentrations decrease with distance toward the bulk soil (Gao et al, 2011) and depend on method of collection, ranging from 50 to 2000 μg C/g soil/day (Cheng, 1996; Gao et al, 2011; de Graaff et al, 2010; Jones and Darrah, 1993; Meharg and Killham, 1991). Due to varying method of collection and their methodological challenges, there is an experimental difficulty in isolating substantial amounts of purified root exudates (Morel et al, 1987).

To overcome these challenges and because of root exudates are mostly composed of polygalacturonic acid (PGA) (Gessa and Deiana, 1990, 1992), which was confirmed by (Morel et al, 1987) where they compared the elemental composition of PGA and root exudates collected in the field from nodal roots of maize plants, most of the laboratory studies use PGA as a model compounds that mimic root exudates (Albalasmeh and Ghezzehei, 2013a,b,c; Barre and Hallett, 2009; Czarnes et al, 2000b; Gessa and Deiana, 1990, 1992; Grimal et al, 2001; Hart et al, 2001; Morel et al, 1987; Peng et al, 2011; Traore et al, 2000; Zhang et al, 2008).

Liquid-phase flow of water in the rhizosphere, as in the bulk soil, is primarily driven by gravitational and matric potential gradients. The main origins of the matric potential of soil water are adsorptive forces on thin films (Tuller and Or, 2005) and capillary forces. The latter is usually associated with pore size distribution. Vapor-phase flow of soil water and water uptake by plant roots are affected by additional osmotic forces that depend on the concentration of dissolved osmolites in the soil water.

Root exudates are believed to play a major role by adding organic matter that can potentially alter soil structure and soil water retention characteristics (Alami et al, 2000; Czarnes et al, 2000b; Kaci et al, 2005; McCully, 1999a; Rosenzweig et al, 2012; Watt et al, 1994). The exact mechanism of how root exudates alter soil water retention is not well understood. According to Bengough (2012) in his recent review "The explanation for the strong dependence of mucilage water potential on water content must lie in the combination of matric and osmotic potentials that together give rise to the water potential". In principle, exudates have the potential of impacting both the capillary and osmotic components of soil water potential and thereby altering liquid and vapor phase flow of soil water and water uptake by roots. The effect of root exudates on osmotic potential is presented elsewhere (Albalasmeh and Ghezze-

hei, 2013c). The overarching goal of this study was to investigate whether exudates provide additional capillary effects. This question was motivated by observations that model exudates as well as natural exudates form gel like structures when their concentration in aqueous solutions is sufficiently high. Thus, the guiding hypothesis of this study was that exudate gels impart capillary forces that strongly retain water. This hypothesized mechanism is analogous to water retention in shrinking-swelling clay matrix. It is important to note here that this capillary effect of exudates is different from what could potentially arise because of soil structural changes.

The specific objectives of this paper are: (a) to demonstrate the formation of exudate gel and enhanced moisture retention using microscopic visualization (b) to quantitatively determine the effect of the capillary and osmotic effects on evaporation and (c) to provide physically based model verification of the experimental findings. Following the presentation of the materials and methods employed in this study to address the first two objectives, we will present a development of the physically based mathematical model that is used to address the third objective.

6.2 Materials and Methods

6.2.1 Porous Media and PGA Preparation

This study involved two sets of experiments that were aimed at visualization and quantification of water retention characteristics of deposited root exudates. For the former experiment, spherical glass beads (Sartorius Stedim Biotech Company, Bohemia, New York) were used as idealized representation of soil. The latter experiments were conducting using 125-250 μm quartz sand (Laguna Clay Company, Indus-

try, California). Similar to the recent study by Albalasmeh et al (2013), an anionic polysaccharide (Polygalacturonic Acid (PGA)) was used to mimic plant root exudates. Prior to the experiments, the glass beads and quartz sand were baked at 440 °C for 16 hours to remove any pre-existing organic matter.

A wide range of concentrations of PGA solution (Table 6.1) were prepared by dissolving known mass of dry PGA powder in 1 L of double Millipore water (DDI). Because PGA is insoluble in water, it was made soluble by adjusting the pH to 12.4 using 1 M potassium hydroxide (KOH) (Albalasmeh et al, 2013).

Table 6.1: PGA concentrations used through out this study

Concentration	
g PGA L^{-1}	g PGA g^{-1} sand
1	0.00039
5	0.00196
15	0.00587
29	0.01135

6.2.2 Microscopic Visualization

Environmental Scanning Electron Microscopy (ESEM), which utilizes water vapor as imaging gas, was used to observe pore-scale moisture dynamics during wetting and drying cycles. ESEM was chosen for this purpose because it enables (a) rapid and dynamic acquisition of images with high-resolution and large depth of field, (b) visualization of hydrated and chemically unaltered samples, and (c) manipulation of the hydration state of the samples by altering the chamber relative humidity. The chamber humidity can be changed by adjusting the pressure of the imaging gas (water vapor) or the stage temperature. The relative humidity of the chamber is expressed as the ratio of the chamber vapor pressure to the saturated vapor pressure corresponding

to the stage temperature as

$$h = \frac{P}{P_s} = \frac{P}{a \ \exp((b - c)/T)} \tag{6.1}$$

where P (Pa) is the chamber vapor pressure; P_s (Pa) is the saturated vapor pressure; T (K) is the stage temperature; and $a = 133.22$, $b = 20.386$ and $c = 5132$ are empirical constants. Evaporation from the sample is suppressed by maintaining the relative humidity of unity $h = 1$. Evaporation from the sample can be initiated by lowering the humidity in the range $h < 1$. Conversely, condensation of vapor on the sample can be triggered by super saturating the chamber with vapor $(h > 1)$.

In this study, we used a Quanta 200 XL30 environmental scanning electron microscope (FEI company, Hillsboro, Oregon) equipped with a field emission electron gun. A gaseous secondary electron detector (GSED), which utilizes ionized water molecules to generate a signal, was used for imaging.

A single layer of glass beads were placed directly on Peltier heating/cooling stage without any preparative treatment. The beads were then bathed with 0.1 g/L of PGA solution. Then sample was frozen to avoid evaporation of the PGA solution during evacuation of the imaging chamber. Then the sample temperature and pressure were gradually adjusted to >0 °C and $h = 1$. In the first drying cycle, the relative humidity of the chamber was lowered in multiple steps to visualize deposition of the PGA within the pore space. Then, the sample was rewetted again by supersaturating the chamber humidity. Note that new organic matter is not added during rewetting as the moisture is derived from condensation of water vapor. The second drying cycle was conducted in identical manner as the first cycle by lowering the chamber humidity. Comparison

between the first and second drying cycles allows to provides visual demonstration of how presence of deposited root exudates mediate pore-scale moisture dynamics.

6.2.3 Isothermal Evaporation Experiment

The goal of this experiment was to provide quantitative description of soil moisture dynamics in the presence of deposited root exudates. For this study, we used plastic (polypropylene) cups of 5.5 cm diameter and 2.5 cm depth. A total of 23 g of sand was placed in the cups and lightly tapped on lab bench. The sand depth was 0.6 cm consistently across all treatments and replicates. The samples were then saturated with 9 mL of the designated PGA solution. Five treatments of PGA concentration (0, 1, 5, 15, and 29 g PGA/L) were conducted in triplicates. The samples were then slowly dried to deposit all the dissolved organic matter (PGA) (Albalasmeh and Ghezzehei, 2013b).

Then, all the samples were resaturated with 9 mL of DDI water. The evaporation experiment was conducted by keeping the samples inside dark temperature-controlled (43° C) chamber (Heraeus oven, Thermo Scientific). The samples were weighed every 20 minutes (XS603S, Mettler Toledo) for up to 17 hours. The gravimetric water content was expressed at all times as

$$\theta_g = \frac{M_t - M_s - M_c}{M_s} \tag{6.2}$$

where M_t, M_s = 23g, and M_c are the total of mass of the container, mass of dry sand, and mass of empty container, respectively.

6.2.4 Isothermal Evaporation Model

The design of the evaporation experiment employed in this study permits us to assume isothermal condition and well mixed ambient air with stable relative humidity. Thus, evaporation from the porous media can be modeled as a Fickian diffusion (Ghezzehei et al, 2004). In the remainder of the model development, the temperature of the system is assumed to remain constant at $T = 316.152$ K and the values of all temperature dependent thermodynamic parameters are provided at this temperature. One-dimensional vapor density flux J_e (kg/m^{-2}s) is given by,

$$J_e = -D_v \frac{\partial C_v}{\partial z} \tag{6.3}$$

where $D_v = 4.33 \times 10^{-4}$ m^2/s is the vapor diffusion coefficient, z is normal distance from the evaporating surface, and C_v (kg/m^{-3}) is vapor mass concentration, which can be expressed as a function of relative humidity (h) using

$$C_v = \frac{M_w \, p_s}{R \, T} h \tag{6.4}$$

where $M_w = 0.018$ kg/m^3 molecular mass of liquid water, $p_s = 1.28 \times 10^4$ Pa is the saturated vapor pressure, and $R = 8.314$ J/K/mol is the universal gas constant. On the evaporating surface ($z = 0$), it is assumed that the relative humidity ($h = h^0$) is in instantaneous equilibrium with the total water potential of the liquid water and

can be described by Kelvin's equation

$$h^0 = \exp\left(\frac{M_w \psi_t}{RT\rho_w}\right) \tag{6.5}$$

where $\rho_w = 998$ kg/m^3 is density of liquid water.

Furthermore, we assume that the relative humidity on the evaporating surface changes slowly enough so that the diffusive process is in quasi-steady state condition. Thus, the humidity concentration decreases linearly with distance from the evaporating surface until it attains the value of the well mixed ambient air ($h = h^\infty$). The thickness of the boundary layer (δ) over which such linear reduction occurs is inversely proportional to the air stream velocity in the evaporating environment (Ghezzehei et al, 2004).

Then, the diffusion equation (6.3) can be further simplified as

$$J_e = -\omega \frac{(\exp(\epsilon \, \psi_t) - h^\infty)}{\delta} \tag{6.6}$$

where the thermodynamic constants at the ambient temperature of $T = 316.152$ K are lumped together as $\omega = (D_v M_w P_s)/(RT) = 2.03 \times 10^{-5}$ kg/m^2/s and $\epsilon = (M_w)/(RT\rho_w) = 6.86 \times 10^{-9}$ Pa^{-1}.

Evaporative loss of mass from cylindrical column of sample can be expressed as

$$J_e = L\theta_g^0 \rho_b \frac{dX}{dt} \tag{6.7}$$

where L (m) is the depth of the sample, ρ_b (kg/m^3) is the bulk density of the sample,

and $X = \theta_g/\theta_g^0$ is the gravimetric water content scaled by the initial gravimetric water θ_g^0. Then, by equating eqs. (6.6) and (6.7) we can rewrite the evaporation model as

$$\frac{dX}{dt} = -\frac{\omega}{\theta_g^0 L \rho_b} \frac{(\exp(\epsilon \, \psi_t) - h^\infty)}{\delta} \tag{6.8}$$

Before Eq. (6.8) can be applied to model evaporation, the relationship between the scaled water content (X) and the total water potential (ψ_t) must be established.

6.2.5 Water Retention Characteristics

The total water potential of the rhizosphere is composed on osmotic and capillary components $\psi_t = \psi_o + \psi_c$, respectively. The osmotic component depends on the concentration of soluble organic matter in aqueous solution. Recent measurements of the osmotic potential of PGA solutions have revealed an inverse relationship with the scaled water content (X) (Albalasmeh and Ghezzehei, 2013c)

$$\psi_o = \frac{a \, C_o}{X} \tag{6.9}$$

where $a = -2.97 \times 10^4 \; Pa \; m^3/kg$ and $C_o \; (kg/m^3)$ is the initial concentration.

The capillary component depends on the size and size distributions of pores. In the rhizosphere, pore size depends on the texture of the mineral fraction as well as the structure of the interstitial pores within the gels formed within the deposited exudates. This capillary potential can be described as function of the scaled water

content using a modified version of the van Genuchten equation

$$\psi_c = \frac{1}{\alpha} \left(X^{-1/m} - 1 \right)^{1-m} \tag{6.10}$$

where α (Pa^{-1}) and m are empirical fitting parameters.

6.2.6 Inverse Modeling

The evaporation model can now be completed by substituting the osmotic (6.9) and capillary potential (6.10) functions in the vapor diffusion equation (6.8)

$$\frac{dX}{dt} = -\frac{\omega}{\theta_g^0 L \rho_b} \frac{1}{\delta} \left\{ \exp\left[\epsilon \left(\frac{a\, C_o}{X} + \frac{1}{\alpha} \left(X^{-1/m} - 1 \right)^{1-m} \right) \right] - h^\infty \right\} \tag{6.11}$$

Under stable evaporative demand, initial evaporation rate from porous media saturated with water of negligible water potential ($\psi_t \approx 0$) occurs at a constant rate $dX/dt = J_e^0$. Then, Eq. (6.11) can be rearranged to express the boundary layer thickness δ as a function of the thermodynamic constants including relative humidity of ambient environment.

$$\delta = -\frac{\omega}{\theta_g^0 L \rho_b} \frac{1}{J_e^0} \left(1 - h^\infty \right) \tag{6.12}$$

The evaporation model can be further simplified by substituting Eq. (6.12) in Eq. (6.11)

$$\frac{dX}{dt} = -\frac{J_e^0}{1 - h^\infty} \left\{ \exp\left[\epsilon \left(\frac{a\, C_o}{X} + \frac{1}{\alpha} \left(X^{-1/m} - 1 \right)^{1-m} \right) \right] - h^\infty \right\} \tag{6.13}$$

There are four unknowns parameters (h^∞, α, m and J_e^0) in this model. The latter (J_e^0) can be determined by fitting to experimental time-series data from evaporation of water. The relative humidity of the chamber is assumed to homogeneous and constant at h^∞. The remaining unknowns are the capillary characteristics of the gel (α and m), which were determined by fitting Eq. (6.13) to time-series data from the various treatments of the isothermal evaporation experiment. Because Eq. (6.13) cannot be solved in closed form for $X(t)$, it was numerically evaluated using the NDSolver function of Mathematica (Wolfram Inc., Champaign, IL).

The goodness of the model fit to the measured data was determined using coefficient of determination (R^2) for each of the treatments,

$$R^2 = 1 - \frac{\sum\limits_{i=1}^{N}(O_i - M_i)^2}{\sum\limits_{i=1}^{N}\left(M_i - \overline{M}\right)^2} \tag{6.14}$$

where N is the number of observations, O_i and M_i denote the ith observed and modeled values of X, and $\overline{M}$ is the mean of the measured values of X.

6.3 Results and Discussion

6.3.1 Visualization of Evaporation Retardation by PGA Gel

The temporal sequence of relative humidity (h) stages and ESEM images of key milestone stages (denoted by enlarged filled symbols) are shown in Fig. 6.1. A subset
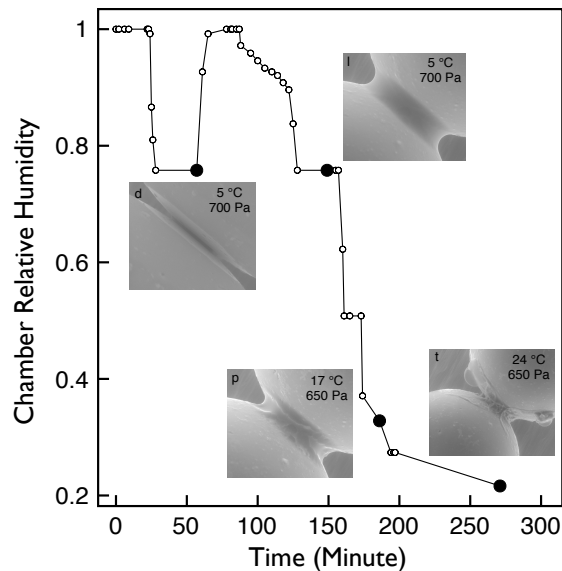
Figure 6.1: Relative humidity at multiple wetting and drying cycles and some ESEM images at different stages and environmental conditions

of the ESEM images taken during the study are shown in to highlight 20 key stages of the visualization experiment. The sequence of images in Fig. 6.2 corresponds to all the points in Fig. 6.1.

We started at $t = 0$ with the glass beads bathed in frozen PGA solution (Fig. 6.2a) to avoid evaporation of the solution before the chamber pressure is adjusted. The sample thawed at slightly unsaturated humidity condition, which retained capillary water between the beads (Fig. 6.2b). Then, when the the relative humidity was reduced to $h \approx 0.75$ (the first drying cycle) the capillary water evaporated in ≈ 6 minutes (see transition from Fig. 6.2b to c). A close-up of the inter-particle contact shows deposition of PGA at the last locations that dry (Fig. 6.2d). The mechanism of this process and its implication to soil structure development were explained by the authors elsewhere (Albalasmeh and Ghezzehei, 2013a,b). This observation implies that the osmotic potential of the dissolved PGA was not strong enough to resist evaporation at $h \approx 0.75$ or less.

Then the sample was resaturated by raising the relative humidity to above unity so that pure water is condensed on the sample (Fig. 6.2f). Then, the second drying cycle started after $\approx$ 85 minutes by gradually lowering the relative humidity down to $\approx$ 0.75 at 149 minutes after the start of the experiment. Note that this stage is identical to the driest stage of the first drying cycle. However, the remaining volume of water is much higher than the first cycle (which was nearly completely dry). The relative humidity was further reduced in stages. After 170 minutes were lapsed, the meniscus surface started to show non-smooth surface. At 186 minutes (Fig. 6.2p) a gel-like fabric emerged to appear vividly. The gel dried further with each drop in relative humidity until $h \approx 0.27$ (Fig. 6.2s). In the last stage, when the relative humidity was lowered to $\approx$ 0.20 the remaining water was removed by boiling as shown Fig. (6.2t).

The series of ESEM images representing the second drying cycle in Fig. 6.2 (i-t) reveal a few important things: (a) the time needed to evaporate the water in the second drying cycle (> 3 hours) was much longer than the first drying cycle (< 10 minutes), which is in agreement with the results found by Roberson and Firestone (1992) who showed similar slow down of evaporation rate by bacterial extracellular polysaccharides (EPS); (b) the deposited organic matter formed gel-like fabric; and (c) under similar humidity conditions the gel fabric held significantly higher water in the contact region. The latter observation is consistent with results reported by Or et al (2007) who observed that EPS "acts as a sponge with considerable capacity to absorb water".

These observation suggest that root exudates are capable of altering the rhizosphere soil-water relations not only though osmotic effects (Albalasmeh and Ghezzehei, 2013c) but also through additional capillary effects of the gel fabric. This finding in part addresses an open question raised by Bengough (2012) "The question then
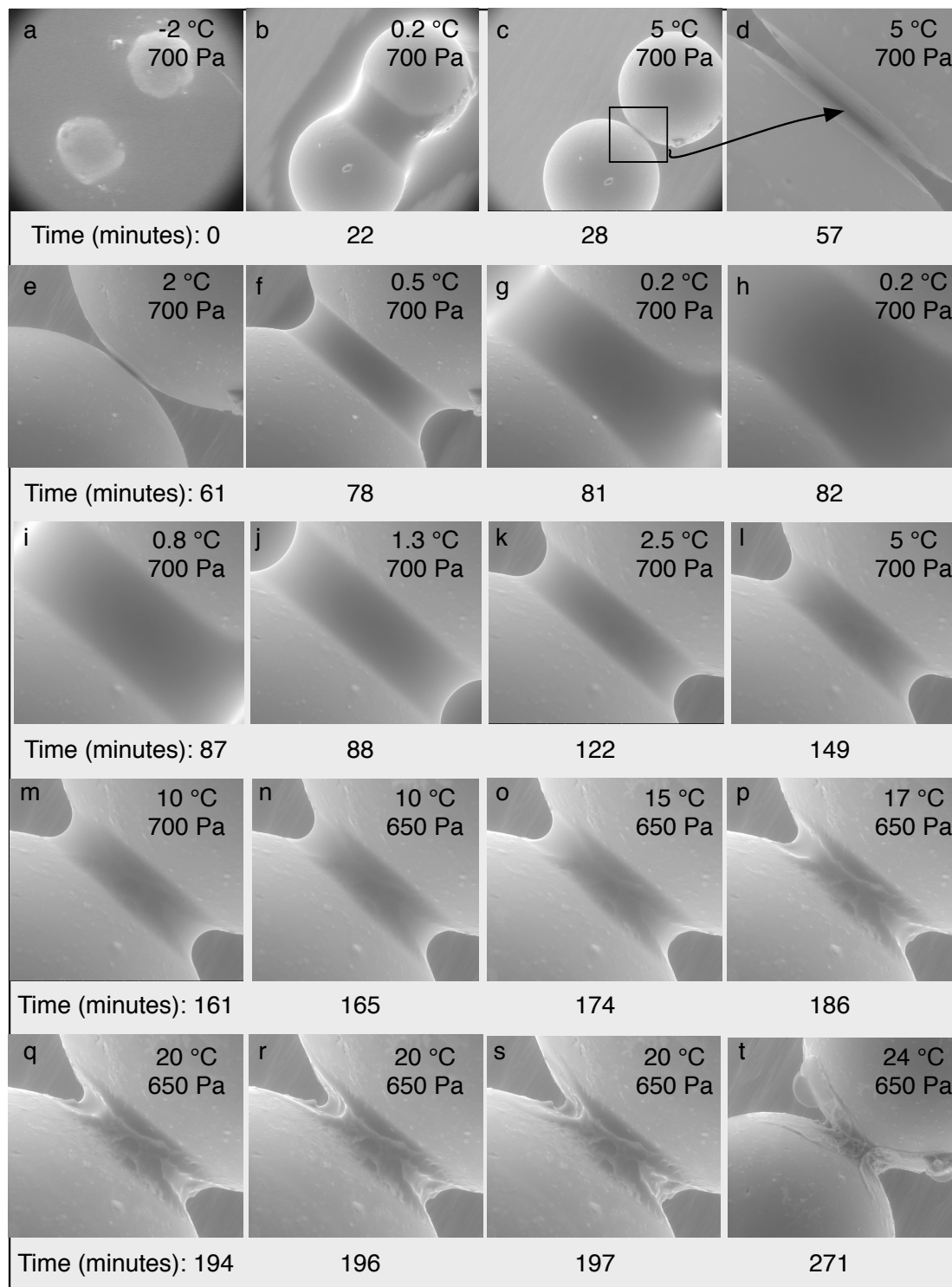
Figure 6.2: Visualization of water at the inter-particle contact between two 300 μ m glass beads under Environmental Scanning Electron Microscopy (ESEM): (a)-(c) drying of glass beads bathed in PGA solution of 0.1 g/L; (d) close-up of deposited organic matter; (e)-(h) rewetting of glass beads by vapor deposition (pure water); (i)-(L) drying of re-wetted organic matter that forming a fabric that binds the particles together under the same conditions and time of the first drying cycle and (m)-(t) drying of re-wetted organic matter at lower pressure, higher temperature and longer time that keep the formed fabric that binds the particles together
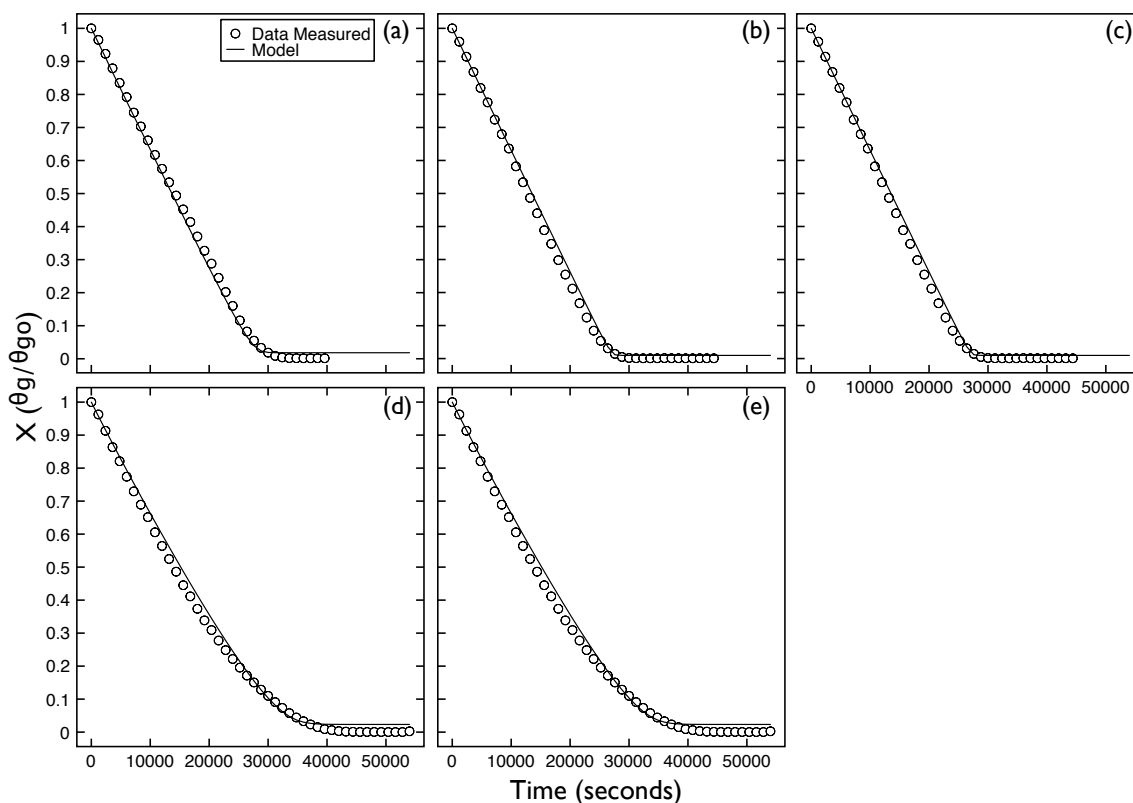
Figure 6.3: Scaled water content retained by sand amended by different concentration of PGA under drying condition. (a) 0 g/L, (b)1 g/L, (c) 5 g/L, (d) 15 g/L and (e) 29 g/L. Each data point is an average of three replicates

arises as to whether the very negative potentials of mucilage at smaller water contents are due to an increased concentration of solutes giving rise to negative osmotic potentials or to the spacing between polymer chains in the gel becoming smaller in the more concentrated gel and giving rise to more negative matric potentials". The isothermal evaporation study was designed to demonstrate this effect quantitatively.

6.3.2 Quantification of Evaporation Rate

The scaled water content ($X = \theta_g/\theta_{go}$) retained by sand media, which contain different amounts of pre-deposited PGA, during evaporation is shown in Fig. 6.3 as

function of elapsed time. The symbols denote means of three replicates. The rate of water evaporation is reflected in the slope of the data shown in Fig. 6.3. Because the sample depth is rather small, most of the evaporation process is assumed to occur in what is commonly referred to as "stage 1 evaporation" (Shokri et al, 2010). In stage 1 evaporation, it is assumed that water is transported to the surface of the porous media via liquid-phase flow and the actual vaporization occurs at the surface (Shokri et al, 2010). Thus, the evaporation rate is primarily controlled by rate of vapor removal from the evaporating surface, which depends on the effective total water potential at the surface. In these experiments, the water potential is primarily controlled by osmotic forces (which depends on dissolved PGA) and capillary forces (which depends on the textural pore size distribution and pore size distributions within PGA gel). The effect of textural capillarity operates consistently across all the treatments. However, the effect of PGA naturally increases with concentration of the applied PGA solution. In addition, the effect of PGA increases with time as the concentration in the dissolved phase rises and the gel gets desaturated. In general, the effect of rising suction (as a result of both capillary and osmotic forces) is responsible for the deviation from linear rate of evaporation. In the case of the control, 1 g/L and 5 g/L treatments, this deviation occurs late during the evaporation experiment after > 90% of the water has evaporated (Fig. 6.3a-c). This implies that that the effect of PGA and textural capillarity are relatively small and comparable to one another for most of the evaporation time.

In the case of 15 g/L and 29 g/L treatments, the deviation from linear evaporation began much earlier. This can only be explained as a result of the combined capillary and osmotic effects of PGA. It is clearly shown in Fig. 6.3d-e that the effect of PGA increases with time as the PGA concentration in aqueous solution increases and the gel gets desaturated. These observations are consistent with the results reported by

Table 6.2: Fitting parameters used to produce Fig. 6.3

PGA (g L^{-1})	α [a]	m [a]	R^2
1	0.00001	0.40	1.000
5	0.000001	0.5	0.998
15	0.0000001	0.63	0.995
29	0.0000001	0.63	0.993

[a] Capillary potential component

Chenu and Roberson (1996), who provided evidence suggesting that EPS-amended sand holds more water than control without EPS treatment. Similar results were reported by Or et al (2007) and Roberson and Firestone (1992).

6.3.3 Fitting Isothermal Evaporation Model to Experimental Data

The time-series data from the control treatment of the evaporation experiment (with no PGA) was used to calculate $J_e^0 = 3.507 \times 10^{-5}$ kg/m^2/s. The relative humidity of the evaporating chamber was assumed to be $h^\infty = 0.47$. Then, the evaporation model Eq. 6.13 was fitted to the experimental time-series data by adjusting the capillary parameters α and m. The osmotic potential of dissolved PGA depends linearly on the aqueous concentration according Eq. (6.9) (Albalasmeh and Ghezzehei, 2013c). The best fit parameters and the coefficient of determination (R^2) for each of the treatments are reported in Table 6.2.

As PGA concentration increase the osmotic component represented by C_o increase as expected. The interesting observation in Table. 6.2 is the increase in the capillary components (α and m) with increase PGA concentration. This could be explained by the capillary effect of the gel formed at the inter-particle contact (Fig. 6.2 i-t). This observation was highlighted by a recent review (Bengough, 2012) where he
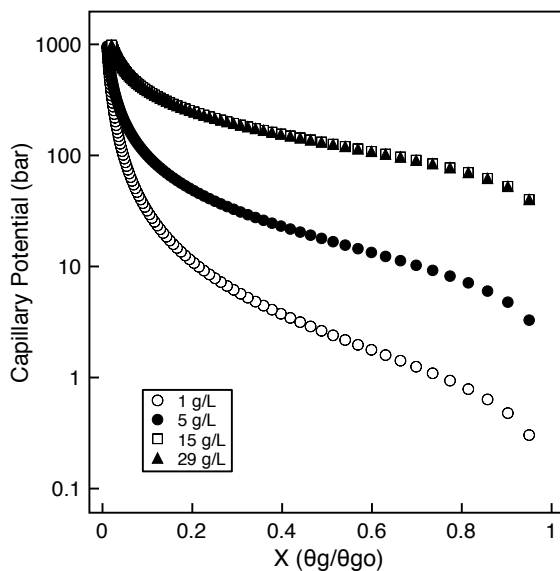
Figure 6.4: Effect of the gel formed at the inter-particle contact on the matric water potential, different symbols represent different PGA concentrations

reported that the total water potential is a combination of matric and osmotic effect of the exudates, which we were able to describe it mathematically (Eq. 6.9 and 6.10). Moreover, we plotted the capillary potential effect of the gel formed as a function of the scaled water content, X at different PGA concentrations in Fig. 6.4.

In Fig. 6.4, we have mainly three lines, the first line represents 1 g/L concentrations where there is a very little amount of PGA which is not enough to form gel, the second line represents 5 g/L concentration and the third line represents 15 and 29 g/L concentrations where have more PGA concentration will not have more effect. Note that the carbon content of 15 g/L PGA (Table 6.1) is equivalent to the maximum carbon content released in the rhizosphere reported by several authors (Cheng, 1996; Gao et al, 2011; de Graaff et al, 2010; Jones and Darrah, 1993; Meharg and Killham, 1991).

6.4   Summary and Conclusion

The role of root exudates on water retention has been generally overlooked due to the narrow zone distribution around the root and because exudates are biodegradable and rapidly assimilated by soil microbes. Recently, we showed that root exudates have the ability to retain considerable amount of water under low water potential. In this work, we have shown the formation of the gel at the inter-particle contact, studied the effects of root exudates at different concentrations on the evaporation rate from porous media using PGA to model plant root exudates and developed a model that describe the effect of root exudates on evaporation rate. Our theoretical and experimental results show that increasing initial PGA concentration increase the amount of water remained in sand at any specific time. Besides, the conducted ESEM imaging experiment confirmed the same conclusion where we showed the ability of root exudate to form gel able on retaining water and reducing the evaporation rate. This study confirmed that using PGA at very low concentrations are able to retain water in soils for longer period of time compared to the control treatment. Therefore, the presence of root exudate play important role in maintaing root water uptake for extended time periods.

Chapter 7

Summary and Conclusion

Soil structure development is controlled by a complex interaction among plant roots and their exudates, microorganisms and their exudates, soil water, ion contents, daily or seasonally wetting and drying cycles and any external forces (i.e. machinery, fire,). Because there is ample empirical evidence that wetting and drying cycles promote soil aggregation, we chose this process as a core for this dissertation. This dissertation presented a framework for in-depth understanding *if* and *how* wetting and drying cycles in the presence of plant root exudates promote soil aggregation and stabilization . The primary focusses addressed are:

1. Association mechanisms between the colloidal cementing agents (plant root and microorganisms exudates) and the neutral surface of sand particles in Chapter 3 using our new method we developed to analyze the solution of these exudates reported in Chapter 2.

2. Wetting and drying cycles as the driving agents for transporting and depositing colloidal cementing agents in Chapter 4.

3. Organic matter deposited during wetting and drying cycles can alter soil water retention in Chapter 5.

4. The effect of the altered water potential status on evaporation rate in Chapter 6.

Due to the large number of samples that needed to be analyzed throughout this work, we developed a rapid and cheap UV spectrophotometry method for carbohydrate concentration analysis in Chapter 2. The new proposed Sulfuric Acid-UV method overcomes drawbacks of the widely used Phenol-Sulfuric Acid method developed by DuBois et al (1956). The new method eliminates the coloration step and avoids the health and environmental hazards associated with phenol use. Moreover, the new method significantly reduces the waiting time prior to light absorption reading. After developing the rapid method for carbohydrate characterization, we investigated *how* plant roots and microorganisms exudates attached and associated to soil surfaces and more specifically to the most neutral sand particles in Chapter 3. We showed that PGA and xanthan as a representation of plant root and microorganisms exudates, respectively, get attached to sand and the mechanism of association involve hydrogen bond between the sand and the polysaccharides. The experimental results presented in this study showed that the association of PGA and xanthan with sand is pH dependent and the association density depend on the molecular configuration and the charge density of the polysaccharides, where lower charge density and more complicated molecular configuration (conformation) lead to more association between the polysaccharides and sand. Because plant root exudates have more capacity to be associated with sand particles more than microorganisms exudates, we focused on plant root exudates only in the rest of the experiments.

In Chapter 4, we developed a mathematical models to distinct the role of wetting and drying cycles in soil aggregate formation by the mechanism of transporting and deposition of colloidal cementing agents (plant root exudates) at the most effective locations (inter-particle contacts). We conducted several visualization experiments to test this hypothesis and we showed for the first time, to the best of our knowledge, the transporting mechanism of root exudates to form bonds between the porous media particles using a series of ESEM snapshots, where the majority of the root exudates was deposited in the contact region between the porous media particles, where the water accumulates during drying. Moreover, these high-resolution images revealed that the deposited root exudates takes the shape of the drying water meniscus (in agreement with our conceptual models). The latter imaging studies also revealed that the root exudates solution turns into gel-like fabric as they dry and the rate of drying drastically slowed down after the gel was formed.

The above findings lead us to investigate the effect of root exudates on water retention in Chapter 5 and evaporation rate in Chapter 6. The experimental results presented in Chapter 5 confirmed that plant root exudates are able to retain a considerable volume of water in soils at low water potential. Moreover, the results differentiate between the different mechanisms by which root exudates deposited during wetting and drying cycles can alter soil water retention where the osmotic potential and capillary effect of the deposited root exudates dwarf the capillary effect of aggregation induced change in pore size distribution. Further experiments were conducted in Chapter 6 to quantitatively describe the effect of the altered water potential status on evaporation rate. These experiments were conducted under isothermal and low-humidity condition and were designed to isolate the effect of the soil-water status from environmental conditions. These experiments show that the osmotic potential induced by PGA in solution causes significant reduction in evaporation rate. Moreover, it was shown that

the effect of root exudates persist even after repeated wetting-drying cycles, with a slight loss of effectiveness with each wetting and drying.

It is well accepted now that rhizospheres physical and chemical properties markedly differ from those of the bulk soil. We have been investigating multiple angles of how biological polymers released into the soil during wetting and drying cycles can alter soil hydrologic functioning and soil mechanical properties. Apparently, plants create a water reserve within the soil that helps them over a short periods of drought. This concept has implications for soil-plant water relations at the plant scale, where these findings could help to understand the water distribution around the plant roots and root water uptake. Water fluxes across the soilroot interface is a dynamic process and critical component to understand and model root water uptake. Although recent architectural models can predict the water uptake pattern across the root length, there is a lack of experimental data on their parameterizations and validations. Indeed, root water uptake is major components of the terrestrial water balance, critical in meeting atmospheric transpiration demand in water-limited environments, represents a process controlling carbon balances and energy exchange between the soil, the atmosphere and crop growth. Moreover, models of root water uptake are sensitive and important inn eco-hydrological models, global climate models and crop production models.

Bibliography

Abiven S, Menasseri S, Angers DA, Leterme P (2007) Dynamics of aggregate stability and biological binding agents during decomposition of organic materials. European Journal of Soil Science 58(1):239–247

Abiven S, Menasseri S, Chenu C (2009) The effects of organic inputs over time on soil aggregate stability - a literature analysis. Soil Biology & Biochemistry 41(1):1–12

Al-Sheraji SH, Ismail A, Manap MY, Mustafa S, Yusof RM, Hassan FA (2012) Purification, characterization and antioxidant activity of polysaccharides extracted from the fibrous pulp of Mangifera pajang fruits. LWT-Food Science and Technolgy 48(2):291–296

Alagoez Z, Yilmaz E (2009) Effects of different sources of organic matter on soil aggregate formation and stability: A laboratory study on a lithic rhodoxeralf from turkey. Soil & Tillage Research 103(2):419–424

Alami Y, Achouak W, Marol C, Heulin T (2000) Rhizosphere soil aggregation and plant growth promotion of sunflowers by an exopolysaccharide-producing rhizobiumsp. strain isolated from sunflower roots. Applied and Environmental Microbiology 66(8):3393–3398

Albalasmeh AA, Ghezzehei TA (2013a) Association of sand and silt particles with organic compounds: Anionic extracellular polymers. Plant and Soil (In Preparation)

Albalasmeh AA, Ghezzehei TA (2013b) Interplay between soil drying and root exudation in rhizosheath development. Vadose Zone Journal (In Preparation)

Albalasmeh AA, Ghezzehei TA (2013c) Role of root exudates on rhizosphere water dynamics: effects on capillary potential and osmotic potential. New Phytologist (In Preparation)

Albalasmeh AA, Berhe AA, Ghezzehei TA (2013) A new method for rapid determination of carbohydrate and total carbon concentrations using uv spectrophotometry. Carbohydrate Polymers (Accepted)

Asghari F, Yoshida H (2006) Acid-catalyzed production of 5-hydroxymethyl furfural from d-fructose in subcritical water. Industrial and Engineering Chemistry Research 45(7):2163–2173

Bai Y, Zhang P, Chen G, Cao J, Huang T, Chen K (2012) Macrophage immunomodulatory activity of extracellular polysaccharide (PEP) of Antarctic bacterium Pseudoaltermonas sp.S-5. International Immunopharmacology 12(4):611–617

Barre P, Hallett PD (2009) Rheological stabilization of wet soils by model root and fungal exudates depends on clay mineralogy. European Journal of Soil Science 60(4):525–538

Bengough A (2012) Water dynamics of the root zone: Rhizosphere biophysics and its control on soil hydrology. Vadose Zone Journal 11(2)

Beruto D, Beruto M, Ciccarelli C, Debergh P (1995) Matric potential evaluations and measurements for gelled substrates. Physiologia Plantarum 94(1):151–157

Bicker M, Hirth J, Vogel H (2003) Dehydration of fructose to 5-hydroxymethylfurfural in sub- and supercritical acetone. Green Chemistry 5(2):280–284

Buckley R (1982) sand rhizosheath of an arid zone grass. Plant and Soil 66(3):417–421

Budavari Se (ed) (1996) The Merck Index - An Encyclopedia of Chemicals, Drugs, and Biologicals. Whitehouse Station, NJ: Merck and Co., Inc.

Cadet F (1999) Measurement of sugar content by multidimensional analysis and mid-infrared spectroscopy. Talanta 48(4):867–875

Carminati A, Vetterlein D (2012) Plasticity of rhizosphere hydraulic properties as a key for efficient utilization of scarce resources. Annals of Botany

Carminati A, Moradi A, Vetterlein D, Vontobel P, Lehmann E, Weller U, Vogel HJ, Oswald S (2010) Dynamics of soil water content in the rhizosphere. Plant and Soil 332:163–176

Cheng W (1996) Measurement of rhizosphere respiration and organic matter decomposition using natural 13c. Plant and Soil 183:263–268

Chenu C (1993) Clay- or sand-polysaccharide associations as models for the interface between micro-organisms and soil: water related properties and microstructure. Geoderma 56(1-4):143 – 156

Chenu C, Guerif J (1991) Mechanical strength of clay-minerals as influenced by an adsorbed polysaccharide. Soil Science Society of America Journal 55(4):1076–1080

Chenu C, Roberson E (1996) Diffusion of glucose in microbial extracellular polysaccharide as affected by water potential. Soil Biology & Biochemistry 28(7):877–884

Chenu C, Pons C, Robert M (1987) Interaction of kaolinite and montmorillonite with neutral polysaccharide. In: LG Shultz, H van Olphen and FA Mumpton, Editors, Proceedings of the International Clay Conference Denver 1985, The Clay Minerals Society, Bloomington pp 375–381

Clapp C, Emerson W (1972) Reactions between ca-montmorillonite and polysaccharides. Soil Science 114(3):210–216

Clapp CE, Davis RJ, Waugaman SH (1962) The effect of rhizobial polysaccharides on aggregate stability. Soil Sci Soc Am J 26:466–469

Copur Y, Kiemle D, Stipanovic A, Koskinen J, Makkonen H (2003) H-1-NMR spectroscopic determination of carbohydrates and yield in pine and maple pulps. Paperi ja Puu-Paper and Timber 85(3):158–162

Cortacero-Ramirez S, Segura-Carretero A, Cruces-Blanco C, de Castro M, Fernandez-Gutierrez A (2004) Analysis of carbohydrates in beverages by capillary electrophoresis with precolumn derivatization and UV detection. Food Chemistry 87(3):471–476

Coura CO, de Araujo IWF, Vanderlei ESO, Rodrigues JAG, Quindere ALG, Fontes BP, de Queiroz INL, de Menezes DB, Bezerra MM, Silva AARE, Chaves HV, Jorge RJB, Evangelista JSAM, Benevides NMB (2012) Antinociceptive and Anti-Inflammatory Activities of Sulphated Polysaccharides from the Red Seaweed Gracilaria cornea. Basic & Clinical Pharmacology & Toxicology 110(4):335–341

Currie LA (1999) Detection and quantification limits: origins and historical overview. Analytica Chimica Acta 391(2):127–134

Czarnes S, DEXTER A, Bartoli F (2000a) Wetting and drying cycles in the maize rhizosphere under controlled conditions. Mechanics of the root-adhering soil. Plant And Soil

Czarnes S, Hallett P, Bengough A, Young I (2000b) Root- and microbial-derived mucilages affect soil structure and water transport. European Journal of Soil Science 51(3):435–443

Dakora F, Phillips D (2002) Root exudates as mediators of mineral acquisition in low-nutrient environments. Plant and Soil 245:35–47

Decagon Devices I (2010) WP4C Dewpoint PotentiaMeter Operator's Manual Version 2, Pullman, WA, USA.

Dontsova K, Bigham J (2005) Anionic polysaccharide sorption by clay minerals. Soil Science Society of America Journal 69(4):1026–1035

Dreywood R (1946) Qualitative test for carbohydrate material. Industrial and Engineering Chemistry-Analytical Edition 18(8):499–499

DuBois M, Gilles K, Hamilton J, Rebers P, Smith F (1956) Colorimetric method for determination of sugars and related substances. Analytical Chemistry 28(3):350–356

Duquesnoy E, Castola V, Casanova J (2008) Identification and quantitative determination of carbohydrates in ethanolic extracts of two conifers using C-13 NMR spectroscopy. Carbohydrates Research 343(5):893–902

ElRassi Z, Mechref Y (1996) Recent advances in capillary electrophoresis of carbohydrates. Electrophoresis 17(2):275–301

Englis D, Becker H (1943) Sugar analysis by alkaline ferricyanide method - determination of ferrocyanide by iodometric and other procedures. Industrial and Engineering Chemistry Analytical Edition 15(4):262–264

Fontes S, Queiroz V, Longo E, Antunes M (2005) Tubular microporous alumina structure for demulsifying vegetable oil/water emulsions and concentrating macromolecular suspensions. Separation and Purification Technology 44(3):235–241

Fujieda T, Kitamura Y, Yamasaki H, Furuishi A, Motobayashi K (2012) An experimental study on whole paddy saccharification and fermentation for rice ethanol production. Biomass & Bioenergy 44:135–141

Fukasawa Y, Tateno O, Hagiwara Y, Hirose D, Osono T (2012) Fungal succession and decomposition of beech cupule litter. Ecological Research 27(4):735–743

Gao Y, Yang Y, Ling W, Kong H, Zhu X (2011) Gradient distribution of root exudates and polycyclic aromatic hydrocarbons in rhizosphere soil. Soil Sci Soc Am J 75:1694–1703

van Genuchten MT (1980) A closed-form equation for predicting the hydraulic conductivity of unsaturated soils1. Soil Sci Soc Am J 44(5):892–898

Gessa C, Deiana S (1990) Fibrillar structure of Ca polygalacturonate as a model for a soil-root interface. Plant And Soil 129(2):211–217

Gessa C, Deiana S (1992) Ca-polygalacturonate as a model for a soil-root interface. Plant and Soil 140:1–13

Ghezzehei TA (2012) Soil structure. In: Huang P, Li Y, Sumner M (eds) Handbook of Soil Science, CRC Press, Boca Raton, Fla., vol 2, pp 1–17

Ghezzehei TA, Or D (2000) Dynamics of soil aggregate coalescence governed by capillary and rheological processes. Water Resources Research 36(2):367–379

Ghezzehei TA, Trautz RC, Finsterle S, Cook PJ, Ahlers CF (2004) Modeling coupled evaporation and seepage in ventilated cavities. Vadose Zone J 3(3):806–818

Godbold D, Hoosbeek M, Lukac M, Cotrufo M, Janssens I, Ceulemans R, Polle A, Velthorst E, Scarascia-Mugnozza G, Angelis P, Miglietta F, Peressotti A (2006) Mycorrhizal hyphal turnover as a dominant process for carbon input into soil organic matter. Plant and Soil 281(1-2):15–24

Golovchenko VV, Khramova DS, Ovodova RG, Shashkov AS, Ovodov YS (2012) Structure of pectic polysaccharides isolated from onion Allium cepa L. using a simulated gastric medium and their effect on intestinal absorption. Food Chemistry 134(4):1813–1822

Goupil P, Benouaret R, Charrier O, ter Halle A, Richard C, Eyheraguibel B, Thiery D, Ledoigt G (2012) Grape marc extract acts as elicitor of plant defence responses. Ecotoxicology 21(5):1541–1549

de Graaff MA, Classen AT, Castro HF, Schadt CW (2010) Labile soil carbon inputs mediate the soil microbial community composition and plant residue decomposition rates. New Phytologist 188(4):1055–1064

Greenland D (1965a) Interaction between clays and organic-compounds in soils .2. adsorption of soil organic-compounds and its effect on soil properties. Soil and Fertilizers 28(6):521–532

Greenland D (1965b) interaction between clays and organic compounds in soils. part 1 mechanisms of interaction between clays and defined organic compounds. Soil and Fertilizers 28(5):415–425

Grimal JY, Frossard E, Morel JL (2001) Maize root mucilage decreases adsorption of phosphate on goethite. Biology and Fertility of Soils 33(3):226–230

Guidi G, Petruzzelli G, Giachetti M (1977) Molecular weight as influencing factor on the adsorption of dextrans on sodium and calcium montmorillonite. Zeitschrift Fur Pflanzenernahrung Und Bodenkunde 140(5):579–586

Guinel F, McCully M (1986) Some water-related physical properties of maize root-cap mucilage. Plant Cell and Environment 9(8):657–666

Hale MG, Foy CL, Shay FJ, Brady NC (1971) Factors Affecting Root Exudation, vol Volume 23, Academic Press, pp 89–109

Hammond G, Modic F (1953) Aromatic Nitration. I. The Ultraviolet Spectra of Aromatic Nitro Compounds in Sulfuric Acid. Journal of the American Chemical Siciety 75(6):1385–1388

Harris R, Chesters G, Allen O (1966) Dynamics of soil aggregation. Advances in Agronomy 18:107–169

Hart T, Lynch J, Chamberlain A (2001) Anion exclusion in microbial and soil polysaccharides. Biology and Fertility of Soils 34(3):201–209

Hayahara T, Takao S (1968) Relationship between polymer concentration and molecular weight in the viscosity behavior of concentrated solution. Kolloid-Zeitschrift und Zeitschrift für Polymere 225:106–111

Hillel D (2004) Introduction to Environmental Soil Physics. Academic Press, San Diego, California

Hinsinger P, Bengough AG, Vetterlein D, Young IM (2009) Rhizosphere: biophysics, biogeochemistry and ecological relevance. Plant and Soil 321(1-2):117–152

Hung C, Selkirk A, Taylor R (1982) A chromatographic quality control procedure based on hplc for 5-hydroxymethylfurfural in autoclaved d-glucose infusion fluids. Journal of Clinical and Hospital Pharmacy 7(1):17–23

ICH Harmonized Tripartite Guidelines (2005) Validation of analytical procedures: text and methodology q2 (r1)

Itagaki H (1994) Saccharification process of cellulose in 97-percent sulfuric-acid monitored by sulfuric-acid induced ultraviolet-absorption behavior. Polymer 35(1):50–52

Jahnel J, Ilieva P, Frimmel F (1998) HPAE-PAD - a sensitive method for the determination of carbohydrates. Fresenius Journal of analytical Chemistry 360(7-8):827–829

Jones D, Darrah P (1993) Re-sorption of organic compounds by roots of zea mays l. and its consequences in the rhizosphere. Plant and Soil 153:47–59

Jucker B, Harms H, Hug S, Zehnder A (1997) Adsorption of bacterial surface polysaccharides on mineral oxides is mediated by hydrogen bonds. Colloids and Surfaces B-Biointerfaces 9(6):331–343

Kaci Y, Heyraud A, Barakat M, Heulin T (2005) Isolation and identification of an eps-producing rhizobium strain from arid soil (algeria): characterization of its eps and the effect of inoculation on wheat rhizosphere soil structure. Research in Microbiology 156(4):522–531

Kanetake T, Otomo M (1988) Extractive Spectrophotometric Determination of Palladium with Di-2-pyridylmethanone 2-(5-Nitro)pyridylhydrazone. Analytical Sciences 4(4):411–415

Kemper W, Rosenau R (1986) Aggregate stability and size distribution. In: Klute A, editor. Methods of Soil Analysis, Part 1. Physical and Mineralogical Methods., 2nd edn, American Society of Agronomy/Soil Science Society of America, Madison, Wisconsion USA, pp 425–461. 9

Khouryieh HA, Herald TJ, Aramouni F, Alavi S (2007) Intrinsic viscosity and viscoelastic properties of xanthan/guar mixtures in dilute solutions: Effect of salt

concentration on the polymer interactions. Food Research International 40(7):883–893

Kögel-Knabner I (2002) The macromolecular organic composition of plant and microbial residues as inputs to soil organic matter. Soil Biology and Biochemistry 34(2):139–162

Labille J, Thomas F, Milas M, Vanhaverbeke C (2005) Flocculation of colloidal clay by bacterial polysaccharides: effect of macromolecule charge and structure. Journal of Colloid and Interface Science 284(1):149–156

Lambers H, Mougel C, Jaillard B, Hinsinger P (2009) Plant-microbe-soil interactions in the rhizosphere: an evolutionary perspective. Plant and Soil 321:83–115

Layne W, Jaffe H, Zimmer H (1963) Basicity of N-Nitrosamines .2. Aqueous Sulfuric Acid Solutions. Journal of the American Chemical Siciety 85(12):1816–&

Lee JG, Hsieh WT, Chen SU, Chiang BH (2012) Hematopoietic and myeloprotective activities of an acidic Angelica sinensis polysaccharide on human CD34(+) stem cells. Journal of Ethnopharmacology 139(3):739–745

de León-González F, Celada-Tornel E, Hidalgo-Moreno CI, Etchevers-Barra JD, Gutiérrez-Castorena MC, Flores-Macías A (2006) Root–soil adhesion as affected by crop species in a volcanic sandy soil of Mexico. Soil and Tillage Research 90(1-2):77–83

Lima S, Antunes MM, Fernandes A, Pillinger M, Ribeiro MF, Valente AA (2010) Acid-catalysed conversion of saccharides into furanic aldehydes in the presence of three-dimensional mesoporous al-tud-1. Molecules 15(6):3863–3877

Lin TM, Lee SS, Lai CS, Lin SD (2006) Phenol burn. Burns 32(4):517–521

LP Z (1974) Spectrophotometric assay of long-chain unsaturated and hydroxy fatty acids in concentrated sulfuric acid. Analytical Biochemistry 58(1):146–154

Ma W, Li XX, Li CJ (2011) Modulation of Soil Particle Size and Nutrient Availability in the Maize Rhizosheath. Pedosphere 21(4):483–490

Marquez C, Garcia V, Cambardella C, Schultz R, Isenhart T (2004) Aggregate-size stability distribution and soil stability. Soil Science Society of America Journal 68(3):725–735

Marschner P (2012) Marschner's Mineral Nutrition of Higher Plants, 3rd Edition. Academic Press, London.

Martin JP (1971) Decomposition and binding action of polysaccharides in soil. Soil Biology and Biochemistry 3(1):33 – 41

Mason BS, Slover HT (1971) Gas-chromatographic method for the determination of sugars in foods. Journal of Agricultural and Food Chemistry 19(3):551–554

McCully M (1999a) Roots in soil: Unearthing the complexities of roots and their rhizospheres. Annual Review of Plant Physiology and Plant Molecular Biology 50:695–718

McCully M, Boyer J (1997) The expansion of maize root-cap mucilage during hydration .3. changes in water potential and water content. Physiologia Plantarum 99(1):169–177

McCully ME (1999b) Root Xylem Embolisms and Refilling. Relation to Water Potentials of Soil, Roots, and Leaves, and Osmotic Potentials of Root Xylem Sap. Plant Physiology 199:1001–1008, URL `http://www.plantphysiol.org/content/119/3/1001.short`

Mecozzi M (2005) Estimation of total carbohydrate amount in environmental samples by the phenol-sulphuric acid method assisted by multivariate calibration. Chemometrics and Intelligent Laboratory Systems 79(1-2):84–90

Meharg A, Killham K (1991) A novel method of quantifying root exudation in the presence of soil microflora. Plant and Soil 133:111–116

Michalowicz J, Duda W (2007) Phenols - Sources and toxicity. Polish Journal of Environmental Studies 16(3):347–362

Milas M, Rinaudo M (1986) Properties of xanthan gum in aqueous solutions: Role of the conformational transition. Carbohydrate Research 158:191–204

Morel J, Andreux F, Habib L, Guckert A (1987) Comparison of the adsorption of maize root mucilage and polygalacturonic acid on montmorillonite homoionic to divalent lead and cadmium. Biology and Fertility of Soils 5(1):13–17

Morel J, Habib L, Plantureux S, Guckert A (1991) Influence of maize root mucilage on soil aggregate stability. Plant and Soil 136(1):111–119

Morgan JAW, Bending GD, White PJ (2005) Biological costs and benefits to plant–microbe interactions in the rhizosphere. Journal of Experimental Botany 56(417):1729–1739

Nam S, Gutierrez M, Diplas P, Petrie J, Wayllace A, Lu N, Muñoz JJ (2010) Comparison of testing techniques and models for establishing the swcc of riverbank soils. Engineering Geology 110(1–2):1–10

Nambiar EKS (1976) Uptake of Zn65 from dry soil by plants. Plant And Soil 44(1):267–271

Neumann G, Römheld V (2007) The Release of Root Exudates as Affected by the Plant Physiological Status, CRC Press, pp 23–72

Old KM, Nicolson TH (1975) Electron microscopical studies of the microflora of roots of sand dune grasses. New Phytologist 74:5I–58

Olness A, Clapp C (1975) Influence of polysaccharide structure on dextran adsorption by montmorillonite. Soil Biology & Biochemistry 7(2):113–118

Or D, Phutane S, Dechesne A (2007) Extracellular polymeric substances affecting pore-scale hydrologic conditions for bacterial activity in unsaturated soils. Vadose Zone Journal 6:298–305

Parfitt R, Greenland DJ (1970) Adsorption of polysaccharides by montmorillonite. Soil Sci Soc Am J 34:862–866

Parfitt RL (1972) Adsorption of charged sugar by montmorillonite. Soil Science 113(6):417–421

Park E, Sul W, Smucker A (2007) Glucose additions to aggregates subjected to drying/wetting cycles promote carbon sequestration and aggregate stability. Soil Biology & Biochemistry 39(11):2758–2768

Peng X, Hallett PD, Zhang B, Horn R (2011) Physical response of rigid and non-rigid soils to analogues of biological exudates. European Journal of Soil Science 62(5):676–684

Pereira LdP, da Silva RO, de Souza Ferreira Bringel PH, Sales da Silva KE, Sampaio Assreuy AM, Pereira MG (2012) Polysaccharide fractions of Caesalpinia ferrea pods: Potential anti-inflammatory usage. Journal of Ethnopharmacology 139(2):642–648

Phares DJ, Smedley GT, Flagan RC (2000) Effect of particle size and material properties on aerodynamic resuspension from surfaces. Journal of Aerosol Science 31(11):1335–1353

Phillips RP, Erlitz Y, Bier R, Bernhardt ES (2008) New approach for capturing soluble root exudates in forest soils. Functional Ecology 22(6):990–999

Pilavtepe M, Sargin S, Celiktas MS, Yesil-Celiktas O (2012) An integrated process for conversion of Zostera marina residues to bioethanol. Journal of Supercritical Fluids 68:117–122

Premakumari J, Roy GAG, Prabhu AAM, Venkatesh G, Subramanian VK, Rajendiran N (2011) Effect of Solvents and pH on beta-Cyclodextrin Inclusion Complexation of 2,4-Dihydroxyazobenzene and 4-Hydroxyazobenzene. JOURNAL OF SOLUTION CHEMISTRY 40(2):327–347

Prodolliet J, Bruelhart M, Lador F, Martinez C, Obert L, Blanc M, Parchet J (1995) Determination of freeand total carbohydrate profile in soluble coffee. Journal od AOAC International 78(3):749–761

Qi L, Laskowskib JS (2006) Adsorption of polysaccharides on minerals. Encyclopedia of Surface and Colloid Science pp 649–668

Rao P, Pattabiraman TN (1989) Reevaluation of the phenol-sulfuric acid reaction for the estimation of hexoses and pentoses. Anal Biochem 181(1):18–22

Raynaud M, Vaxelaire J, Olivier J, Dieude-Fauvel E, Baudez JC (2012) Compression dewatering of municipal activated sludge: Effects of salt and pH. Water Research 46(14):4448–4456

Read D, Gregory P, Bell A (1999) Physical properties of axenic maize root mucilage. Plant and Soil 211:87–91

Reid C, Mexal J (1977) Water stress effects on root exudation by lodgepole pine. Soil Biology and Biochemistry 9(6):417 – 421

Reid J, Goss M (1981) Effect of living roots of different plant-species on the aggregate stability of two arable soils. Journal of Soil Science 32(4):521–541

Reid J, Goss M (1982) interactions between soil drying due to plant water-use and decreases in aggregate stability caused by maize roots. Journal of Soil Science 33(1):47–53

Roberson E, Firestone M (1992) Relationship between desiccation and exopolysaccharide production in a soil pseudomonas sp. Applied and Environmental Microbiology 58(4):1284–1291

Robert C, Cadet F (1998) Analysis of near-infrared spectra of some carbohydrates. Applied Spectroscopy Reviews 33(3):253–266

Rondan-Sanabria GG, Valcarcel-Yamani B, Finardi-Filho F (2012) Effects on starch and amylolytic enzymes during Lepidium meyenii Walpers root storage. Food Chemistry 134(3):1461–1467

Rosenzweig R, Shavit U, Furman A (2012) Water retention curves of biofilm-affected soils using xanthan as an analogue. Soil Sci Soc Am J 76(1):61–69

Sealey L, McCully M, Canny M (1995) The expansion of maize root-cap mucilage during hydration .1. kinetics. Physiologia Plantarum 93(1):38–46

Sharp RE, Poroyko V, Hejlek LG, Spollen WG, Springer GK, Bohnert HJ, Nguyen HT (2004) Root growth maintenance during water deficits: physiology to functional genomics. Journal of Experimental Botany 55(407):2343–2351

Sheu SC, Lai MH (2012) Composition analysis and immuno-modulatory effect of okra (Abelmoschus esculentus L.) extract. Food Chemistry 134(4):1906–1911

Shokri N, Lehmann P, Or D (2010) Evaporation from layered porous media. JOURNAL OF GEOPHYSICAL RESEARCH-SOLID EARTH 115

Sideri D (1936) On the formation of structure in soil ii synthesis of aggregates, on the bonds uniting clay with sand and clay with humus. Soil Science 42(6):461–481

Smith RJ, Hopper SD, Shane MW (2011) Sand-binding roots in Haemodoraceae: global survey and morphology in a phylogenetic context. Plant And Soil 348(1-2):453–470

Soga T, Serwe M (2000) Determination of carbohydrates in food samples by capillary electrophoresis with indirect UV detection. Food Chemistry 69(3):339–344

Somasundaran P (1969) Adsorption of starch and oleate and interaction between them on calcite in aqueous solutions. Journal of Colloid and Interface Science 31(4):557–565

Song F, Han X, Zhu X, Herbert SJ (2012) Response to water stress of soil enzymes and root exudates from drought and non-drought tolerant corn hybrids at different growth stages. Canadian Journal of Soil Science 92(3):501–507

Sprent JI (1975) Adherence of sand particles to soybean roots under water stress. New Phytologist 74:461–463

Srivastava KP, Kumar A (2007) Solvent dependence of the electronic absorption spectra of mercury-phthalocyanine. ASIAN JOURNAL OF CHEMISTRY 19(1):361–365

Suortti T, Gorenstein M, Roger P (1998) Determination of the molecular mass of amylose. Journal of Chromatography A 828(1-2):515–521

Sutherland IW (2001) Exopolysaccharides in biofilms, flocs and related structures. Water Science and Technology 43(6):77–86

Takei Y, Bartolo RC, Fujihara H, Ueta Y, Donald JA (2012) Water deprivation induces appetite and alters metabolic strategy in Notomys alexis: unique mechanisms for water production in the desert. Proceedings of the Royal Society B-Biological Sciences 279(1738):2599–2608

Theng B (1982) Clay-polymer interactions - summary and perspectives. Clays and Clay Minerals 30(1):1–10

Tisdall J, Oades J (1982) Organic matter and water-stable aggregates in soils. Journal of Soil Science 33(2):141–163

Traore O, Groleau-Renaud V, Plantureux S, Tubeileh A, Boeuf-Tremblay V (2000) Effect of root mucilage and modelled root exudates on soil structure. European Journal of Soil Science 51(4):575–581

Trzcinski AP, Hernandez E, Webb C (2012) A novel process for enhancing oil production in algae biorefineries through bioconversion of solid by-products. Bioresource Technology 116:295–301

Tuller M, Or D (2005) Water films and scaling of soil characteristic curves at low water contents. WATER RESOURCES RESEARCH 41(9)

Vogt KA, Grier CC, Vogt DJ (1986) Production, turnover, and nutrient dynamics of above- and belowground detritus of world forests. Academic Press, London; Orlando

Vriesmann LC, Teofilo RF, de Oliveira Petkowicz CL (2012) Extraction and characterization of pectin from cacao pod husks (Theobroma cacao L.) with citric acid. LWT-Food Science and Technolgy 49(1):108–116

Walker T, Bais H, Grotewold E, Vivanco J (2003) Root exudation and rhizosphere biology. Plant Physiology 132(1):44–51

Wang HC (1990) Effects of inceptive motion on particle detachment from surfaces. Aerosol Science and Technology 13(3):386–393

Wang Z, Liu X, Li R, Chang X, Jing R (2011) Development of Near-Infrared Reflectance Spectroscopy Models for Quantitative Determination of Water-Soluble Carbohydrate Content in Wheat Stem and Glume. Analytical Letters 44(15):2478–2490

Watt M, McCully M, Jeffree C (1993) Plant and bacterial mucilages of the maize rhizosphere: Comparison of their soil binding properties and histochemistry in a model system. Plant and Soil 151:151–165

Watt M, McCully ME, Canny MJ (1994) Formation and Stabilization of Rhizosheaths of Zea mays L. (Effect of Soil Water Content). Plant Physiology 106:179–186

Watt M, SILK WK, PASSIOURA JB (2006) Rates of root and organism growth, soil conditions, and temporal and spatial development of the rhizosphere. Annals of Botany 97(5):839–855

Weisseborn PK, Warren LJ, Dunn JG (1995) Selective flocculation of ultrafine iron ore. 1. mechanism of adsorption of starch onto hematite. Colloids and Surfaces A: Physicochemical and Engineering Aspects 99(1):11–27

Wright K, Northcote DH (1974) The relationship of root-cap slimes to proteins. Biochem Journal 139(3):525–534

Yu J, Lv L, Lan P, Zhang S, Pan B, Zhang W (2012) Effect of effluent organic matter on the adsorption of perfluorinated compounds onto activated carbon. Journal of Hazardous Materials 225:99–106

Zha XQ, Pan LH, Luo JP, Wang JH, Wei P, Bansal V (2012) Enzymatic fingerprints of polysaccharides of Dendrobium officinale and their application in identification of Dendrobium species. Journal of Natural Medicines 66(3):525–534

Zhang B, Hallett PD, Zhang G (2008) Increase in the fracture toughness and bond energy of clay by a root exudate. European Journal of Soil Science 59(5):855–862

Zhang ML, Sheng GP, Yu HQ (2008) Determination of proteins and carbohydrates in the effluents from wastewater treatment bioreactors using resonance light-scattering method. Water Research 42(13):3464–3472

Zhang Y, Banks CJ, Heaven S (2012) Anaerobic digestion of two biodegradable municipal waste streams. Journal of Environmental Management 104:166–174

Zhao MX, Yan Q, Ruan WQ, Miao HF, Ren HY, Xu Y (2012) A Comparative Study of Sequential Hydrogen-methane and Independent Methane Production from Kitchen Wastes. Energy Sources, Part A: Recovery, Utilization, and Environmental Effects 34(11):1046–1054

Zheng Y, Yu C, Cheng YS, Lee C, Simmons CW, Dooley TM, Zhang R, Jenkins BM, VanderGheynst JS (2012) Integrating sugar beet pulp storage, hydrolysis and fermentation for fuel ethanol production. Applied Energy 93(SI):168–175
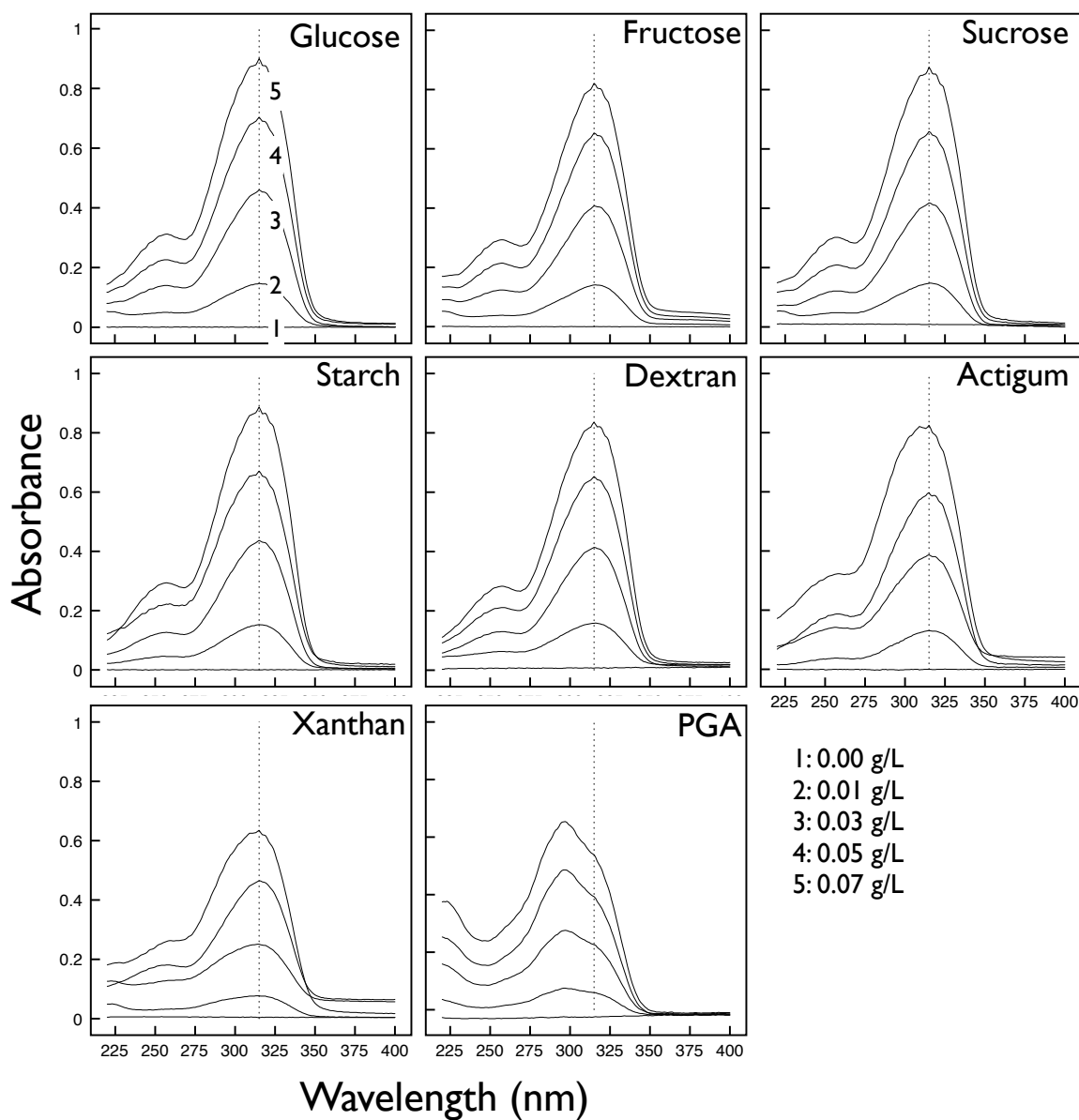
Appendix A

UV-VIS Spectra

Figure A.1: UV spectra formed under the Sulfuric Acid-UV method using concentrated sulfuric acid only. Note that the dotted line shows the maximum spectra at 315 nmVisible spectra formed under the Phenol-Sulfuric Acid method using concentrated sulfuric acid and phenol. Note that the dotted line shows the maximum spectra at 490 nm
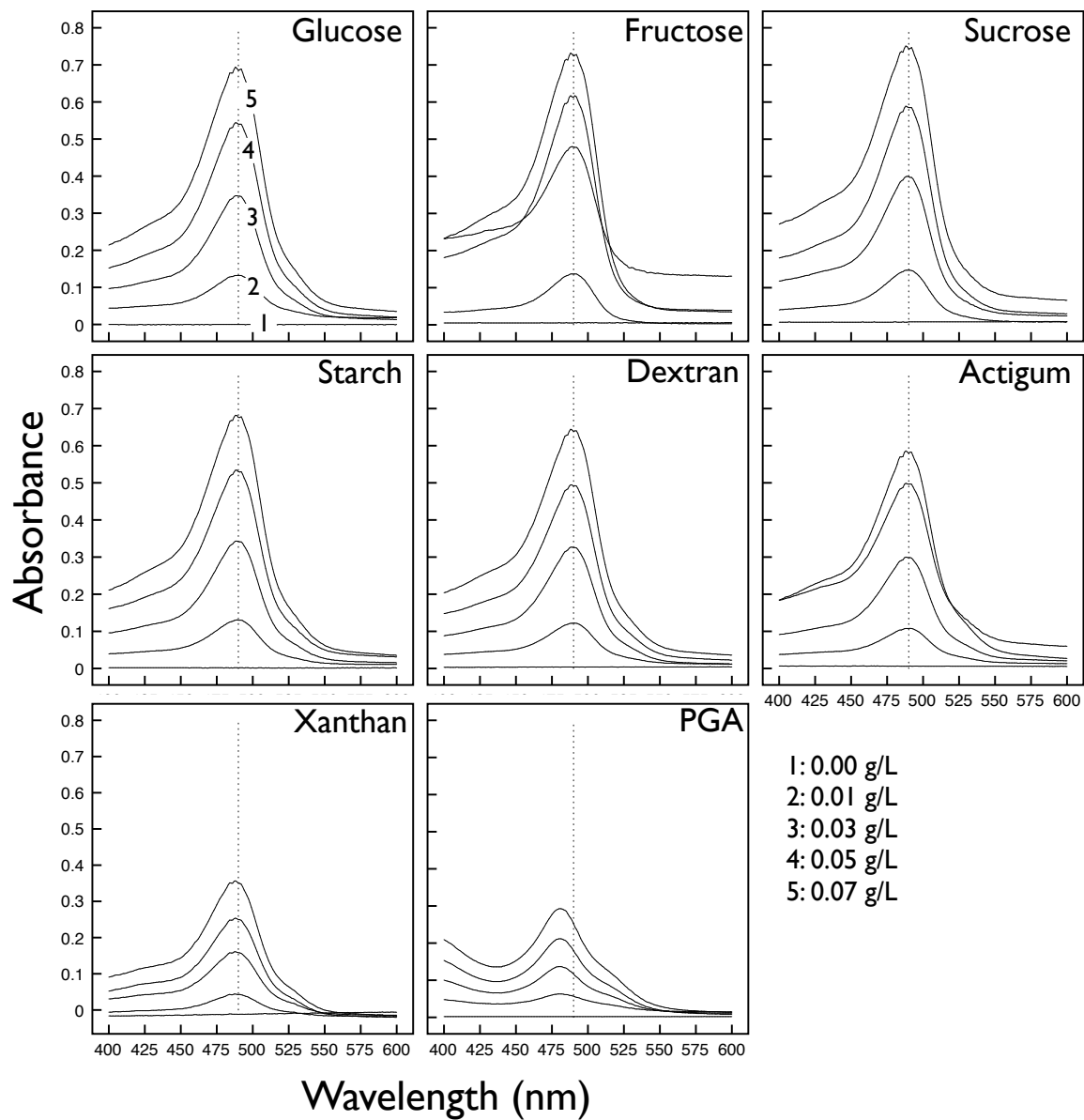
Figure A.2: Visible spectra formed under the Phenol-Sulfuric Acid method using concen- trated sulfuric acid and phenol. Note that the dotted line shows the maximum spectra at 490 nm

Appendix B

Geometrical Considerations

B.1 Radii of Curvature

Recall the dimensionless of Young-Laplace equation (equation 4.5)

$$\psi = \frac{1}{r_1} - \frac{1}{r_2} \tag{B.1}$$

From the right angle triangle in Fig. B.1 using Pythagorean equation we have

$$(r_1 + r_2)^2 + 1 = (r_2 + 1)^2 \tag{B.2}$$

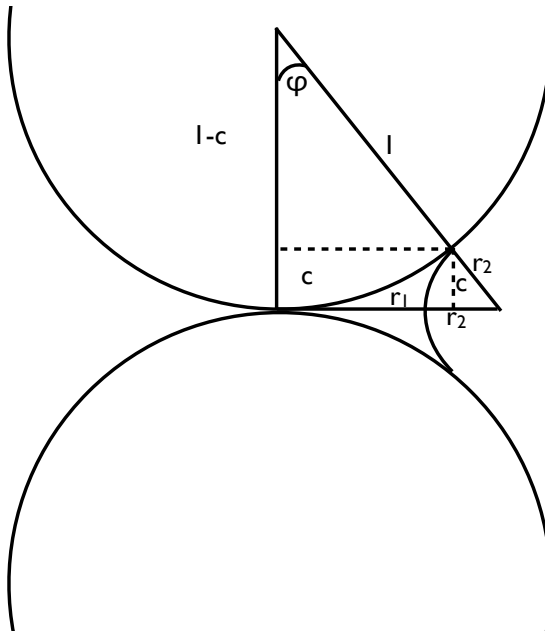By solving equations B.1 and B.2 simultaneously, analytical expression for r_1 and r_2

Figure B.1: Dimensionless geometric definitions of capillary water

can be written as

$$r_1 = \frac{4}{3 + \sqrt{9 - 8\psi}} \tag{B.3}$$

$$r_2 = \frac{4}{3 + \sqrt{9 - 8\psi} - 4\psi} \tag{B.4}$$

From Fig. B.1 we can calculate the half wetting angle (φ) as

$$\varphi = ArcCos(\frac{1}{1 + r_2}) \tag{B.5}$$

B.2 Pendular Liquid Volume

The volume of liquid-vapor interface is described by the volume of revolution equation as

$$f(z) = \sqrt{r_2^2 - z^2} + r_1 + r_2 \tag{B.6}$$

where the total volume (V_t) retained behind the interface is a solid of revolution around the z axis, given by

$$V_t = \pi \int_0^c (f(z))^2 dz \tag{B.7}$$

The volume of solid (V_s) behind the meniscus represented by spherical cap of radius R and cap c, given by

$$V_s = \frac{1}{3}\pi c^2 (3 - c) \tag{B.8}$$

where c is obtained from simple geometric relation from Fig. B.1 as

$$c = \frac{r_2}{1 + r_2} \tag{B.9}$$

The volume of liquid (V_l) can be found by subtracting equation B.8 from equation B.7, given by

$$V_l = \frac{\pi r_2 \left(3(r_2 + 1)^2 \left(2r_1 + \sqrt{\frac{r_2^3(r_2+2)}{(r_2+1)^2}} + 2r_2 + r_2(r_2 + 1)\sec^{-1}(r_2 + 1) \right) - 2r_2(2r_2 + 3) \right)}{3(r_2 + 1)^3}$$

$$(\text{B.10})$$